



National Library
of Canada

Bibliothèque nationale
du Canada

Canadian Theses Service

Service des thèses canadiennes

Ottawa, Canada
K1A 0N4

NOTICE

The quality of this microform is heavily dependent upon the quality of the original thesis submitted for microfilming. Every effort has been made to ensure the highest quality of reproduction possible.

If pages are missing, contact the university which granted the degree.

Some pages may have indistinct print especially if the original pages were typed with a poor typewriter ribbon or if the university sent us an inferior photocopy.

Reproduction in full or in part of this microform is governed by the Canadian Copyright Act, R.S.C. 1970, c. C-30, and subsequent amendments.

AVIS

La qualité de cette microforme dépend grandement de la qualité de la thèse soumise au microfilmage. Nous avons tout fait pour assurer une qualité supérieure de reproduction.

S'il manque des pages, veuillez communiquer avec l'université qui a conféré le grade.

La qualité d'impression de certaines pages peut laisser à désirer, surtout si les pages originales ont été dactylographiées à l'aide d'un ruban usé ou si l'université nous a fait parvenir une photocopie de qualité inférieure.

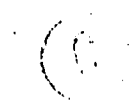
La reproduction, même partielle, de cette microforme est soumise à la Loi canadienne sur le droit d'auteur, SRC 1970, c. C-30, et ses amendements subséquents.

THE UNIVERSITY OF ALBERTA

Reduction of Electrode Sheath Potentials in CO₂ Lasers

by

Andrew Henry Labun



A THESIS

SUBMITTED TO THE FACULTY OF GRADUATE STUDIES AND RESEARCH
IN PARTIAL FULFILMENT OF THE REQUIREMENTS FOR THE DEGREE
OF Doctor of Philosophy

Department of Electrical Engineering

EDMONTON, ALBERTA

FALL, 1991



National Library
of Canada

Bibliothèque nationale
du Canada

Canadian Theses Service Service des thèses canadiennes

Ottawa, Canada
K1A 0N4

The author has granted an irrevocable non-exclusive licence allowing the National Library of Canada to reproduce, loan, distribute or sell copies of his/her thesis by any means and in any form or format, making this thesis available to interested persons.

The author retains ownership of the copyright in his/her thesis. Neither the thesis nor substantial extracts from it may be printed or otherwise reproduced without his/her permission.

L'auteur a accordé une licence irrévocable et non exclusive permettant à la Bibliothèque nationale du Canada de reproduire, prêter, distribuer ou vendre des copies de sa thèse de quelque manière et sous quelque forme que ce soit pour mettre des exemplaires de cette thèse à la disposition des personnes intéressées.

L'auteur conserve la propriété du droit d'auteur qui protège sa thèse. Ni la thèse ni des extraits substantiels de celle-ci ne doivent être imprimés ou autrement reproduits sans son autorisation.

ISBN 0-315-69992-2

Canada

THE UNIVERSITY OF ALBERTA

RELEASE FORM

NAME OF AUTHOR Andrew Henry Labun
TITLE OF THESIS Reduction of Electrode Sheath
Potentials in CO2 Lasers
DEGREE FOR WHICH THESIS WAS PRESENTED Doctor of Philosophy
YEAR THIS DEGREE GRANTED FALL, 1991

Permission is hereby granted to THE UNIVERSITY OF ALBERTA LIBRARY to reproduce single copies of this thesis and to lend or sell such copies for private, scholarly or scientific research purposes only.

The author reserves other publication rights, and neither the thesis nor extensive extracts from it may be printed or otherwise reproduced without the author's written permission.

(SIGNED) 

PERMANENT ADDRESS:
11615 134 St.
.....
Edmonton, Alberta.....
T5M 1J3.....

DATED September 23, 1991

THE UNIVERSITY OF ALBERTA
FACULTY OF GRADUATE STUDIES AND RESEARCH

The undersigned certify that they have read, and recommend to the Faculty of Graduate Studies and Research, for acceptance, a thesis entitled Reduction of Electrode Sheath Potentials in CO₂ Lasers submitted by Andrew Henry Labun in partial fulfilment of the requirements for the degree of Doctor of Philosophy.

Dr. C. E. Capjack

..... *P.P. Capjack*

Supervisor

Dr. H. J. J. Seguin

..... *H. J. J. Seguin*

Supervisor

Dr. P. R. Smy

..... *Peter R. Smy*

Dr. W. Finlay

..... *W. Finlay*

Dr. A. M. Robinson

..... *A. M. Robinson*

.....

Dr. G. D. Enright

..... *G. D. Enright*

External Examiner

Date..... *September 23, 1991*

ABSTRACT

Electrodes in glow discharges are surrounded by sheath regions characterised by electric potentials on the order of a few hundred volts and thicknesses less than a millimetre. In CO₂ transverse discharge lasers, where the potential across the entire discharge is a few thousand volts, these sheaths can dissipate as much as a third of the power deposited in the gas, resulting in considerable inefficiency. As well, the cathode sheath region figures strongly in the development of thermally induced discharge instabilities. It is therefore desirable to develop techniques to reduce these potentials and also to stabilise the discharge.

Through experiments in a photo-initiated, impulse enhanced, electrically excited (PIE) CO₂ laser discharge, two techniques have been found which substantially reduce or perhaps even eliminate the sheath potentials. The first is to apply high-voltage, short duration impulses (~10 kV, 0.2 μs) across the discharge at a frequency of about 10 kHz or more, rather than at the 5 kHz rate typical of PIE lasers. This seems to reduce the concentration of negative ions in the discharge sufficiently to substantially reduce the anode sheath potential with no appreciable increase in pulse power consumption. The second technique is to develop a repetitive, fully ionised spark channel on the cathode or anode. This results in a plasma electrode. At repetition frequencies of 10 kHz or more the sheath potentials are reduced below measurable values (i.e. below ~20 V).

Computer simulations of electron dynamics in the cathode sheath reveal that it is possible to increase the production of electrons in the cathode sheath by an applied transverse magnetic field. This implies that the electrode sheath potentials may be reduced by altering the collision statistics of the sheaths. As well, it is demonstrated that the strength of magnetic field necessary to stabilise high pressure discharges, such as found in pulsed transversely excited atmospheric (TEA) lasers, scales as the pressure squared. This suggests that very large magnetic field are necessary to stabilise TEA pulse discharges.

Acknowledgement

I would like to thank my supervisors, Dr. H. J. J. Seguin and Dr. C. E. Capjack, for their patient and conscientious encouragement and support during the course of my degree.

I would like to thank various colleagues and staff in the high power laser group: Dr. Suwas Nikumb, Vladimir Pohnert, Don Presakarchuk, and Hugo Reshef. I have also greatly benefited from association with my fellow graduate students Dale Akitt, Walter Bilida, Chris Sellathamby, James Strohschein, and Eugene Yelden.

Finally, I would like to thank my mother Lydia for fostering in me a love of learning and my wife Carolyn for her love and wise counsel.

Table of Contents

<u>Chapter</u>	<u>Page</u>
I. The significance of electrode sheaths to high power lasers.	1
A. Introduction	1
Challenges in high power laser technology	7
Reduction of electrode sheath potentials	9
B. Structure of the thesis	10
II. Energy Deposition in the electrode sheaths of a PIE CO ₂ laser discharge	16
A. Introduction	16
B. Experiment	21
PIE discharge apparatus	21
Electrostatic probe measurements	25
C. Results and discussion	30
The cathode fall region	30
E/p in the positive column	38
The anode fall region	42
D. Conclusion	46
III. Electron dynamics in magnetised CO ₂ laser and He discharges	49
A. Introduction	49

Computational considerations	51
B. The computer simulation	52
C. Results of the simulation	60
Electron flux in the non-magnetised cathode region	61
The effective pressure concept in a magnetised cathode region	66
Electron flux in the magnetised cathode region	70
Efficiency of the magnetised cathode region	76
D. Conclusions	82
IV. Magnetic laser discharge stabilisation -- scaling to high pressure systems	85
A. Introduction	85
B. Instability mechanisms	86
C. Magnetic discharge stabilisation concept	87
D. Scaling law for the transverse discharge velocity	87
E. Required magnetic field -- scaling law	96
F. Conclusions	99
V. A spark channel plasma electrode for a CO ₂ laser gas discharge.	102
A. Introduction	102
The cathode fall region	103

The PIE excitation process	104
The plasma electrode concept	105
B. Plasma electrode operation	107
C. DC potential reduction measurements	111
Potentials in externally ionised discharges	111
Data collection	112
Ionisation effects and pin electrodes	115
Plasma electrode frequency effects	120
D. Discharge conductivity tests	121
E. Efficiency considerations	125
F. Conclusions	127
VI. General Discussion and Conclusions	130
A. Conclusions	134
VII. Appendix: A listing of the MAGSIM code.	136

List of Tables

<u>Table</u>	<u>Page</u>
II.1 Typical recombination and attachment reactions in CO ₂ laser discharges.	19
II.2 Variation of V_a with I and f_p	45
III.1 Propagation of electrons in the cathode region of magnetised He normal glow discharges (30 Torr, 600 K). The electron multiplication is normalised to the initial number of electrons.	79
III.2 Propagation of electrons in the cathode region of magnetised He:N ₂ :CO ₂ normal glow discharges (30 Torr, 600 K). The electron multiplication is normalised to the initial number of electrons.	80
IV.1 Comparison of v_{tr} obtained from Monte Carlo and fluid model (Eq. (7)) predictions.	97
IV.2 Values of c_{tr} for various CO ₂ laser mixtures.	98

List of Figures

<u>Figure</u>	<u>Page</u>
I.1 Vibrational modes and transitions of CO ₂ and N ₂ significant in laser operation.	2
I.2 Fractional electron power transfer for a CO ₂ :N ₂ :He mixture in the proportions (1:1:8).	4
II.1 Configuration of the discharge system, based on a transverse discharge laser.	22
II.2 Schematic of the PIE discharge circuit.	24
II.3 The configuration of the probe in the discharge, illustrating the three degrees of freedom.	26
II.4 Probe measurements of V for $I=2.0$ A and various pulser frequencies, with a quadratic ^c fit.	32
II.5 Contours of fitted V values based on probe measurement. Only the contours for $P_{PIE} >^c 1$ kW are not affected by the probe sheath.	33
II.6 The conductive region and flux lines for a pin cathode. In (a), P_{PIE} is small, while in (b), P_{PIE} is large.	36
II.7 Variation in E/p with pulser power P_{PIE} . The data points represent 1 kV ^a increments to the pulser input potential starting from 2 kV.	39
II.8 E/p trends for a non-attaching (He:N ₂ = 39:8 Torr) and an attaching mixture (He:N ₂ :CO ₂ :CO = 39:8:1.5:1.5 Torr).	41
II.9 The anode fall V_a for $I = 2.0$ A. The scatter in the data is largest for low f_p	43
III.1 Collision cross sections for electrons at 1 Torr with (a) He, (b) N ₂ , and (c) CO ₂	55
III.2 The electron free path computation. The total length of the free path S is the sum of N segments S_i	57
III.3 The electron energy sampling and recording techniques. Collision energies are recorded at the last plane crossed and interpolated quadratically.	58
III.4 The energy density of the electron flux (EDEF) in the He cathode region (Full scattering):(a) forward flux and (b) reverse flux.	62
III.5 The mean energy of the He cathode region EDEF:(a) forward scattering;(b) full scattering, forward flux; and (c) full scattering, reverse flux.	64
III.6 The evolution of the EDEF in the He:N ₂ :CO ₂ cathode region: (a) forward flux and (b) reverse flux.	65

III.7	The mean energy of the EDEF in the He:N ₂ :CO ₂ cathode region: (a) forward flux and (b) reverse flux.	67
III.8	The mean energy of the EDEF in the He:N ₂ :CO ₂ cathode region (forward flux): (a) 30 Torr and 0 T, (b) 30 Torr and 0.1 T, and (c) 27.6 Torr and 0.1 T; and in the He cathode region (forward flux): (d) 30 Torr and 0 T, (e) 30 Torr and 0.1 T, and (f) 26.1 Torr and 0.1 T.	69
III.9	The evolution of the EDEF of the forward flux in the He cathode region at 30 Torr and 0.1 T.	71
III.10	The attrition of the cohort of collisionless electrons in the He cathode region. The closed squares represent the 0 T case and the closed circles represent the 0.1 T case.	73
III.11	The evolution of the EDEF of the forward flux in the He:N ₂ :CO ₂ cathode region at 30 Torr and 0.1 T.	74
III.12	The EDEF for forward flux at $z/D = 0.98$ in the He:N ₂ :CO ₂ cathode region (the dashed line represents the EDEF for 0.1 T).	75
III.13	The growth of the electron avalanche in the He cathode region for various magnetic fields.	77
III.14	The growth of the electron avalanche in the He:N ₂ :CO ₂ cathode region for various magnetic fields.	78
IV.1	Geometry of a magnetised cathode glow discharge region.	88
IV.2	Monte Carlo simulation results for the average electron energy and ionisation distributions and β_e (B=0 T) for a [20:8:2] laser mix.	91
IV.3	Electron Hall parameter as a function of electron energy for a 30 Torr laser mixture of He:N ₂ :CO ₂ in the proportions [20:8:2].	93
IV.4	The lateral displacement of the electron avalanche according to Eq. (3). The dots are Monte Carlo results. The magnetic field strength is 0.1 T.	94
V.1	The double-pin electrode, with transverse pins fixed to two rods connected through the water-cooled Delrin block to the pulser circuits. The spark channel between the pin tips acts as a plasma electrode.	108
V.2	The discharge geometry. The positive column extends from the double-pin electrode to a broad region on the ballasted multi-pin electrode.	109
V.3	Discharge circuit schematic.	110
V.4	The overall potential reduction δV vs. the plasma electrode frequency f for the N ₂ plasma cathode. The closed squares represent data for $P_{PIE} = 625$ W and $I = 69$ mA, the closed circles represent data for 675 W and 54 mA, and the closed triangles represent data for 725 W and 89 mA, respectively.	113

V.5	The overall potential reduction δV^{tot} vs. the plasma electrode frequency f for the He:N ₂ :CO ₂ plasma cathode. The closed circles represent data for $P_{PIE} = 216$ W, the closed squares represent data for 234 W, the closed triangles represent data for 282 W, and the inverted closed triangles represent data for 340 W, while $I = 69$ mA for each case.	114
V.6	The overall potential reduction δV^{tot} vs. the plasma electrode frequency f for the He:N ₂ :CO ₂ plasma anode. The closed squares represent data for $P_{PIE} = 295$ W and the closed circles represent data for 370 W. $I = 26$ mA for each case.	116
V.7	V^{tot} and δV^{tot} vs. P_{PIE} for the He:N ₂ :CO ₂ plasma electrode. The closed circles represent data for δV^{tot} for the plasma cathode and the closed squares represent data for δV^{tot} for the plasma anode. The open circles represent data for V^{tot} for the plasma cathode and the open squares represent data for V^{tot} for the plasma anode.	117
V.8	The externally ionised glow discharge for a pin cathode. In (a) P_{PIE} is much less than in (b), resulting in a narrower conductive zone.	119
V.9	The conductivity probe. The current drawn between two probes is proportional to the conductivity at the mid-point of the discharge volume.	122
V.10	The probe current vs. the bulk conductivity with and without the plasma cathode. The open circles conform to the probe characteristic.	124

List of Symbols

B	magnetic field
c	electron recombination rate
d_c	cathode fall distance
e	electron charge
E_{pc}	positive column electric field
f	energy density of electron flux
f_p	volume pulser frequency
f_{pe}	plasma electrode pulser frequency
I	dc current
k	Boltzmann constant
n	electron or ion density
\bar{n}	average electron density
n_0	electron density immediately following PIE pulse
n_e	electron density
n_i	ion density
p	pressure
P_{PIE}	input power to PIE pulser circuit
R	random number
r	radius of cycloid-defining circle
R_e	electric Reynolds number
r_p	probe radius

S	electron trajectory length
t	time
T_e	electron temperature
V_a	anode fall potential
V_c	cathode fall potential
V_p	probe-to-plasma potential
V_{pc}	positive column potential
V_{tot}	total dc power supply potential
v_{tr}	discharge velocity
v_x, v_y, v_z	electron velocities
x, y, z	spatial dimensions
α	electron attachment rate
a	normalised probe radius
α	collisionless electron cohort attrition rate
β_e	electron hall parameter
β_i	ion hall parameter
ϵ_0	permittivity of free space
λ	mean free path
λ_D	Debye length
μ_{\perp}	electron mobility perpendicular to magnetic field
μ_e	electron mobility
μ_i	ion mobility
μ_T	electron mobility transverse to magnetic field

ν_{en}	electron momentum transfer collision frequency
σ	electrical conductivity
τ_d	instability growth time
τ_l	ion transit time in cathode fall region
χ	normalised sheath potential
ω_{ce}	electron cyclotron frequency

I. The significance of electrode sheaths to high power lasers.

A. Introduction

This thesis is concerned with the physics and engineering of the electric gas discharge, which plays a vital role in high power CO₂ lasers. Consequently, it is helpful to consider in a general way the function of the discharge in such lasers and the advances toward higher power which have been made through improvements in discharge technology.

Quantum physics has revealed that gas molecules composed of three or more atoms can vibrate in different modes, either "stretching" the bonds between atoms or "bending" them. Vibration occurs at specific frequencies, which correspond to discrete quantities of energy. Figure I.1 depicts the lowest energy levels of the CO₂ and N₂ molecules with their associated energies.¹ Transitions between vibrational modes occur via collisions between the molecules and other particles, or alternatively through the absorption or emission of photons. Some of these transitions have greater probability than others. For example, if two vibrational modes have similar energy, it is likely that in a collision between a vibrating and a non-vibrating molecule, energy will be transferred between molecules. This occurs between the N₂ ($\nu=1$) mode and the CO₂ 001 mode and between the CO₂ 100 and 020 modes. Since all such transitions are equally likely in both directions, the populations of molecules with the modes participating in these transitions rapidly adjust towards equilibrium. In the case of the 020 mode, collisions with ground-state (000) molecules result in a further rapid transition to the metastable 010 mode of the CO₂ molecule. The tendency of the 100 mode to equilibrate with the 020 and 010 modes can be exploited to reduce its population relative to the 001 mode. The admixture of He gas with the CO₂ depopulates the 010 mode and so reduces the populations of the 100 and 020 modes. N₂ is added to the mixture since its $\nu=1$ mode repopulates the CO₂ 001 mode. Bombardment with electrons of the appropriate energy (selectively inducing the N₂ $\nu=1$ mode) results in a large number of CO₂ 001 molecules but only a small number of 100 molecules. In this way a He:N₂:CO₂ electric gas discharge can

This figure is not reproduced here due to copyright restrictions. See Ref. 1.

Fig. 1.1 Vibrational modes and transitions of CO_2 and N_2 significant in laser operation.

create and sustain a significant population inversion. This has a profound implication for photons corresponding to the energy difference between the 100 and 001 modes (i.e. 10.6 μm). These photons are more likely to encounter the high energy 001 molecules than the low energy 100 molecules. The result of such an encounter is that a 001 molecule emits a second 10.6 μm photon with identical properties to the first, while a 100 molecule absorbs the incident photon. Thus, a net gain of 10.6 μm photons is to be expected in the inverted population. This gain provides the basis for amplification in the CO_2 laser system.

The electrons which populate the $\text{N}_2(\nu=1)$ mode also collide with other gas species. Thus they populate every vibrational mode to some extent and also ionise the bulk gas to some degree. The latter process is vital to maintaining the electrical conductivity of the gas. However, ionisation is most effective at a higher electron energy than the $\text{N}_2(\nu=1)$ vibrational pumping collisions (see Fig. 1.2).² The average energy of the electrons in a dc gas discharge is determined by the ratio of the electric field to the density of the gas (i.e. the E/N ratio). Essentially, this ratio determines the average electron energy that is gained between collisions. As can be seen in Fig. 1.2, for a given gas mixture this ratio sets the fraction of total electrical power deposited in the various modes by electron collisions. Through its influence on the population levels of the various modes, E/N directly controls the degree of population inversion and thus laser gain.

The process of generating laser (light amplification through stimulated emission of radiation) beams is critically dependent on the maintenance of population inversions corresponding to the radiative transitions of the CO_2 molecules. By devising that the radiation is emitted directionally through the introduction of an optically resonant cavity, the energy deposited in the gas by collisions may be extracted in the form of infrared light. The wavelength of this stimulated radiation corresponds to the energy of the transition in question.

From its invention in 1964 by C. K. N. Patel, the CO_2 laser has been associated with high power.^{3,4} Initially, 11.9 W of 10.6 μm radiation was reported with a $\text{He:N}_2:\text{CO}_2$ gas

This figure is not reproduced here due to copyright restrictions.

See Ref. 2.

Fig. 1.2 Fractional electron power transfer for a $\text{CO}_2:\text{N}_2:\text{He}$ mixture in the proportions (1:1:8).

mixture. Even higher output powers were ultimately achieved by controlling the chemical reactions in the glow discharge⁵ and by the rapid transport of the heated gas from the discharge region by high speed blowers.⁶ This convective cooling of the gas overcame a thermal rate-limiting step in the de-excitation of the 010 bending mode of the CO₂ molecule to the ground state by conveying the 010 molecules out of the optical resonating cavity and replacing them with ground state molecules. Thus the population inversion between the upper and lower laser levels of the CO₂ molecule, and hence the gain, was enhanced.⁷ This technique, used with combined dc and rf excitation, allowed cw lasers to operate with optical outputs in excess of 25 kW as early as 1970.⁸

Alternative methods to electric discharges were also developed for pumping high power cw CO₂ lasers in the late 1960's, including chemical lasers⁹ and gasdynamic lasers of 60 kW output power.¹⁰ Despite impressive output powers, non-electrical lasers have not proven successful in the industrial marketplace and are not much in evidence at present.

In order to achieve large amplification volumes at atmospheric pressure with only modest applied electric potentials, transversely excited atmospheric (TEA) lasers were developed.¹¹ Such devices feature discharges only centimeters in length but meters in width. These lasers had to be operated in a pulse mode due to the onset of glow-to-arc instabilities. The successful extension of the transverse excitation concept to cw lasers has required some form of external ionisation of the gas to improve the discharge's stability and uniformity. One technique developed to achieve this end is the photoinitiated, impulse-enhanced, electrically excited (PIE) discharge.¹² A PIE device first photoionises the discharge volume via pulsed ultraviolet (UV) radiation and subsequently avalanches these diffuse photoelectrons by means of the same high voltage impulse. The persistence of this ionisation over a pulse duty cycle of approximately 0.2 ms results in a steady-state conductive medium through which a non-self-sustained dc current may be propagated to pump the laser amplification medium. Further details of the operation of the PIE discharge are presented in the body of this dissertation. Subsequent progress in the PIE discharge has been made through the introduction

of multi-element, fluid-ballasted electrodes,¹³ which permit the generation of the UV radiation from a pulsed corona to be combined with the high voltage impulse on a single structure (viz. the pin electrode). Very large PIE lasers have been constructed with this technology. A device capable of over 20 kW of pulsed or cw laser output power has been demonstrated.¹⁴

The CO₂ laser's efficiency at converting electrical power into laser radiation is extremely high relative to other lasers. The quantum efficiency of the CO₂ laser is given by the energy of the laser transition divided by the energy of the 001 state and has a value of approximately 41%. The fraction of the upper laser level molecules which do not undergo the laser transition reduces the efficiency expected in the laser. Yariv takes only these two factors into account in estimating CO₂ laser efficiency at 30%.¹⁵ However, the efficiency with which the processes in the laser discharge (primarily the electron bombardment of N₂ populate the upper laser level must also be considered, and this may be expected to vary according to the method of exciting the discharge.

When measured efficiencies of lasers are quoted in the scientific literature, however, it is not always clear how these numbers were obtained. For example, Harry and Evans give an "electrical conversion efficiency" of up to 23% in a 3.5 kW, multi-electrode, fast axial flow laser with a 0.6m discharge length.¹⁶ It seems unlikely that the power dissipated in the ballast resistance is included in this figure. The power dissipated by the sheath potentials are not as significant to the electrical efficiency of lasers with long discharges as to those with short, transverse discharges. This consideration may explain why a much lower efficiency of 12.2% was obtained by Wu in a 3.1 kW laser with a ballasted, multi-pin electrode having only a 28 mm discharge length.¹⁷ Presumably, Wu also does not include energy dissipated by his ballast resistance. It is difficult to compare such efficiencies with the information provided by vendors of high power lasers, which stresses the overall power requirement of a laser system. For example, an article in the trade literature on the Majestic Laser Systems' 20 kW PIE, transverse discharge laser quotes 8% efficiency from 260 kW of input power, "a large fraction

of which was deposited in the gas."¹⁴ This efficiency, apparently, does include ballast dissipation but not mechanical power.

Of course, the users of large laser systems are concerned not with the efficiency of the electric discharge *per se* but with the installation requirements and the total electricity consumption necessary to provide a given laser output power (the "wallplug" efficiency). This is the approach followed in the information brochure for the United Technologies SM41-25 25 kW dc-excited, transverse discharge laser, which cites a requirement for 600 A, 460 VAC three-phase power. If this requirement were fully utilised to provide a 25 kW laser beam, an efficiency of only 5.2% at unity power factor would result. Another measure of efficiency is the cooling water requirement, which in this case specifies 400 kW of heat dissipation, implying an efficiency no worse than 6%, including ballast resistance dissipation and possibly mechanical heating.

Challenges in high power laser technology

The development of progressively higher power lasers within even more compact packages is desirable in order to limit the cost of the devices and thus make them more competitive with alternative technologies in industrial materials processing applications. Two factors which currently limit laser output power are discharge instabilities and thermal bottle-necking. The latter factor stems from the inability to relax the population from the lower laser state to the ground state, which results in reduced population inversions.

Nighan and Wiegand¹⁸ demonstrated that a thermal instability was largely responsible for the tendency of dc glow discharges to collapse into arcs. Local increases in gas temperature lead to decreased gas density and thus increased conductivity. Positive feedback thus occurs in which electron collisional heating of the gas tends to produce filaments of high current which then develop into arcs. Reduction of these instabilities has traditionally been achieved by external ionisation schemes and by conveying the gas from the discharge in a time less than that required for thermal instability growth, typically on the order of milliseconds.¹⁸

More recently, a technique of preventing the onset of thermal instabilities by a magnetic field transverse to the electric field has been demonstrated.^{19,20} The $\mathbf{j} \times \mathbf{B}$ (Lorentz) force exerted on the electrons in the cathode fall region of the glow discharge translates the discharge across the electrode surface. This effect hinders the development of the stationary high current density filaments which lead to arcs. A computer simulation of this process was developed which allowed quantitative predictions of this process to be made.^{21,22} Successful implementations of the concept of magnetic stabilisation have been made^{23,24} which allow higher levels of power to be achieved before instability onset in these systems. The technique has recently been applied to multi-kilowatt lasers by Macken.²³

Another development towards increasing power by instability reduction has been PIF-burst-mode operation.^{25,26} Since the PIE discharge is non-self-sustained, extinguishing it by ceasing the high frequency, high voltage pulses also results in the extinction of thermal instabilities. Although the process is not completely understood, measurements of output power indicate that significantly higher dc currents can be sustained before instability onset. Also, at a given current, more output power may be extracted. This has resulted in the effective doubling of the output power available from the device.²⁷

As the amount of dc current which can be sustained in stable transverse discharges increases, more stringent demands are placed on the cooling subsystems of these high power lasers. Cooling is of extreme importance in maintaining gain. While one approach to cooling would be to install more heat exchangers, the approach taken in this project has been to investigate more efficient discharge technology. In this work, particular attention has been paid to the electrode potential sheaths. By reducing the waste heat generated in the discharge it should be possible to achieve greater output power with the same cooling apparatus currently in use.

Reduction of electrode sheath potentials

A corollary to the low potential transverse discharge geometry is that the electrode sheath potentials, the cathode fall V_c and the anode fall V_a , are of the same order of magnitude as the positive column potential V_{pc} . This implies a large power dissipation in the discharge, since the same dc current must pass through all these potentials. Unfortunately, V_c and V_a only span sheaths about 1 mm in thickness on the electrode surface and thus play no role in laser amplification. That role is filled by the positive column, which extends from the boundary of the cathode sheath to the boundary of the anode sheath. The cathode sheath region is the subject of chapter III of this dissertation and is discussed briefly, as well, in chapters II and V. In self-sustained discharges, the cathode sheath is responsible for providing most of the charge carriers through the mechanism of electron impact ionisation. The magnitude of V_c for normal glow discharges, between clean planar electrodes, is a property of the metal and gas.²⁸ For stainless steel pin cathodes in CO₂ lasers V_c typically amounts to 300 V. The corresponding anode sheath serves to collect charge carriers into the anode and it has a potential fall similar to that of the cathode sheath in the case mentioned above. It is described more fully in chapter II.

The positive column, which serves as the laser amplification medium, is discussed briefly in chapter II, but has not been the focus of this research project. The details of the PIE process are treated at more length in chapters II and V. Measurements of the various potential drops are reported in chapter II, which indicate that the total potential in the two sheath regions can amount to 700 V. This represents 25-30% of the applied dc potential.

Some possible routes to power savings in the cathode sheath may be discerned after considering the fundamental processes occurring in it. Briefly, positive ions drift through the cathode sheath, accelerated by V_c , to collide with the cathode. In about 10% of such collisions secondary electrons are emitted by various processes²⁹ and are accelerated away from the cathode, ionising neutral molecules. In the strong field present in the cathode region a substantial fraction of the ionisation energy may be acquired between collisions. The electron

flux grows exponentially through an avalanche process, although the electron density remains very low in the sheath because of the alacrity with which electrons move away from the cathode. At the boundary of the cathode sheath region the electron multiplication must result in enough free electrons to balance the ion current to the cathode. The electric field at this point becomes zero, or even reverses slightly,³⁰ due to the positive space charge of the cathode fall region. From the boundary of the cathode fall region to the anode fall region the current is due primarily to electron drift in a relatively low electric field.

Since V_c is influenced by the cathode material's secondary emission properties, it would seem that a lower value of V_c might suffice to balance the current if the probability of secondary emission of electrons by ion bombardment could be increased.³¹ In addition, V_c could be lowered by making the conversion from ion to electron current more efficient.

Abnormal glow discharges commonly occur in gas lasers, especially as current density increases. Small-area cathodes (such as pins) readily maintain very large current densities. These result in values of V_c considerably greater than those for normal glow discharges.³² Another unwanted effect of a small electrode area is the large electric field necessary to concentrate the current onto the electrode. Therefore, distribution of the currents over larger surface areas would result in reduced potential drops over the cathode sheath.

Less conventional approaches might also be fruitful in reducing electrode sheaths. It is well known, for example, that arcs maintain sheath potentials on the order of 10 V.³³ Their high electron density results in very thin sheaths with concomitant low sheath potentials. This low V_c property of arcs has been exploited on a pulsed basis in some TEA lasers.³⁴ However, the arc technique for reducing V_c has not been extended to cw lasers.

B. Structure of the thesis

The papers which comprise this thesis represent investigations into new techniques for reducing the sheath potentials in PIE CO₂ lasers. The effects of the degree of external ionisation, attachment/recombination chemistry, pin electrode geometry, and the dc current

level in a conventional PIE discharge are analysed in chapter II. This investigation led to the discovery of a potentially significant means of reducing the anode fall by controlling the pulse repetition frequency. The analysis also introduces the reader to the experimental apparatus used in chapter V. There is also some explanation of the difficulties involved in probe measurements of electrode sheath potentials in a quasi-operational laser system.

Deeper insight into the physics of the cathode sheath has been obtained through a computer simulation of the electron dynamics in the cathode sheath. A Monte Carlo simulation originally developed by Razdan²¹ was revised and restructured to record the energy distribution of the electron flux (called the energy density of the electron flux (EDEF) in chapter III), as well as ionisation events. The influence of the magnetic field on electron multiplication in the sheath and on the total generation of electrons through collisions has thus been calculated. Although there is a large influence of the magnetic field on the types of collisions that occur, especially by high energy electrons, this simulation alone is incapable of ascertaining whether V_c can be substantially reduced by a judicious application of a magnetic field. However, it does provide motivation for further work in this area, as well as some quantitative results regarding the effects of subtle changes in the collision statistics in the cathode region.

Thermal instabilities are also a limiting factor in high power laser technology. Thus, it is appropriate that results from Monte Carlo simulations relating to the stabilising effect of magnetic fields also be presented here as chapter IV. It had been previously observed³⁵ that TEA laser discharges were not stabilised by magnetic fields. Based upon the electron energies and ionisation information available from the simulation, it was possible to estimate the necessary magnetic field strength to stabilise a discharge as a function of pressure. This outcome is valid for dc discharges and so provides information relevant to both high power cw and TEA laser research.

Finally, chapter V describes the design and performance of a repetitive spark channel plasma electrode. This device employs a separate high voltage pulse circuit to create a spark

between two closely-spaced electrodes in the discharge chamber. The spark also constitutes one side of a PIE glow discharge circuit, the other side being a conventional multi-element electrode. By this means, it has been possible to eliminate the electrode sheath on the plasma electrode side. The amount of the reduction depends on such factors as the pulse repetition rate and the external ionisation. Some of these effects have been explained, but a detailed evaluation of the physics of this device and its possible ultimate worth in a laser system requires further research.

Two approaches to electrode sheath potential reduction which are not reported in this thesis are those of selecting optimal electrode materials and electrode geometries. The former was not attempted, since experience has shown that stainless steel provides many benefits, including long life. It was therefore not considered profitable to investigate this aspect of electrode sheath potentials. The latter approach was, however, pursued at some length. Many probe measurements were performed with cathodes of varying geometries, predominantly hollow cathodes. Measurements of geometric effects suffered from two defects. The first was that the results were not consistent or reproducible, even during the same run. There is a considerable interaction between the probe and a single electrode element. This can be seen from the single plot of such measurements in Fig. II.4. Under these conditions it was not possible to determine if, say, a variation in geometry resulted in a 20 V reduction in V_c , or under which conditions that would be the case. The second is that measurements of the total potential with different electrodes could not be compared with each other or with those of bare pins because of the way in which the different geometries were realised. Since it was necessary to use the same fluid-ballasted electrode blocks with projecting pins for all experiments, steel sleeves with alternative tip geometries, such as grooves or hollows, were placed over the pins. This altered several chamber parameters such as the discharge gap, flow pattern, and electrode surface area. In retrospect a more rigorous approach to such measurements might have led to usable results. However, it is unlikely that any probe measurement such as that undertaken in the course of this project can provide satisfactory

results in a PIE discharge.

It should be noted that an important consideration when employing these diverse techniques to sheath potential reduction is that the method must not impinge on the properties of the positive column. This is implicit in the choice of techniques put forward in this dissertation. For example, massive external ionisation could prevent the abnormal glow from developing on pin electrodes (chapter II), but would also have the effect of reducing E/N in the positive column to such an extent that little if any laser output could be obtained. For this reason, care was taken in the plasma electrode experiments to ensure that the plasma electrode was not adversely affecting the conductivity of the positive column. The goal of this research is to provide the laser developer with new avenues to system improvement, which implies that they should result in greater laser output power per unit of electrical input power.

REFERENCES

- [1] P.W. Milonni, J.H. Eberly, *Lasers* (Wiley-Interscience, New York, 1988), p. 438.
- [2] R.H. Bullis, W.L. Nighan, M.C. Fowler, W.J. Wiegand, *AIAA J.* **10**, 407 (1972).
- [3] C.K.N. Patel, *Appl. Phys. Lett.*, **7**, 15 (1965).
- [4] C.K.N. Patel, P.K. Tien, J.H. McFee, *Appl. Phys. Lett.*, **7**, 290 (1965).
- [5] W.J. Witteman, *Appl. Phys. Lett.* **11**, 337 (1967).
- [6] T.A. Cool, J.A. Shirley, *Appl. Phys. Lett.* **14**, 70 (1969).
- [7] A.J. DeMaria, *Proc. IEEE* **61**, 731 (1973).
- [8] C.O. Brown, J.W. Davis, *Appl. Phys. Lett.* **21**, 480 (1972).
- [9] T.A. Cool, R.R. Stephens, T.J. Falk, *Int. J. Chem. Kinetics* **1**, 495 (1969).
- [10] E.T. Gerry, *IEEE Spectrum* **7**, 51 (1970).
- [11] A.J. Beaulieu, *Appl. Phys. Lett* **16**, 504 (1970).
- [12] H.J.J. Seguin, A.K. Nam, and J. Tulip, *Appl. Phys. Lett.*, **32**, 418 (1978).
- [13] H.J.J. Seguin, A.K. Nam, and J. Tulip, *J. Appl. Phys.*, **49**, 4566 (1978).
- [14] V.E. Merchant, *Laser Focus/Electro-Optics*, May (1985).
- [15] A. Yariv, *Quantum Electronics, 3rd ed.* (Wiley, New York, 1989), p. 218.
- [16] J.E. Harry, D.R. Evans, *Appl. Phys. Lett.* **50**, 313 (1987).
- [17] K.H. Wu, *Optics Communications* **61**, 45 (1987).
- [18] W. Nighan, W. Wiegand, *Appl. Phys. Lett.*, **25** 633 (1974).
- [19] H.J.J. Seguin, C.E. Capjack, D. Antoniuk, K.A. Nam, *Appl. Phys. Lett.*, **37**, 130 (1980).
- [20] C.E. Capjack, D.M. Antoniuk, H.J.J. Seguin, *J. Appl. Phys.*, **52**, 4517 (1981).
- [21] R. Razdan, C.E. Capjack, H.J.J. Seguin, *J. Appl. Phys.* **57**, 4954(1985).
- [22] R. Razdan, C.E. Capjack, H.J.J. Seguin, *Appl. Optics* **25**, 2915(1986).
- [23] J.A. Macken, U.S. Pat. 4755999 (1988).
- [24] V.A. Seguin, H.J.J. Seguin, C.E. Capjack, and S.K. Nikumb, *J. Appl. Phys.*, **60**, 3088 (1986).

- [25] S.K. Nikumb, H.J.J. Seguin, V.A. Seguin, and H. Reshef, *J. Phys. E: Sci. Instrum.*, **20**, 911 (1987).
- [26] S.K. Nikumb, H.J.J. Seguin, V.A. Seguin, D. Presakarchuk, *Appl. Phys. Lett.* **53**, 254 (1988).
- [27] S.K. Nikumb, H.J.J. Seguin, V.A. Seguin, R.J. Willis, H.W. Reshef, *IEEE J. Quant. Electron.*, **QE-25**, 1725 (1989).
- [28] A. von Engel, *Ionised Gases* (Oxford University Press, London, 1965), p. 229.
- [29] G. Carter, J.S. Colligon, *Ion Bombardment of Solids*, (Heinemann, London, 1968), p. 38.
- [30] R.A. Gottscho, *Phys. Rev. A*, **36**, 2233 (1987).
- [31] G. Francis, *Handbuch der Physik*, ed. S. Flügge, **22**, (Springer Verlag, Berlin, 1956), p. 56.
- [32] A. von Engel, *op. cit.*, p. 135.
- [33] R. Holmes in *Electrical Breakdown of Gases*, ed. J.M. Meek and J.D. Craggs (Wiley-Interscience, Chichester, 1978), p. 847.
- [34] V.P. Gorkovskii, N.V. Karlov, I.O. Kovalev, B.M. Koval'chuk, G.P. Kuz'min, G.A. Mesyats, and A.M. Prokhorov, *Sov. J. Quant. Elect.*, **14**, 1253 (1984).
- [35] W.D. Bilida, M.Sc. Thesis, The University of Alberta, 1989.

II. Energy Deposition in the electrode sheaths of a PIE CO₂ laser discharge

A. Introduction

High-power CO₂ lasers are being exploited in an increasing number of industrial processes which call for precisely controlled and delivered, high-intensity, radiant energy. As progressively higher powers are attained, it is important in laser design to consider the efficiency of the processes which transform electrical power into laser radiation.

The common feature of all electrically excited CO₂ lasers is the formation of a glow discharge in the amplifying medium. This weakly ionised plasma can be divided into three zones: the cathode fall region, which in a 50 Torr discharge is slightly less than 1 mm in thickness; the positive column, the length of which is determined by the separation of the electrodes; and the anode fall region, also less than 1 mm thick. Ionisation in the positive column is the result of collisions between the drifting electrons and the neutral gas molecules; a process which is in equilibrium with recombination of the plasma for a self-sustained discharge. Non-self-sustained discharges are supported by external ionisation of the positive column, for example by flashlamps or electron beams, and may thus be far from ionisational equilibrium. The energy transfer between a laser's electrical power supply and the vibrational modes of the CO₂ molecules which emit the 10.6 μm laser radiation generally occurs in the positive column of a glow discharge. Specifically, this transfer occurs by means of vibrational excitation collisions of electrons with neutral gas molecules. These collisions often result in the molecules' absorbing quanta of energy corresponding to stretching or flexing of the intra-molecular bonds or rotation of the molecules about their axes. Provided that the appropriate excitation collisions occur more frequently than de-excitation events, such as intermolecular collisions or emissions of radiation, a non-equilibrium population of excited molecules can be maintained. The necessary environment for this to occur in is a medium with a sufficient number of free electrons to conduct a considerable current but still having a predominance of neutral molecules (i.e. a glow discharge). A fundamental design objective

for high-power lasers is to fill a volume of extended dimensions with a homogeneous laser amplification medium, which remains stable and retains a high gain even when large quantities of electrical energy are deposited into it.

An important class of high-power lasers is that featuring a transverse-discharge convection cooled geometry with continuous optical output. These devices are designed such that the gas flow, current flow, and optical resonance are mutually orthogonal. For example, the discharge volume of the most recently constructed PIE (Photo-initiated, Impulse-enhanced, Electrically-excited) laser, capable of 30 kW of continuous output power, has dimensions 20 cm x 10 cm x 400 cm in the gas flow, current flow, and resonator directions, respectively. The device maintains a gas velocity of 45 m/s. This arrangement allows the gas in the entire resonator volume to be subjected to intense and homogeneous electrical power deposition and subsequent optical energy extraction, while spending only a few milliseconds in the discharge. A key aspect of this approach is that discharge instabilities are transported out of the discharge before they can develop into arcs.

The PIE discharge technology is particularly well-suited for transversely excited lasers. Sub-microsecond pulses on the order of 10 kV create a non-self-sustained plasma and thereby provides a medium which can be optimised for continuous deposition of energy into the CO₂ laser medium. A dc sustaining current with a potential of a few kV is then adequate for vibrational pumping. A benefit of the independent optimisation of two aspects of the glow discharge is that the PIE discharge is exceptionally stable and uniform. Further improvement of this technology has come about through the development of burst-mode excitation. This approach circumvents thermal instabilities in the laser plasma by effectively switching the current through the discharge off and on before the instability growth time is exceeded. In this manner, the average power of the PIE laser has been more than doubled.¹

While the PIE discharge has been demonstrated to be highly effective in producing a uniform, stable amplification medium for cw laser operation, the implications of some aspects of its dynamic behaviour for optimising laser operation have not been investigated. Among

these are the influence of the large periodic variations in E/N on the plasma chemistry and the effect this has on the potential drops in different regions of the discharge.

The plasma-chemical processes of recombination and attachment, the latter incidentally resulting in reduced stability,² are of particular significance in the PIE discharge. This aspect follows from the repetitive creation of a transient high electron density regime with a high E/N during the pulses. Electrons recombine with positive ions during the inter-pulse period and are also attached by electronegative neutral species. Typical reactions and reaction rates chosen from those compiled by Smith *et al.*³ for illustration are shown in Table II.1. Other chemical reactions⁴ also occur which affect the proportions of the various chemical species present in the discharge. The principal result of the attachment and recombination processes is to cause the electron density to decay rapidly after the pulse. Assuming that the plasma is weakly ionised, so that the reaction rates a of attachment and c of recombination are limited by electron density (and assuming positive ion density $n_i = n_e = n$, which is not valid for highly attaching species), a simple differential equation results:

$$dn/dt = -c n^2 - a n \quad (1)$$

with the initial condition $n(t) = n_0$. This has the solution

$$n(t) = \frac{a n_0 e^{-at}}{a + c n_0 (1 - e^{-at})} \quad (2)$$

In the actual discharge, reaction rates (which are derived from energy-dependent cross sections) vary too greatly during the pulse period for these equations to be useful except as heuristic devices. Also not considered in these equations are the changes in the chemical composition of the discharge which occur during the pulse. High electron energies favour ionisation and detachment reactions, among others, over recombination and attachment (evident from the cross-sections in Fig. 1 of Labun *et al.*⁵). The above equations indicate that the decay of electron density proceeds exponentially at different rates, depending on the relative dominance of attachment and recombination reactions in the plasma.

Higher fields are necessary in the positive column of attaching gases to conduct current, since fewer free electrons remain. A similar effect occurs in the anode fall region. It

Table II.1 Typical recombination and attachment reactions in CO₂ laser discharges.

<u>recombination</u>	<u>k (cm³ s⁻¹)</u>
$N_2^+ + e^- \rightarrow 2 N$	2.8×10^{-7}
$CO_2^+ + e^- \rightarrow CO + O$	6×10^{-8}
<u>attachment</u>	
$CO_2 + e^- \rightarrow CO + O^-$	5×10^{-13}
$CO + e^- \rightarrow C + O^-$	3×10^{-14}

has been calculated^{3,4} that negative ion concentrations, especially CO_2^- , can approach and exceed that of free electrons in self-sustained discharges in favourable E/N regimes. The potential drop in the cathode region is not much affected by negative ions, since they are not likely to be created there in large quantity by the high energy electrons. Nor do they drift into the region from elsewhere because of the repulsive field.

Several factors combine to produce anode falls in PIE discharges which have potential drops of approximately the same magnitude as the cathode fall. The anode fall arises from the space charge created by the highly mobile electrons as they accelerate towards the anode. In the process, they ionise enough molecules to balance the flow of ions into the cathode region. In brief treatments of the anode fall region, in which only planar anodes are discussed, V_a is said to be on the order of the ionisation potential of the gas, typically a few tens of volts.^{6,7} In fact, V_a as measured in PIE discharges is on the order of a few hundreds of volts. Francis⁸ notes three factors relevant to the PIE discharge which affect the anode fall, all of which tend to increase it: a small anode requires a large anode fall, high current density increases the anode fall and gives rise to intensely bright anode "spots" (observed in all PIE discharges), and the introduction of electronegative gases causes a large increase in the anode fall of up to hundreds of volts. This last effect is due to the low mobility of negative ions mentioned above, which prevents them from acquiring the energy necessary to ionise neutral molecules. The electrons must therefore ionise correspondingly more molecules each. As well, a lower free electron density implies that a higher drift velocity is necessary to produce a given current. These two factors result in an increase in V_a . Since the negative ion density is susceptible to changes in the dynamic processes in the discharge, it is possible in principle to reduce V_a by altering the parameters of the pulse cycle.

The cathode fall V_c is also subject to geometric and current density factors given by Francis.⁸ A strong electric field extends approximately 0.5 mm from the cathode surface and accelerates electrons emitted by the cathode by the processes of ionic bombardment and the photoelectric effect. These electrons then undergo high-energy (tens of eV) ionising collisions

with neutrals, which create an avalanche. The process ultimately results in an electron current equal to the ion current incident on the cathode.⁶

Previous research has shown that V_c in dc glow discharges can be reduced by choosing materials which most readily emit secondary electrons or by employing hollow-cathode geometries,⁹ especially with transverse magnetic fields.^{10,11,12} The pin geometry currently used in PIE discharges actually results in a large V_c , since it concentrates current. It would thus be advantageous to determine which electrode geometry minimises V_c and thereby enhances the overall system efficiency. One technique for economically testing various geometries is to place larger pins manufactured with these geometries over the existing pins on the electrode blocks. In this case a direct measurement of V_c for a variety of pin geometries would be preferable to indirect measures such as V-I characteristics. Variable quantities such as the resistance of the ballast network and the separation between cathode and anode could be isolated from the results obtained. It is therefore of interest to attempt a direct measurement of V_c under various discharge conditions in order to determine a control value for V_c .

The sensitivity of the electric field in various regions of the PIE discharge to the dynamic behaviour of the plasma may merit close investigation, particularly if the effects on laser performance prove significant. This investigation thus seeks to ascertain the importance of the effects of certain aspects of the PIE discharge's dynamic behaviour. These include the high-voltage pulse amplitude, its repetition frequency, and the magnitude of the sustaining dc potential on the cathode fall potential, the electric field in the positive column, and the anode fall potential.

B. Experiment

PIE discharge apparatus

The experiments reported in this paper were conducted in a discharge chamber which was part of a modified transverse discharge laser (Fig. II.1). The principal modification was

GAS TRANSPORT AND EXCITATION SYSTEM

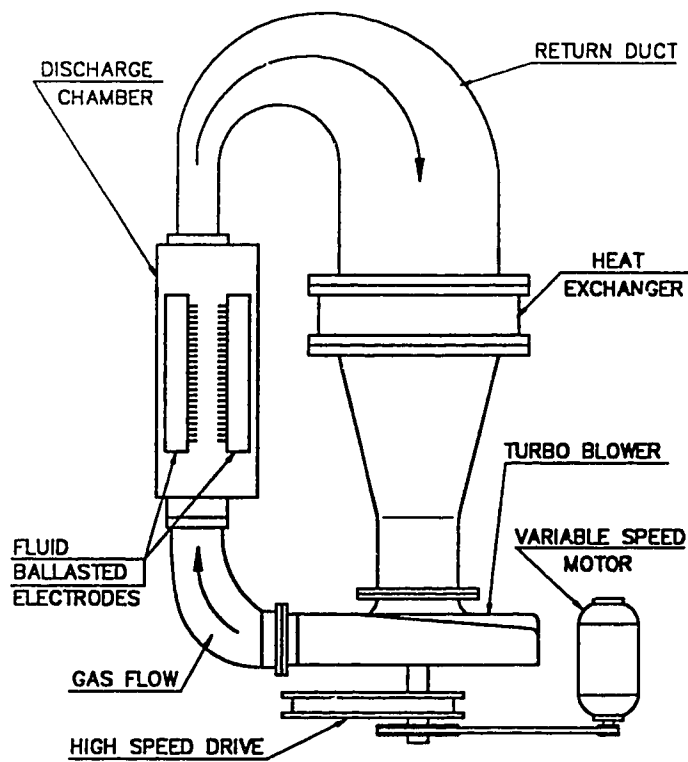


Fig. II.1 Configuration of the discharge system, based on a transverse discharge laser.

the replacement of the optical assemblies by rectangular plexiglas viewports to allow observation of the entire discharge and the introduction of a movable electrostatic probe into the centre of the discharge volume. A centrifugal compressor forced an appropriate CO₂ gas mixture through a heat exchanger and into the rectangular discharge chamber at 30 m/s.

The gas mixture used throughout this experiment (He:N₂:CO₂:CO = 39:8:1.5:1.5 Torr) had been found earlier to give satisfactory laser amplification in PIE lasers. The role of the added CO was to reduce the tendency of the equilibrium CO₂ concentration in the gas to be lowered excessively through dissociation into CO and O. H₂ is sometimes added to discharges to remove O from the discharge, but this practice is not followed in PIE discharges, which add CO as stated above.

It was intended that this device be used as a "test bed" for modifications of the technology used in larger PIE systems. Consequently, electrode modules designed for these bigger lasers were installed, similar to those described by Seguin *et al.*¹³ These modules featured solid delrin blocks provided with internal fluid-ballasting and cooling for an 27 cm x 21 cm array of 187 equally-spaced stainless steel sub-electrode pins. The separation of the tips of the anode pins from the tips of the cathode pins was 9.0 cm, while the exposed pin length was 2.5 cm.

The schematic diagram in Fig. II. 2 indicates that the PIE discharge circuit comprised two independent excitation circuits, one featuring a hydrogen thyratron switch to provide rapid discharging of a high-voltage capacitor through a step-up transformer, and the other a regulated dc power supply. Both circuits are necessary in the three-step process by which excitation of the inter-electrode volume is accomplished. Initially, a multi-kilovolt electrical pulse rising on the order of 100 GV/s with a full-width at half-maximum of 0.2 μ s initiates a corona breakdown on the pins. This process photoionises the volume via ultraviolet (UV) radiation. Free electrons are accelerated by the same pulse and collide with neutral molecules, creating a brief, efficient ionisation avalanche. The high-frequency, repetitive application of these pulses maintains the conductivity of plasma at a level necessary to support a dc

PIE Laser Discharge System

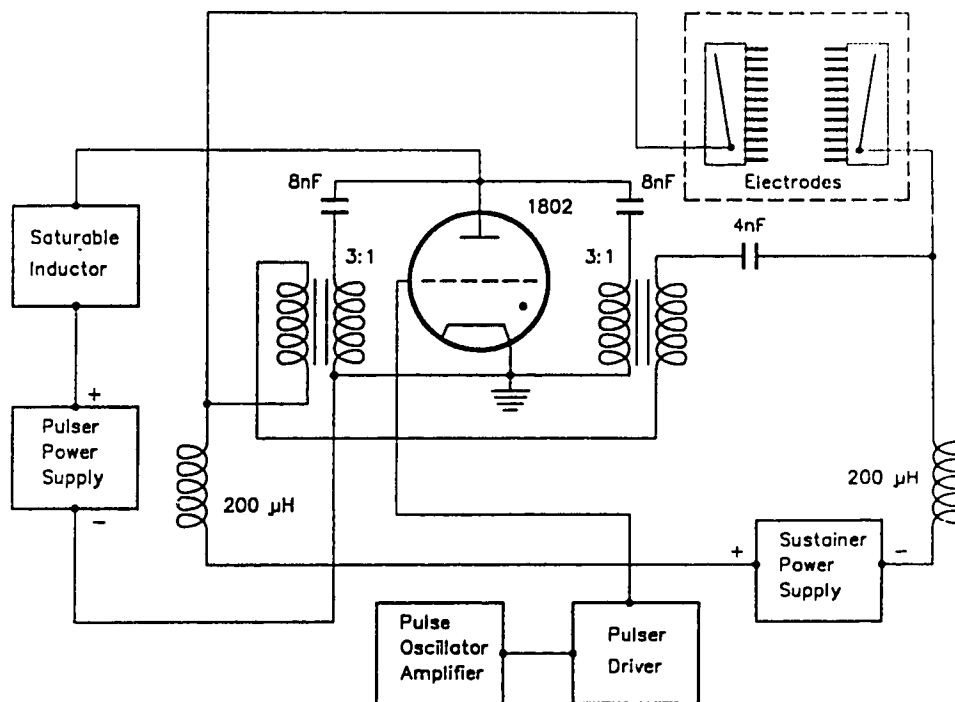


Fig. II.2 Schematic of the PIE discharge circuit.

discharge. A dc potential then sustains a high current in the discharge. This dc pumping generally accounts for over 99% of the power deposition in an optimised discharge in a large laser.¹³ In the experiments reported herein, the pulse power was occasionally of the same order as the dc power. This was not therefore representative of normal operating conditions.

As the gas is transported through the discharge, its temperature and hence its conductivity rise. The spatial temperature profile cannot be accurately computed on the basis of equilibrium thermodynamics since significant quantities of power are deposited in internal degrees of freedom of the CO₂ molecules. These molecules then relax on millisecond time scales, comparable to the transit time of the gas in the discharge region. Nevertheless, the ballast resistance ratio in the electrode blocks was graded in the flow direction to approximately accommodate increasing temperature. This resulted in a fairly uniform current density over the entire discharge volume.

Electrostatic probe measurements

The probe consisted of a bare copper wire of diameter 0.7 mm housed in a quartz sleeve and extended into the plasma with only a small length (~2 mm) at the end exposed (Fig. II.3). It was mounted eccentrically on a rotating plate and could itself be rotated and translated along its length into and out of the discharge. With three degrees of freedom, the probe tip could be positioned anywhere within the discharge chamber, as well as contacting the electrode pins. Since the PIE discharge imposed pulses of several kV on the probe, a high-voltage low-pass filter was inserted between the probe and the AVO mechanical voltmeter. Thus, a steady potential was recorded by the voltmeter.

During the experiments reported herein, the probe was positioned at specific distances between the cathode and anode. The average electric field between the electrodes was obtained by measurements centred on the mid-plane 4.0 ± 0.3 cm apart, far from the high field regions near the electrodes. Measurement of the cathode and anode falls was made by subtracting the potential measured 1.0 ± 0.5 mm away from the electrode surface from the potential

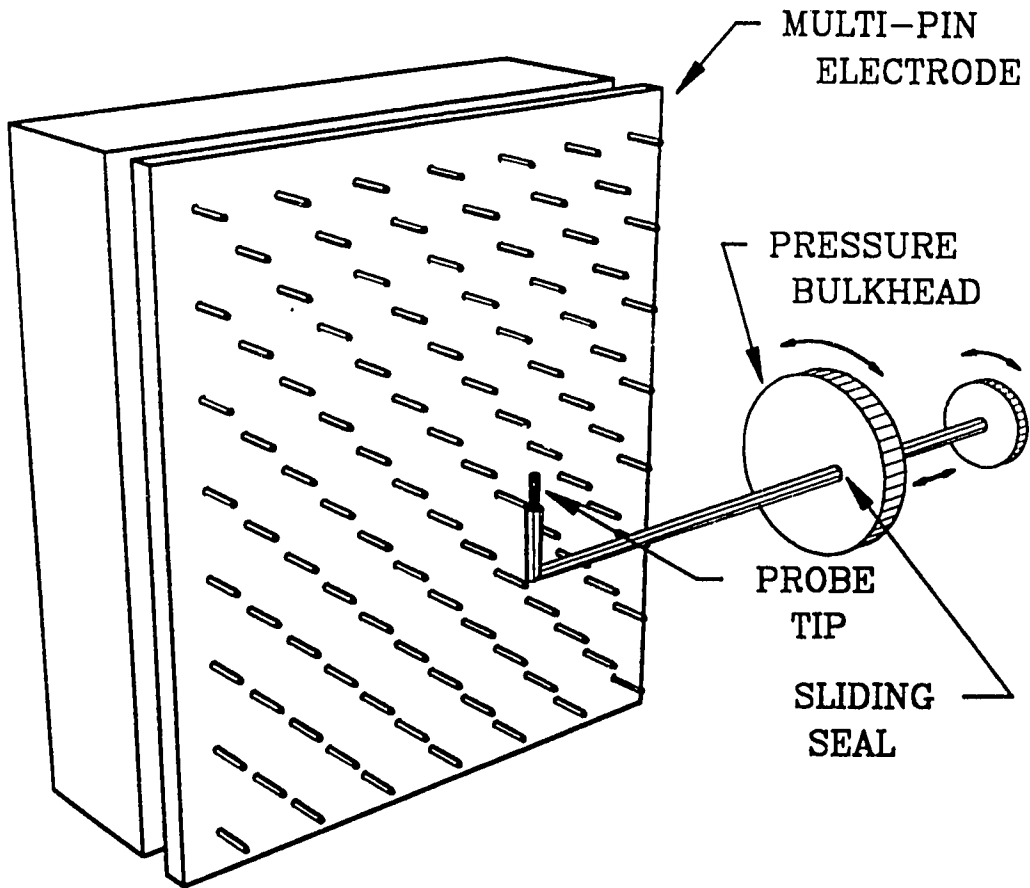


Fig. II.3 The configuration of the probe in the discharge, illustrating the three degrees of freedom.

measured when the probe contacted the electrode. The probe first contacted the pin at or near the tip and was then drawn slightly away from the pin. Unfortunately, the probe's position relative to the the pin tip could not be precisely reproduced, due to the slightly jerky motion of the probe. As a result, the probe shadowed the pin tip from the discharge to varying degrees, as well as being separated from it by the variable distance given above. This no doubt accounts for much of the scatter in the data for V_a and V_c , as discussed in the following section. The presence of this scatter due to slight variations in the probe's position emphasises that the length scale of interest is on the order of a millimeter.

Although an unbiased plasma probe provides the most straightforward means of measuring potential drops in a glow discharge, the potential indicated by the probe is not that of the plasma in which it is immersed. This is a consequence of the fact that charged species diffuse to the surface of such a probe at rates proportional to their mobility (which is inversely proportional to their mass). If no bias potential is applied to the probe, it will float to a negative potential with respect to the plasma, repelling free electrons sufficiently to result in a balanced electron and ion current. Provided that this negative potential does not vary as the probe is moved from one position in the plasma to another, the probe's potential drop between two positions will equal the plasma's potential drop. Only if the discharge possesses spatially uniform properties will this be generally the case. In this experiment, this condition is only fully satisfied in the positive column, where the electric field strength is relatively constant over dimensions of a few millimetres.

Loeb¹⁴ provides an extensive discussion of the pitfalls of probe measurements, especially as used to determine electron energy distributions in low pressure discharges. Included among the physical effects which can falsify probe potential measurements is the presence of negative ions, which affects the current to the probe. This would tend to cast doubt on simple theories of probe current which assume the negative carriers are electrons and take advantage of their high mobility. Gottscho¹⁵ has investigated the sheaths in low-frequency (dc, 50 kHz, and 10 MHz) rf discharges in attaching and non-attaching gases.

He determined that the negative ions influence the dynamic behaviour of the sheath only in the middle frequency range, well below their plasma frequency (in his case, the ion plasma frequency $f_i \sim 3$ MHz, while in the present case, $f_i > 30$ MHz). At higher frequencies the ions are relatively immobile and react to the average conditions in the discharge. In the experiment reported here, then, the ions are fairly insensitive to the actual PIE pulses, reacting only to the resultant fluctuations in the electron density which persist somewhat longer. Indeed, for the present investigation where only floating potentials are recorded and potential differences are measured in hundreds of volts, the possible errors due to negative ions which Loeb identifies (typically on the order of a few volts) may be safely neglected. Indeed, the analysis here does not consider the effect of negative ions on probe values.

The large impulses may also be expected to affect the probe potential as they give rise to high energy electrons, resulting in larger negative probe potentials. This and other similar effects such as secondary ionisation by ions bombarding the probe and ionisation in the probe sheath may be neglected as small and are in any event negated when potentials are subtracted to determine the field strength.

More significant difficulties arise due to high pressure effects. Two complicating factors mentioned by Loeb are changes in potential over the dimensions of the probe, certainly a factor near the electrodes, and the presence of probe sheaths. The effect of a potential gradient on the probe's potential, and the corollary effect of the probe's equipotential surface on the discharge, are discussed in the analysis of the cathode fall measurements. The probe sheath is present for all measurements, however, and so is considered here.

A sheath forms around an unbiased probe in which there are fewer electrons than positive ions (negative ions are neglected). The width of the sheath is related to the Debye length

$$\lambda_D = (\epsilon_0 k T_e / n e^2)^{0.5} \quad (3)$$

where n is the charge density in the plasma far from the probe, T_e is the electron

temperature, ϵ_0 is the permittivity of free space, e is the elementary electric charge, and k is Boltzmann's constant. As the pressure is increased, the mean free path λ can be reduced to values much less than the probe diameter. The ionisation near the probe is severely reduced as electrons and ions near the probe are more likely to collide with it. Thus, high pressures and low bulk ionisation densities both imply large probe sheaths. As well, a large probe diameter relative to λ results in a relatively slow ion drift velocity toward the probe. So at sufficiently high pressures, the gas flow velocity of a convection laser is comparable to drift velocity near the probe. This effect could be significant if comparisons were made of probe potentials under different gas density or flow conditions.

Smy has published a review of analyses of spherical probe sheaths in high-pressure plasmas as they pertain to Langmuir probe measurements.¹⁶ Since the unbiased plasma probe is merely a special case of Langmuir probe, many of his results are applicable to the measurements taken in this experiment. In particular, the ion current to the probe can be characterised as falling into three distinct sheath regimes in high-pressure plasmas, as determined by three dimensionless parameters. These parameters are the normalised probe radius $a = \lambda_D/r_p$, the normalised sheath potential $\chi = eV_p/kT_e$, and the electric Reynolds number $R_e = 2v_f r_p e/kT_e$. Here V_p is the probe-to-plasma potential, v_f is the gas flow velocity, and r_p is the probe radius. In discharges for which $R_e a^2 \chi^2 \ll 1$, known as the diffusion-convection regime, the sheath is thin compared to the probe radius and sheath effects can be ignored. Two thick-sheath cases (for which $R_e a^2 \chi^2 \gg 1$) can be identified: sheath-convection ($R_e a^2 < 1$), in which all ions convected into the sheath are drawn to the probe by the electric field, and E field-convection ($R_e a^2 > 1$), in which the electric field is only strong enough to draw a fraction of the ions convected into the sheath to the probe. No measurements of probe current were attempted in the experiments reported herein, but, as will be shown, the behaviour of the probe sheath is of significance to the results.

C. Results and discussion

Three parameters affecting the performance of PIE lasers were varied over a wide range of values in order to determine the nature of their effects and whether these could be optimised. The three parameters were the dc current, the power deposition of the ionisation pulses, and the pulse frequency. They were examined in the ranges 0.5-4.0 A for the dc current I , 144-2850 W for the pulser power P_{PIE} (as measured by the high voltage power supply to the pulse transformer), and 5-14 kHz for the pulse frequency f_p . The range of P_{PIE} significantly exceeded that encountered in useful laser discharges, which in this system had been typically less than 500 W. Experience has shown that much larger lasers make more effective use of these pulses than small ones. By way of an example, Nikumb *et al.*¹³ obtained optimal small signal gain at $P_{PIE} = 300$ W in a laser consisting of 12 pairs of modules of the same design as the pair in this study. Efficient design of the overall excitation system, therefore, can result in substantial power savings. A corollary is that the actual values of extensive parameters such as power deposition cited in this investigation should not be simply extrapolated to laser systems of different scales.

Physical insight into the processes active in the discharge in its different regions can be obtained by examining the effects of variation of the three parameters I , P_{PIE} , and f_p . The dc current I , for instance: affects the surface area of the negative glow on the cathode pins; determines, along with the discharge electrical conductivity σ , the strength of the concentrating field near the anode; and also fixes the rate of power deposition into the laser amplification medium. The following discussion is accordingly divided into three sections according to region, whether the cathode region, the positive column, or the anode region. Within each of these regions the effects of all three parameters are discussed.

The cathode fall region

Measurements of the cathode fall potential V_c in a one-dimensional normal glow discharge would be expected to yield a constant value close to 190 V. This figure is based

upon the values collected by von Engel.⁶ In fact, probe potentials recorded 1 mm from the pin tips varied greatly, apparently displaying sensitivity to uncontrollable factors (for example, the potentials measured for $I=2.0$ A in Fig. II.4). Since many data points, each obtained during different runs, were available, statistical analysis was considered appropriate. A fit to a polynomial of order two was obtained using the IMSL FORTRAN subroutine library. The domain of Fig. II.4 was divided into several segments and the mean and variance of the data within each segment was used to obtain a weighted fit. Although no dependence on f_p is evident, the value of V_c obtained through the fit to data measured by the probe does vary greatly over a wide range of ionisation and current densities (Fig. II.5), from a low of 50 V to a high of approximately 300 V. This variability is due in part to an actual change in V_c and in part to the capture of ions by the probe sheath. When the potentials in Fig. II.5 are interpreted in light of these two effects, reliable values of V_c may be discerned.

The probe sheath's effects on the ion current in the vicinity of the probe may be deduced by estimating the values of the dimensionless parameters α , χ , and R_e defined previously. Most of the factors involved in this estimate in this experiment were either fixed, such as r_p , or did not change greatly, such as V_p . The notable exception was n , which was not measured. Previous experimenters have, however, made measurements of n which indicate the range of values possible. Sedgwick⁹, performing tests on a self-sustained, transverse flow discharge, recorded a maximum n of $7 \times 10^{11} \text{ cm}^{-3}$ with a gas flow of 35 m/s at low pressure ($\text{CO}_2:\text{N}_2:\text{He} = 4:4:6$ Torr). Seguin *et al.* measured n in a 10.5 litre coaxial magnetised PIE discharge with a Langmuir probe.¹⁷ They found in a 25 Torr gas mixture ($\text{CO}_2:\text{N}_2:\text{He} = 1:4:20$) that the self-sustained discharge had $n = 4.4 \times 10^{11} \text{ cm}^{-3}$, while with 1000 W of pulser power this was raised by a factor of 100. Results obtained in a different device by Willis¹⁸ indicate that the electron density was not reduced when a dc current was imposed on the discharge, as reported by Seguin *et al.*¹⁷, but that the pulser had been loaded by the dc circuit and so was unable to ionise effectively. Observations of the impulse amplitude in the apparatus used in the present work revealed no dc loading effect. It seems, then, that n is a

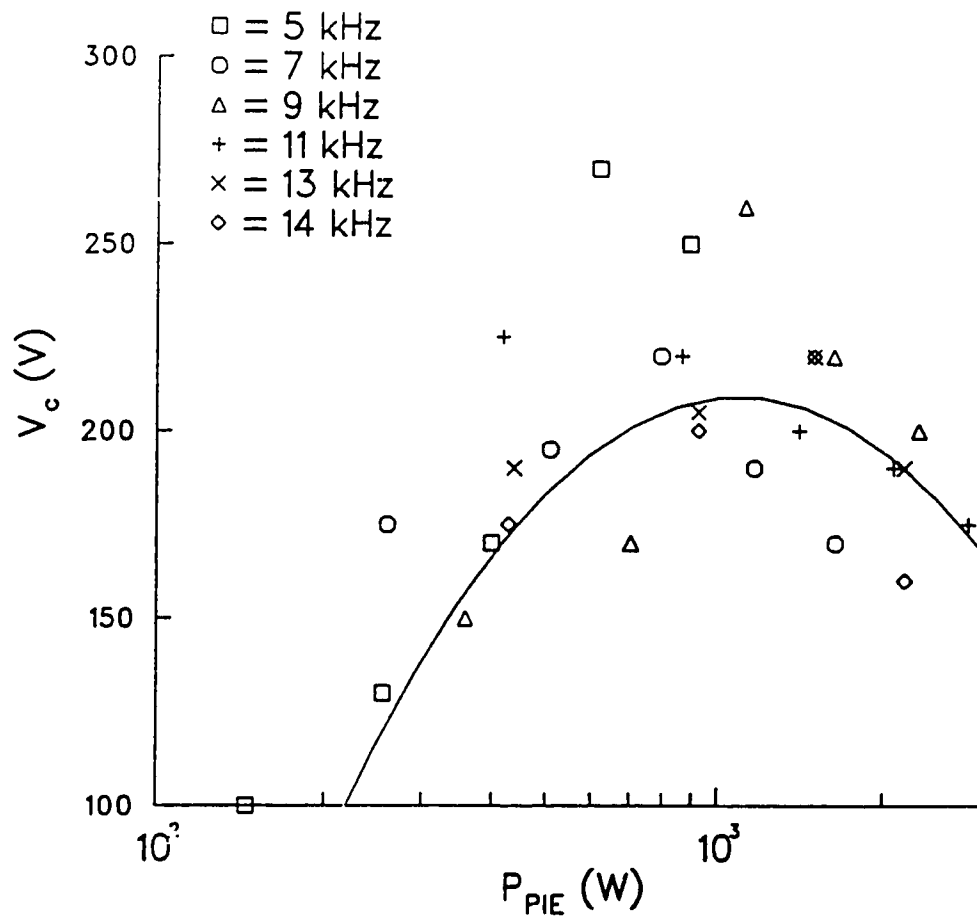


Fig. II.4 Probe measurements of V_c for $I=2.0$ A and various pulser frequencies, with a quadratic fit.

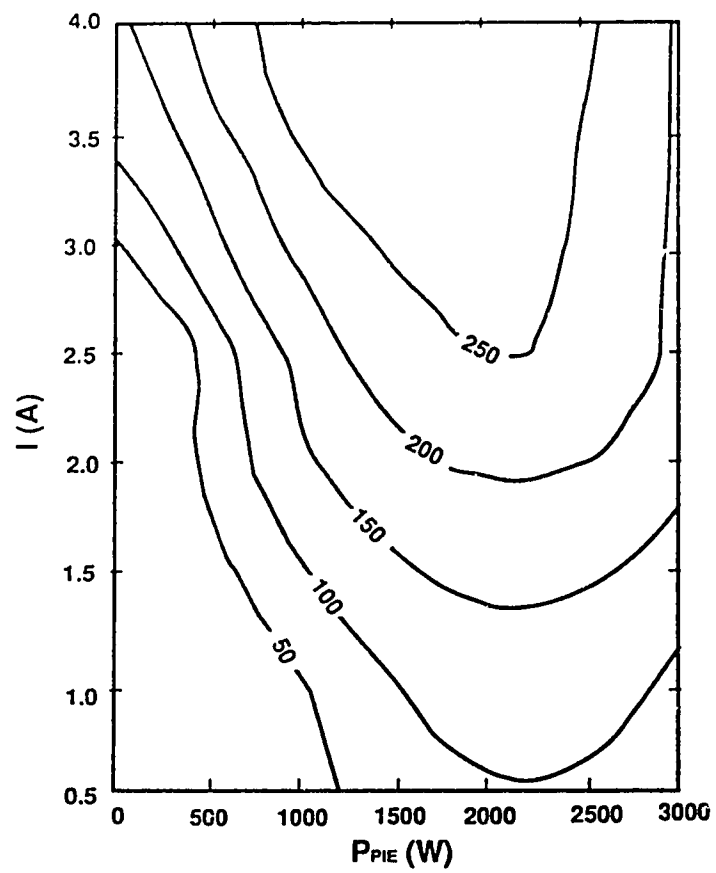


Fig. II.5 Contours of fitted V_c values based on probe measurement. Only the contours for $P_{PIE} > 1$ kW are not affected by the probe sheath.

function of P_{PIE} but not of I .

The probe-to-plasma potential V_p near the cathode in a PIE discharge is not simply related to that of a dc plasma. The large negative pulses applied to the cathode create a population of high energy electrons. Thus, V_p is driven to a larger negative value near the cathode than in the central region of the discharge volume where the pulses are attenuated. This effect must increase as higher pulser voltages are applied. Seguin¹⁷ determined a sheath potential of -40 V far from the electrodes, which suggests that a slightly greater magnitude sheath potential may be expected near the cathode.

Assuming, for the purpose of illustration, that Seguin *et al.*'s values of n are valid for the present work, the self-sustained discharge's values of the dimensionless parameters were $a = 4 \times 10^{-3}$, $\chi = 1.3 \times 10^3$, and $R_e = 0.75$. Thus, in the self-sustained discharge, $R_e a^2 \chi^2 = 20$ and $R_e a^2 = 1.2 \times 10^{-5}$. The thick probe sheath is therefore a sink for ions. In the case of the non-self-sustained discharge with 1000 W of pulser power, $R_e a^2 \chi^2 = 0.2$, implying a thin sheath. It would appear, then, that in the probe measurements made in these tests both thin and thick sheath considerations applied, with thin sheaths characteristic of highly ionised glows and thick sheaths which absorb all incident ions characteristic of slightly ionised glows.

In addition to the effect of the pulser on the probe's measurement of V_c , there was also a direct effect on V_c due to the geometry of the cathode, which will now be considered.

The value of V_c given above is a constant only for a normal glow discharge. This condition prevails when the current density at the cathode does not exceed some critical value. If enough surface exists on the cathode for emitting current, the region of the glow will spread so as to maintain the current density below that value. The glow in the PIE discharge was, however, not always normal. Since the cathode was in the form of 187 individually ballasted pins, and the area at the tip of the pin was very restricted, the glow region extended progressively further down the pin shaft to acquire more surface area as the current in the discharge increased. However, the length of a flux path from the pin tip to the anode was much shorter than the length of such a path from midway down the pin shaft. As well, the

region of ionisation emanated from the pin tip. Thus, there was an interaction between the degree of ionisation and the current drawn from the pin which determined the current density and thus V_c . In Fig. II.6(a), a moderately ionised discharge can be seen to concentrate current on the pin tip, while from Fig. II.6(b) a distributed current results from a highly ionised discharge. In the moderately ionised case, not only is the high cathode current density likely to result in an abnormal glow, but the electric field near the cathode will be particularly strong because of the high current density. The highly ionised case is characterised by lower current densities both at the tip of the electrode and in the volume, as ionisation results in more high-conductivity flux paths being open to the current. These effects resulted in lower measured values of V_c for the highly ionised glow discharge.

The variation in the measured value of V_c in Fig. II.5 can be seen to result from the interplay between I and P_{PIE} . For low values of P_{PIE} and I , the current-emitting region of the cathode was limited to the pin tips, while the probe sheath radius was approximately equal to the pin radius. In the act of measurement, the probe was about 1 mm from the pin tip, between it and the anode. Thus, the probe, by capturing the ions that would otherwise have fallen upon the pin tip and sustained the discharge, extinguished the discharge on the pin. The probe then assumed a potential which would provide the current drawn by the probe circuit (approximately 300 μ A, 10% of the pin current when a total of 0.5 A was drawn by the discharge). This resulted in some value between the cathode potential and the potential in the plasma a few millimetres from the cathode. As I increased with P_{PIE} kept low, the probe continued to extinguish the glow near the pin and thus the measured value of V_c rose only slowly. For very slightly preionised discharges from pins, then, the probe's thick sheath precluded a true measure of V_c .

For intermediate values of P_{PIE} , the probe entered the thin-sheath regime and no longer extinguished the discharge on the pin tip. While the pin tip was still highly favoured for discharge current, the progressively higher conductivity which accompanies increased P_{PIE} allowed current emission from the pin shaft. Since the electric field along the flux lines

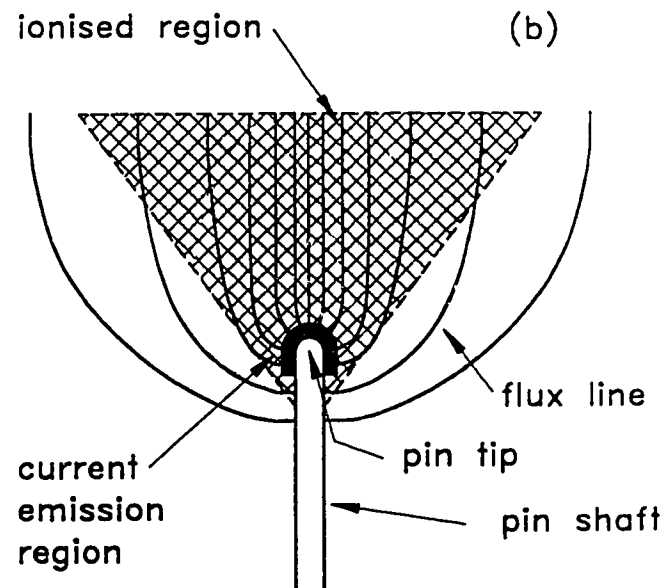
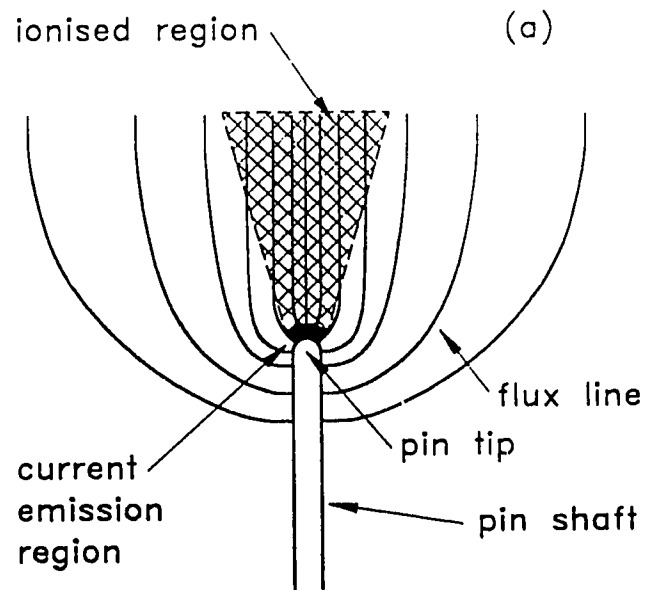


Fig. II.6 The conductive region and flux lines for a pin cathode. In (a), P_{PIE} is small, while in (b), P_{PIE} is large.

emanating from the shaft was weaker than that emitted from the tip, the density of the current drawn from the shaft tended to be less than that drawn from the tip. The normal glow, however, requires a minimum current density in order to be sustained. Thus, in order to draw a large current from the pin, which entailed emission of current from much of its surface, it was necessary to impose such a large potential on the discharge that it entered the abnormal glow at the tip in order to support a normal glow on the shaft of the cathode pin. Since the tip was where the probe measurement is taken, the abnormal glow potential was recorded at large currents for intermediately ionised discharges.

Finally, at high pulser powers (in Fig. II.5, $P_{PIE} > 2000$ W), the high degree of uniform ionisation permitted the current to be conducted through the entire volume. Unlike the intermediate ionisation case mentioned in the previous paragraph, though, this current emission from the pin shaft did not require an abnormal glow at the pin tip for the currents drawn in this investigation. As will be shown, the total positive column potential was low for this high degree of ionisation and thus the proportional increase to this potential necessary to draw current from part way down the pin shaft was too small in absolute terms to drive the pin tip into the abnormal glow. Thus, in this region, high current operation led to a stable value of V_c at approximately the value predicted by von Engel.

While there was relatively close agreement between the predicted and measured values of V_c at higher discharge currents, the measured values of V_c for currents below 1.0-1.5 A were substantially less than predicted. This may be attributed to the fact that the probe drew a finite current, regardless of its sheath radius, which amounted to a loading effect. Since the cathode was fixed at ground potential and the probe measured all potentials relative to ground, it would tend to "pull" potentials toward more negative values. Thus, when the probe drew enough current to perturb the local discharge (as it would for small I), it measured a value of V_c below the actual value.

In summary, the electrostatic probe measurements of cathode fall, when suitably averaged, varied with discharge current and ionisation. Qualitative consideration of the effects

of ionisation, cathode pin geometry, and the finite impedance of the probe leads to the conclusion that only the high current measurements of V_c with $P_{PIE} > 1000$ W yielded accurate results. These results suggest that with only moderate degrees of ionisation, similar to those used in actual laser discharges, the abnormal glow regime was encountered at currents sufficiently high to entail current emission from the shafts of the cathode pins. In cases of even higher ionisation, in this system $P_{PIE} > 2000$ W, the abnormal glow regime was not encountered for practical currents since the highly ionised gas did not require large electric fields.

This attempt at a direct measurement of V_c has also revealed that certain characteristics of electrostatic probes, notably the sheath, limit the value of this approach so severely as to make it not worthwhile. The favoured regime for laser operation, with only a moderately ionised gas, is precisely the one in which the probe most perturbs the discharge, rendering the measurements valueless. In addition, some cathode geometries may be more affected by the presence of a probe than others, making probe-based comparisons of V_c dubious, at best. It would seem that non-invasive methods of *in situ* cathode fall measurement are necessary, such as laser optogalvanometry^{19,20} or spectroscopic measurements.²¹

E/p in the positive column

While the measurement of E_{pc}/p was the most straightforward probe measurement and the data accordingly shows little scatter, its dependence on P_{PIE} and f_p implies a complicated interaction of the plasma composition and discharge conditions. The behaviour of E_{pc}/p for $I = 2.0$ A as shown in Fig. II.7 was typical of that for all values of I , although at higher currents the discharge could not be maintained over such a wide parameter range due to power supply limitations.

Figure II.7 shows the complex dependence of E_{pc}/p on P_{PIE} . Three observations may be made in regard to Fig. II.7. First, for a wide range of values of P_{PIE} above 300 W, the slope of E_{pc}/p vs. P_{PIE} was extremely steep. Second, there was an inflection in the E_{pc}/p

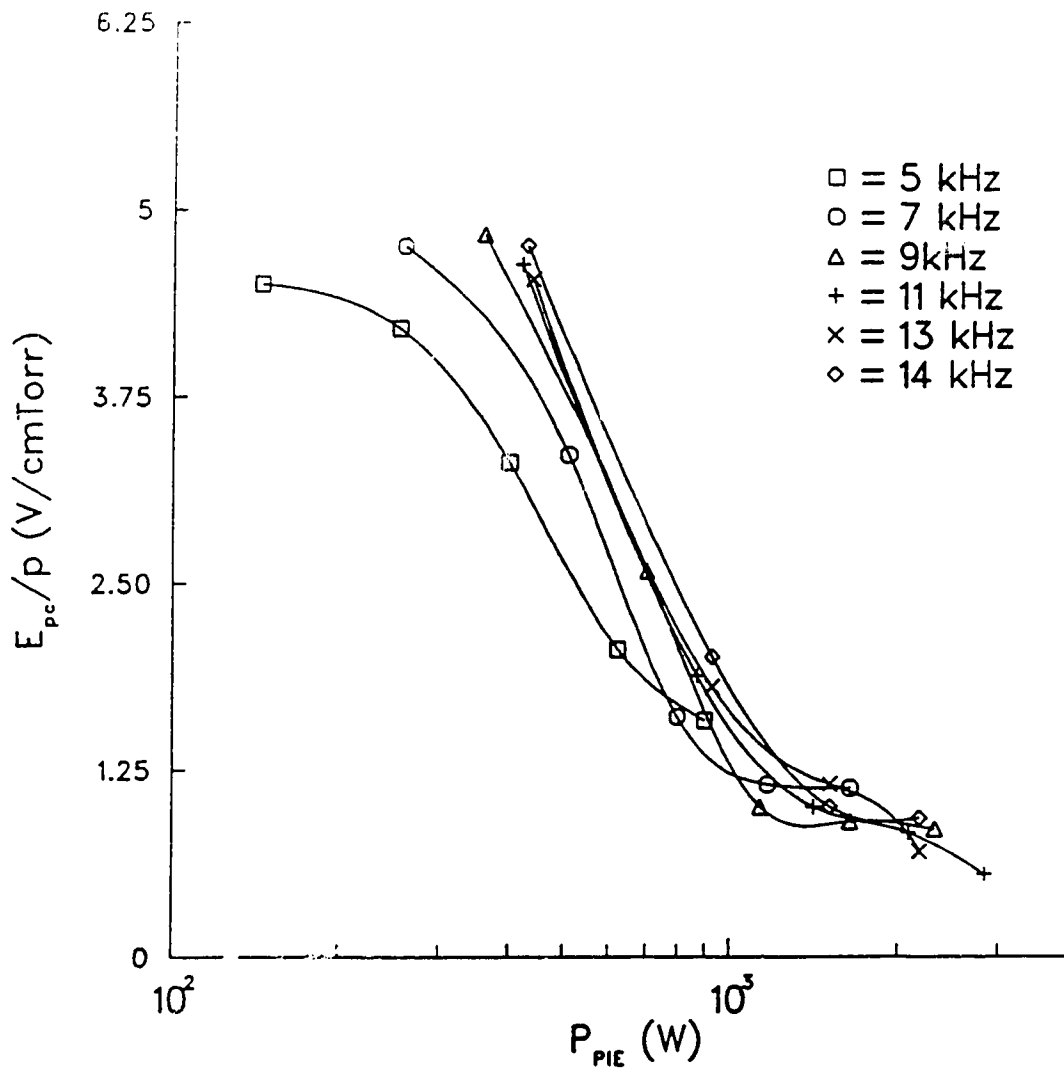


Fig. II.7 Variation in E_{pc}/p with pulser power P_{PIE} . The data points represent 1 kV increments to the pulser input potential starting from 2 kV.

trend, such that for sufficiently large P_{PIE} , E_{pc}/p declined much more gradually. Third, E_{pc}/p was not uniquely determined by P_{PIE} , as was V_c (at constant I), but rather by some other function of f_p and impulse potential (recall that $P_{PIE} \propto f_p \times \text{input potential}$). In Fig. II.7, the data points at the tops of the curves represent pulser power supply input potentials of 2 kV, with the following points on each curve corresponding to 3 kV, 4 kV, and so on. It will be argued here in conjunction with Fig. II.8 that the steep slope is due to attachment and recombination, that beyond the inflection recombination dominates, and that the third effect is due to the nonlinear decay of n .

Comparison of the variation in E_{pc}/p in a non-attaching gas (He:N₂ = 39:8 Torr) with $I = 3.0$ A (Fig. II.8) highlights the effects due to the combined pulsed/continuous PIE discharge and those due to attaching gases derived from CO₂ and CO. The pulser power supply potentials at the top of each curve are 3 kV in all cases, increasing by 1 kV increments.

In both mixtures there is a similar frequency dependence of the E_{pc}/p vs. P_{PIE} curve. Simply put, more frequent ionisation impulses result in a higher average electron density \bar{n} and thus a lower E_{pc}/p , for a given impulse potential. That \bar{n} varies inversely with f_p at a given P_{PIE} (e.g. in Fig. II.8, consider 1 kW) is due to the fact that n decreases exponentially. Averaging the expression for n in Eq. 2 yields

$$\bar{n} = \frac{I}{e} \ln\left[1 + \frac{c n_0}{a}(1 - e^{-a/f_p})\right] \quad (4)$$

(Recall that $E_{pc}/p \propto \bar{n}^{-1}$.) It is evident that \bar{n} increases less than linearly with f_p , due to the density-dependent recombination and attachment. Although P_{PIE} is a simple product of input potential (i.e. n_0) and f_p , \bar{n} is not a function of this product and thus not of P_{PIE} .

It would appear that negative ions undergo detachment reactions during the actual PIE pulses and then reform between pulses by attachment reactions. The implication of the foregoing is that at lower pulser frequencies there is a greater density of negative ions. During the long inter-pulse period when electron and ion densities are fairly low, the attachment reaction predominates because it is first order in n (Eq. 1). The negative ions themselves are long-lived and would persist longer than the inter-pulse period, except for the pulses. The

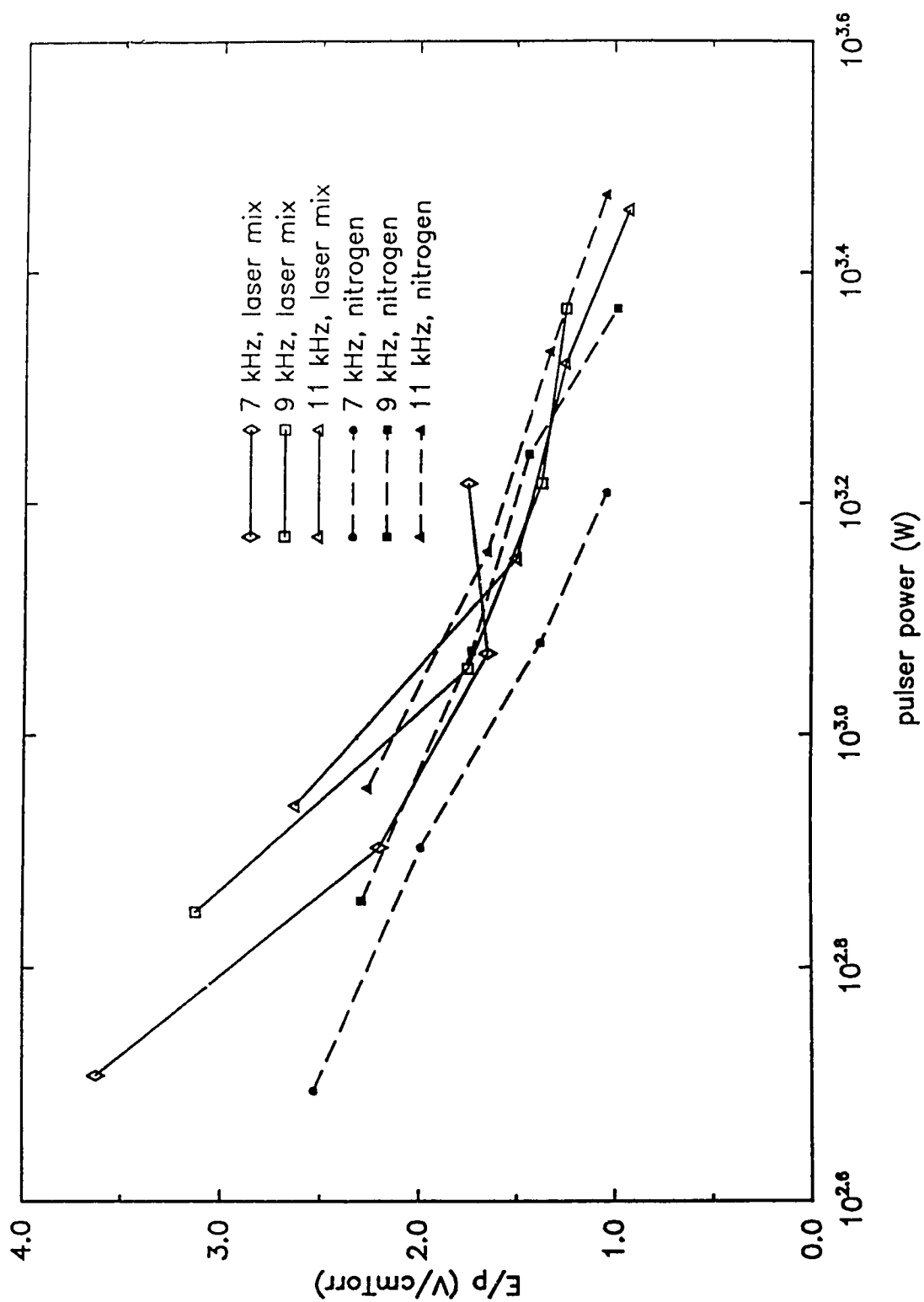


Fig. II.8 E_{pc}/p trends for a non-attaching ($\text{He}:\text{N}_2 = 39:8$ Torr) and an attaching mixture ($\text{He}:\text{N}_2:\text{CO}_2:\text{CO} = 39:8:1.5:1.5$ Torr).

overall effect of combined attachment and recombination is that the electron density decays rapidly and so accounts for the steeply sloped E_{pc}/p vs. P_{PIE} in the moderately ionised regime.

The inflection in Fig. II.8 of the E_{pc}/p vs. P_{PIE} curve for values of P_{PIE} corresponding to large pulse amplitudes in the He:N₂:CO₂:CO laser mixture is related to the action of CO₂ and CO. For progressively higher input potentials, and concomitantly higher electron impulse energies, E_{pc}/p declines at a lower rate in keeping with that of the non-attaching He:N₂ mixture. It seems likely that at this point the very high electron densities contribute more to \bar{n} than at lower input potentials and thus reduce the relative contribution of the attachment process, which is prevalent for lower electron densities. At both higher potential and higher pulse frequency, indeed, the frequency-dependence of E_{pc}/p is reduced.

The region on the E_{pc}/p vs. P_{PIE} curve beyond the inflection is never encountered in normal laser operation since the E_{pc}/p is too low, suggesting that attachment plays an important role in determining electron density in PIE lasers. As well, it would appear that f_p substantially affects the plasma composition through its influence on the concentration of attached electrons as well as the E_{pc}/p , complicating the determination of the optimal laser operating point.

The anode fall region

Consideration of Fig. II.9 and similar graphs (not reproduced here) for the entire range of I leads to the observation that there was no consistent trend of V_a with P_{PIE} . Although there was much variation with P_{PIE} , this appears to be nothing more than scatter in the data. This observation is consistent with the behaviour expected for electrodes in the absence of electrode geometry-related effects as noted earlier in the case of the cathode fall region. That is, the sheath potential is not affected by the degree of external ionisation of the positive column *per se* over a wide range of values. Rather, it is determined by the requirement that the ion drift into the cathode region be balanced by ion production in the

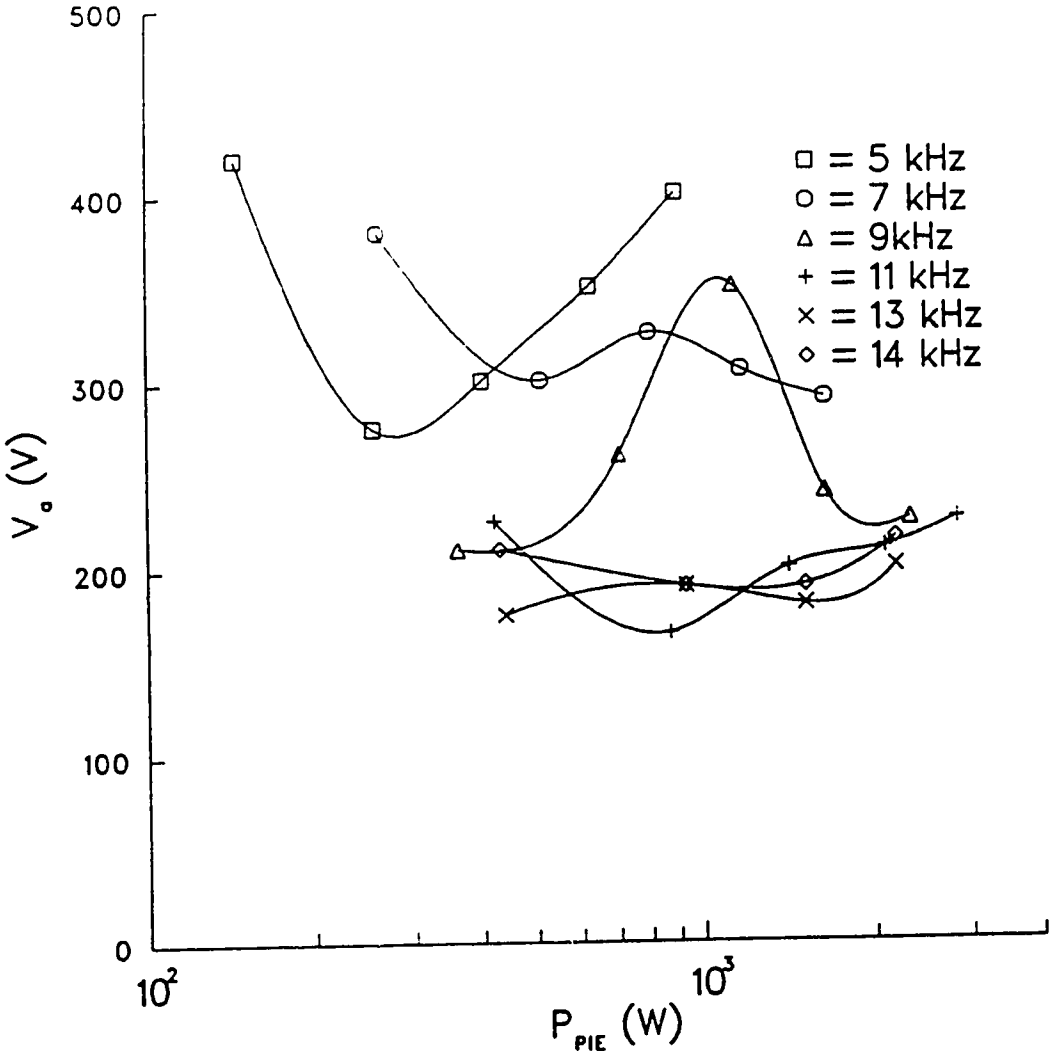


Fig. II.9 The anode fall V_a for $I = 2.0$ A. The scatter in the data is largest for low f_p .

anode region. The cathode ion sink must be balanced by the anode ion source. It is thus appropriate to speak of a single value of V_a for a range of P_{PIE} in the discharge. The average value of V_a for all P_{PIE} at a given I and f_p is thus a valid quantity and is tabulated in Table II.2 along with its standard deviation. The average standard deviation σ_{ave} for each row and column is also given, along with an overall average.

From Table II.2 it may be seen that V_a increased with I by 100-150 V due to increasing current density and that it decreased by the same amount with f_p . In addition, the degree of scatter, as measured by the standard deviation, decreased with f_p . While the increase of V_a with I is intuitive, the absence of an effect of P_{PIE} and the presence of an effect of f_p is contrary to the situation in the cathode fall region.

The frequency dependence of V_a supports the proposition that a lower frequency of ionisation impulses results in a greater proportion of negative ions in the discharge. The increase in V_a with I is probably due to an increase in the electron collection potential and thus is expected to be extended through a large space. In contrast, the influence of negative ions on the space charge which produces the anode fall is probably local to the anode sheath region.⁸ The resultant steep potential gradient would tend to increase the effect of the slight irreproducibility in the probe position on the probe potential. The presence of negative ions thus raises V_a and also the degree of scatter to be expected from V_a measurements.

The possibility of separate optimisation of the anode fall potential and the laser gain medium presents itself on the basis of this hypothesis. Conceivably, the anode fall could be reduced through a suitable choice of f_p and then the desired E_{pc}/p could be obtained by adjustment of the pulse amplitude. Since P_{PIE} is much smaller than the total discharge power, this adjustment could occur over an almost arbitrary range at no significant cost to the laser input power. As a direct result of V_a control, then, laser efficiency could be increased by up to 5% for a 2000-3000 V discharge.

Table II.2 Variation of V_a with I and f_p

$f_p \setminus I$	0.5 A	1.0 A	1.5 A	2.0 A	2.5 A	3.0 A	3.5 A	4.0 A	σ_{ave}
5 kHz	251 ± 40	291 ± 49	335 ± 58	349 ± 62	345 ± 41	363 ± 55	380 ± 53	400	51
7 kHz	251 ± 35	248 ± 44	285 ± 12	320 ± 36	350 ± 63	373 ± 14	373 ± 17	356 ± 40	33
9 kHz	218 ± 24	219 ± 27	232 ± 27	257 ± 55	280 ± 41	291 ± 46	296 ± 33	325 ± 20	34
11 kHz	128 ± 39	179 ± 32	213 ± 21	205 ± 25	233 ± 16	250 ± 18	271 ± 25	286 ± 21	25
13 kHz	121 ± 36	144 ± 24	186 ± 11	186 ± 11	205 ± 20	240 ± 16	253 ± 31	275 ± 35	23
14 kHz	116 ± 30	143 ± 29	185 ± 17	201 ± 13	213 ± 21	223 ± 12	235 ± 9	250 ± 17	19
σ_{ave}	34	34	24	34	34	27	28	27	31

D. Conclusion

A parametric study of the electric potential drops in the PIE discharge has demonstrated that variations in the high-voltage pulses can have a substantial effect on the discharge characteristics. The total power of the pulser affects the degree of ionisation in the vicinity of the cathode. If a great deal of pulser power is expended, the cathode will not be required to operate in the abnormal glow regime in order to support the discharge current. Unfortunately, since the electrostatic probe measurements of V_c for the pin geometry are also affected by the amount of pulser power (and hence electron density), it is not feasible to accurately measure V_c through this simplistic technique. Both the pulse amplitude and pulse frequency influence the dc electric field strength in the positive column through processes of ionisation and attachment. Pulse frequency alone influences the anode fall, due to the attachment process.

Since each region is affected by different parameters of pulser operation, it should be possible to optimise the overall performance of the laser by separately varying them. This prospect warrants further, more detailed investigation.

REFERENCES

- [1] S.K. Nikumb, H.J.J. Seguin, V.A. Seguin, R.J. Willis, H.W. Reshef, *IEEE J. Quant. Electron.*, **QE-25**, 1725 (1989).
- [2] R. Haas, *Phys. Rev. A* **8**, 1017 (1973).
- [3] K. Smith, R.M. Thomson, *Computer Modelling of CO₂ Lasers* (Plenum, New York, 1978), p. 211
- [4] W. Wiegand, W. Nighan, *Appl. Phys. Lett.*, **22**, 583 (1973).
- [5] Chapter III of this thesis.
- [6] A. von Engel, *Ionised Gases* (Oxford University Press, London, 1965), p. 229.
- [7] E. Nasser, *ibid.*, p. 421.
- [8] G. Francis, *Handbuch der Physik*, ed. S. Flügge, **22**, (Springer Verlag, Berlin, 1956), p. 145.
- [9] G.E. Sedgwick, Ph.D. thesis, University of Alberta, 1974.
- [10] C. Popovici, M. Somesan, *Appl. Phys. Lett.* **5**, 103 (1966).
- [11] V.M. Tkachenko, V.B. Tyutyunnik, *Zh. Tekh. Fiz.* **38**, 896 (1968).
- [12] V.M. Tkachenko, V.B. Tyutyunnik, *Zh. Tekh. Fiz.* **42**, 67 (1972).
- [13] S.K. Nikumb, H.J.J. Seguin, V.A. Seguin, and H. Reshef, *J. Phys. E: Sci. Instrum.*, **20**, 911 (1987).
- [14] L.B. Loeb, *Basic Processes of Gaseous Electronics*, (University of California Press, Berkeley, 1961), p. 361.
- [15] R.A. Gottscho, *Phys. Rev. A*, **36**, 2233 (1987).
- [16] P.R. Smy, *Adv. Phys.*, **25**, 517 (1976).
- [17] V.A. Seguin, H.J.J. Seguin, C.E. Capjack, and S.K. Nikumb, *J. Appl. Phys.*, **60**, 3088 (1986).
- [18] R. Willis, Ph.D. thesis, University of Alberta, 1987.
- [19] R. Walkup, R.W. Dreyfus, Ph. Avouris, *Phys. Rev. Lett.* **50**, 1846 (1983).
- [20] R.A. Gottscho, A. Mitchell, G.R. Scheller, Y.-Y. Chan, D.B. Graves, *Phys. Rev. A*,

40, 6407 (1989).

[21] C. Barbeau, J. Jolly, *Appl. Phys. Lett.* **58**, 238 (1991).

III. Electron dynamics in magnetised CO₂ laser and He discharges

A. Introduction

The increased adoption of high powered lasers within the materials processing and fabrication industry has generated a persistent demand for more efficient, compact, and reliable laser energy sources. Since the carbon dioxide system continues to dominate the high power laser field, considerable attention has been devoted to improving the operational characteristics of this type of discharge-pumped machine.

This goal has been pursued through extensive research, both theoretical and experimental, on cold-cathode plasma creation and maintenance, within a gaseous mixture of helium, nitrogen, and carbon dioxide, under elevated electrical energy deposition. Discharge instability mechanisms and attempts to develop novel techniques to ameliorate this singularly important limiting aspect in this class of laser have figured prominently in past studies.

A case in point is the concept of Magnetic Stabilization, advanced for enhancing the specific discharge power loading within a CO₂ laser plasma.¹ The technique, which features the superposition of a strong magnetic field transverse to the pumping electric field, causes localised areas of incipient thermal instability to be swept away by the externally impressed ExB drift of the electron flux.

The influence of these specially profiled magnetic fields upon the glow-to-arc instability threshold of a positive column active medium has been extensively examined and is reasonably well understood.^{2,3,4} In addition, the ability of the sweeping effect of the transverse ExB drift to suppress instabilities in the cathode region has been established.^{5,6} However, the effect of the magnetic field on the evolution of the electron flux in the cathode region has not been addressed. This particular aspect could be of major significance in CO₂ lasers, because electrodes are known to play a dominant role in cold-cathode glow dynamics.

¹A version of this chapter has been published: A.H. Labun, C.E. Capjack, H.J.J. Seguin, J. Appl. Phys. 68, 3935 (1990).

Electrode potential drops determine, in large measure, the electrical excitation efficiency of these devices. It is conceivable that magnetic field effects on charge carriers in the high field regions immediately adjacent to the cathode surface could appreciably affect the performance of glow discharge pumped lasers.

An important question to be answered is the effect of a strong transverse magnetic field on the production of electrons at or near the cathode surface. Heylen and Dargan⁷ have shown that the number of ionizations per volt in nitrogen is dependent on the magnetic field strength for all values of E/p . This suggests that the magnetic field in the cathode region can be varied to control electron production, which could result in a changed cathode fall potential⁸ or cathode fall distance. The cathode fall potential in present day, narrow-gap, gas transport, high powered lasers constitutes a sizable portion of the applied excitation potential. Consequently, magnetically enhanced cathodes could have a profound beneficial impact on the efficiency of these systems.

A further consideration is the reduction of the electron density in the negative glow region by the elimination of high energy electrons emitted from the cathode region. Ionization beyond the cathode region plays a role in the strength and sign of the electric field in the negative glow and positive column. Three possible situations exist with regard to electron production through impact ionization: ionization might occur only in the cathode region, significant ionization might also occur in the negative glow, and ionization might occur throughout the discharge. If all the ionization were to take place in the cathode region, only an electron current would exist in the positive column and no field reversal would be required to maintain the ion current in the cathode region. If, however, significant ionization took place in a well-defined region beyond the cathode region, such as the negative glow, a local potential minimum would develop, with attendant field reversals. (It is possible that such a field reversal could be responsible for the anomalous, but beneficial, low cathode potential reported by V. A. Seguin, *et al*⁸ in a CO₂ laser with a transverse magnetic field. The cathode fall was measured to be only 50 V under conditions of zero gas flow and a 0.0083 T magnetic

field, rather than the 350 V measured with gas flow.) If ionization were to take place over a broad region in the positive column, the relatively low ionic mobility would give rise to an increased ion density in the discharge. The resultant field reversal beyond the cathode region would accelerate ions towards both the cathode and the anode. Gottscho *et al.*,⁹ recently reported detecting such a reversal in N₂ and mixtures of N₂ and Ar.

Since the cathode region is also the boundary-layer for the gas flow, the magnetic trapping of high energy electrons in this region could also cause increased heating. This would have a negative effect on the instability threshold of the positive column gain medium immediately adjacent to the cathode region. The considerations above are of sufficient importance to the further enhancement of CO₂ laser performance to warrant an in-depth investigation. Consequently, this paper will address some of the questions posed. Specifically, the results of an extensive computer simulation of cold-cathode, normal glow phenomena, under the influence of a strong, transverse magnetic field are presented. Results are reported for pure helium gas and for a helium, nitrogen, carbon dioxide mixture typically found in CO₂ lasers. [Subsequent to the publication of this article, a different interpretation has been placed on V. A. Seguin's measurement by A. H. L. It is now believed that under the zero gas flow condition, the temperature rose enough to reduce the gas density and thus increase the cathode fall distance by a simple scaling effect. The probe may then have been *inside* the cathode fall region. In such a situation, its measurement could not be considered reliable.]

Computational considerations

Electron dynamics in the cathode region of glow discharges are at present not well understood. This is due to the nonequilibrium nature of the electron population, which is accelerated by a very large electric field. Since nonequilibrium has in the past rendered the traditional Boltzmann equation analysis intractable, recent research has concentrated on Monte Carlo simulations of the cathode region.^{5,6,10,11,12,13,14,15,16,17} These simulations do not rely on the assumption of equilibrium since they only require a knowledge of the collision

cross-sections. However, until now most Monte Carlo simulations have been restricted to noble gases and the consideration of the electric field only. The Monte Carlo technique used in the simulations reported herein consists of analytical electron trajectory computations terminated by randomly determined collisions. This technique allows the inclusion of the effects of a transverse magnetic field in the cathode region. These simulations produce distributions of the energy density of the electron flux (EDEF) throughout the cathode region which permit an analysis of the evolution of the electron avalanche in a magnetised discharge.

A brief comparison of results obtained for the case of an unmagnetised helium normal glow discharge with those of other researchers is made in order to impart confidence in the Monte Carlo approach used for this investigation. A comparison of results for pure He with those for the He:N₂:CO₂ mixture under various magnetic fields is made both to extend the body of knowledge concerned with the He discharge and to highlight magnetic field effects in the CO₂ laser mixture.

B. The computer simulation

The Monte Carlo code utilised in this simulation is an extension of the code reported by Razdan, Capjack, and Seguin for the description of the cathode region of magnetised He:N₂:CO₂ glow discharges.^{5,6} Since the algorithm will only be briefly described here, the interested reader is referred to these two papers. Changes made to the code will be described in greater detail.

The algorithm consists of computing the sequence of accelerations and collisions for a primary electron from its emission from the cathode to its final passage past the cathode fall distance, D_c . Secondary electrons are similarly followed through the cathode region from their points of creation. In an extension to the original code, all further generations of electrons (e.g. tertiary electrons created by the secondaries) are also treated in the same manner; consequently, complete avalanches may be simulated. Optionally, electrons with an energy equal to or greater than the ionization energy may be followed beyond the cathode region into

a region of extremely low field strength to observe how many additional electrons they would create in the negative glow. Such avalanches are computed for many primary electrons, resulting in an accurate sample of the EDEF. The electric field is not computed in a self-consistent manner, but is approximated by the linearly decreasing function

$$E(z) = (2V_0/D_c)[1 - (z/D_c)] \quad (1)$$

where V_0 is the cathode fall voltage. The magnetic field is assumed transverse to the electric field (in the x-direction) and results in an electron drift in the negative y-direction. The mean free path is determined from an assumed pressure (30 Torr) and temperature (600 K), typical of the cathode regions of CO₂ lasers. Although in some discharge geometries a significant temperature and hence neutral density gradient may exist, in this analysis the simplifying assumption of an isothermal cathode region has been made. The normal cathode glow cathode region parameters used are, for He gas, $V_0 = 150$ V and $D_c = 0.866$ mm, and for He:N₂:CO₂ (20:8:2), $D_c = 0.751$ mm and $V_0 = 187$ V. These values are based on a pressure-weighted average of the values for the various species.¹⁸

The validity of these discharge parameters and equation (1) under conditions of strong magnetic fields is not established, thereby making it advisable to only consider magnetic fields which are minor perturbations on the discharge. A calculation of the effect of magnetic fields on electron-neutral collision rates permits an estimate of the maximum value of magnetic field which may be treated as a slight perturbation on the cathode region parameters. According to Blevin and Haydon,¹⁹ the crossed electric and magnetic fields induce an effective gas pressure p' for the electrons:

$$p' = p[1 + (\omega_{ce}/\nu_{en})^2]^{1/2} = p[1 + \beta^2]^{1/2} \quad (2)$$

where ω_{ce} is the electron cyclotron frequency, ν_{en} is the electron momentum transfer collision frequency (assumed constant), and the ratio β is the Hall parameter. This expression was obtained for the electron drift conditions characteristic of the positive column of an electric

discharge and assumes a constant collision frequency and isotropic scattering. For $B=0.1$ T, the predicted ratio of the effective pressure to the actual pressure is $p'/p=1.088$ in the He:N₂:CO₂ mixture and $p'/p=1.150$ in He. The estimates are based on collision data for the entire cathode region obtained by running the computer simulation with no magnetic field. Since the effective pressure change is an order of magnitude smaller than the primary pressure, this strength of magnetic field is deemed to be a minor perturbation on the discharge. Since discharges are stabilised by magnetic fields of less than 0.01 T, this does not constitute a severe limitation on the applicability of the simulation.

Inelastic and elastic collisions of electrons with gas atoms are included in the simulation. The determination of collision type is made randomly, according to the collision probability cross-section for each type of collision for each gas in the mixture. These cross-sections⁶ (Fig. III.1) are highly sensitive to the electron energy. The set of collision probability cross-sections for elastic and inelastic collisions extends over the range 1-200 eV, while the set of differential scattering cross-sections extends over the energy range 1-100 eV. Electrons with energies beyond these ranges are treated as if they were at the top of the ranges. This approximation does not significantly affect the results of these simulations. The resulting two electrons in electron ionization or dissociative attachment reactions are assumed to divide or share the remaining energy equally.⁵ This simplifying approximation thus under-estimates the number of high energy electrons (and low energy electrons) present in the EDEF. All scattering is anisotropic, with high energy collisions resulting primarily in forward scattering. Scattering is isotropically distributed about the collision axis.

The gas in which the discharge takes place is modeled by stationary gas atoms, with the presence of ions and other electrons neglected because of the low fractional ionization density in the glow (about 10^{-7}). The temperature of the gas would not normally affect the outcome or the energy of the collisions, but is used to scale the gas density. In Razdan's simulations, the electron's path between collisions is randomly distributed about the mean free path according to the formula

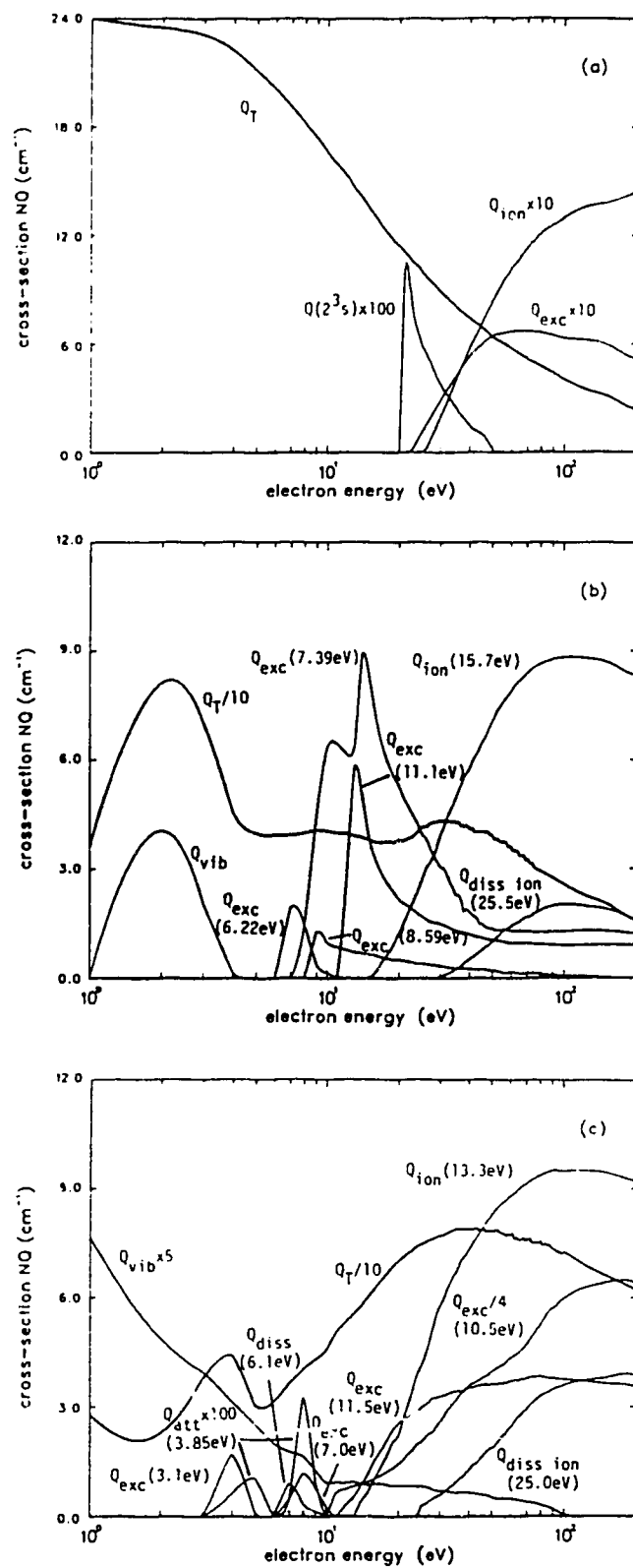


Fig. III.1 Collision cross sections for electrons at 1 Torr with (a) He, (b) N₂, and (c) CO₂.

$$S = -\lambda \ln(R), \quad (3)$$

where for a mixture of He, N₂, and CO₂,

$$\lambda^{-1} = \lambda_{\text{He}}^{-1} + \lambda_{\text{N}_2}^{-1} + \lambda_{\text{CO}_2}^{-1}. \quad (4)$$

One value of λ is computed for the entire trajectory. The random number R is uniformly distributed between 0 and 1. The electron trajectory is computed analytically based upon the path length S and the initial velocities v_x , v_y , and v_z .

This technique was found to be inadequate for the representation of the highly energy dependent mean free path lengths implied by the energy dependent cross-sections. In fact, a single value for the mean free path cannot be determined for the electron at the initiation of its trajectory, since the mean free path changes continuously while the particle is *en route* and its kinetic energy is changing. Therefore, resort must be made to a stepping technique (Fig. III.2). The cross-section for collision at position 1 is used to compute a fraction S_1 of the trajectory. The energy at position 2 is used to compute another fraction S_2 of the trajectory, and so on until N steps have been made. The total length of the trajectory S is then

$$S = -(\ln R/N) \sum_{i=1}^N \lambda(\epsilon_i). \quad (5)$$

A single value of R is used for the computation of the trajectory. In the limit as N becomes large, S approaches the true length of the trajectory. The results reported herein were obtained with $N=6$.

The major extension to Razdan's work reported in this paper is the monitoring of the energy of electrons as they pass through the cathode region. This was accomplished by the device of fixing imaginary planes perpendicular to the field direction at 0.033 mm intervals (Fig. III.3). As an electron undergoes a collision, after having crossed one or more of these planes, its crossing is noted. The program records its energy by incrementing a corresponding element in a histogram. Thus, when a 14 eV electron makes a collision at, say, $z=0.71$ mm, a histogram element corresponding to 14 eV at the 0.066 mm plane is incremented by 1. Since

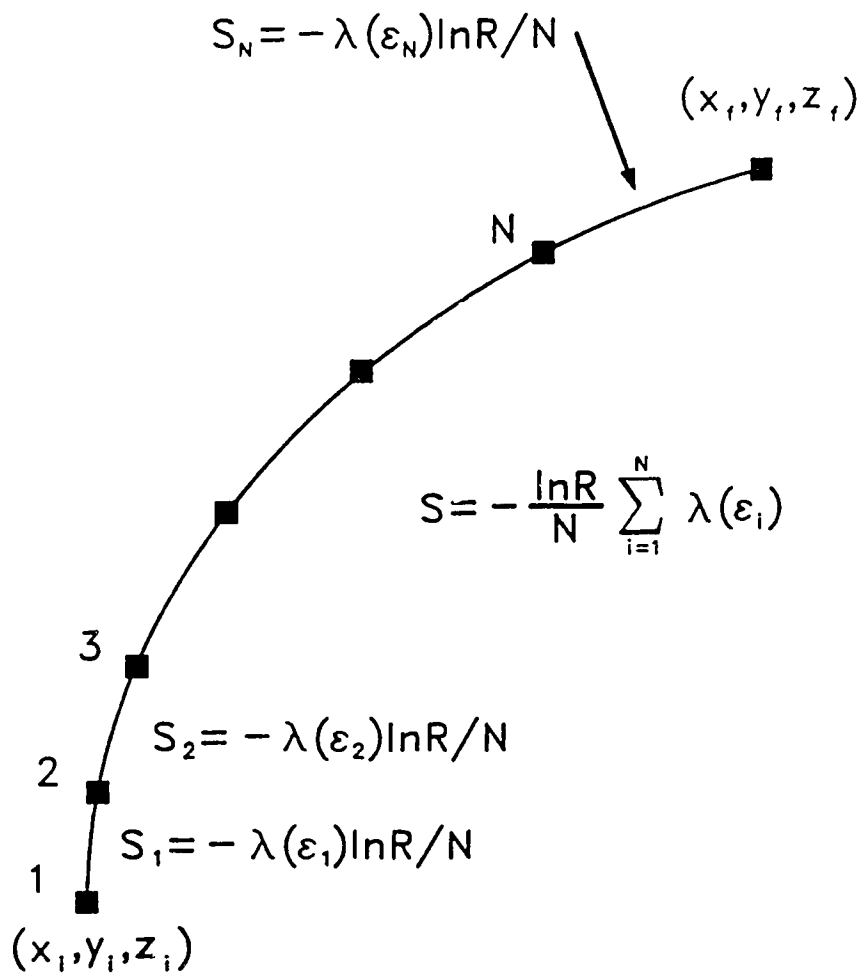


Fig. III.2 The electron free path computation. The total length of the free path S is the sum of N segments S_i .

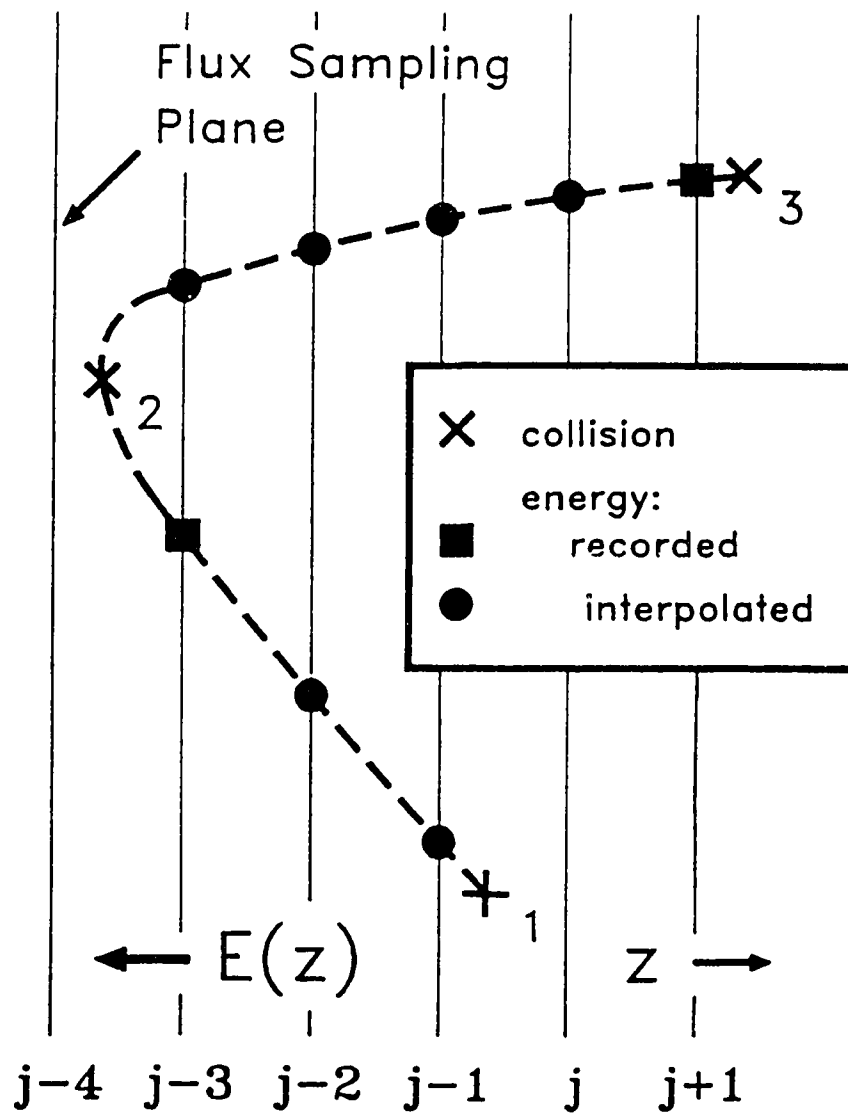


Fig. III.3 The electron energy sampling and recording techniques. Collision energies are recorded at the last plane crossed and interpolated quadratically.

the electric field varies linearly with z , the energy gained by an electron varies quadratically with z . Therefore, for electrons that cross more than one plane between collisions, a quadratic interpolation of the energy is performed to determine which histogram element to increment at each plane crossed before the collision plane.

The series of histograms corresponding to each of the planes represents the evolution of the energy distribution of the electron flux. The term "electron flux" is used here in the sense of a particle flux (i.e. the number of electrons passing through a plane perpendicular to the equipotential). This is different from the one-dimensional flux, which measures only the vector component of the particle flux oriented in the field direction. This distinction is not made in simulations considering forward scattering only, as these simulations have no electrons with lateral velocity components.

As well as the electron energy, the sense of the electron's velocity is also detected at the crossing. In this paper, forward and reverse flux are defined in the following manner: forward electron flux is motion from the cathode to the edge of the negative glow, while reverse electron flux refers to movement in the opposite direction. Forward electron flux is computed by incrementing the histogram at each plane only when an electron's trajectory began on the side of the plane closer to the cathode and ended it on the side closer to the anode, and *vice versa* for reverse flux. The net flux of electrons is taken as the difference between the forward and reverse fluxes. The orbital motion of the electrons in the yz -plane does not contribute to the net flux, and is not in fact directly detectable since the trajectory computations only make use of the end-points of the electron trajectories (or fractions thereof). Ionic contributions to flux are not dealt with in this paper.

The output from the simulation is a series of arrays containing the number of electrons of each energy passing through the various planes, as well as a summation for the entire simulation of the occurrences of the various types of collisions possible. From these it is possible to compare the energy distributions of the electron flux passing through the planes, to see how the thermalization of the flux proceeds through the cathode region. As well, the

growth of the electron flux may be measured by summing the electrons enumerated at each plane. It is not possible, however, by using this advancement technique to compute a true electron energy distribution function directly. While the speed of electrons may be derived at each plane from the energy, the direction is not readily obtainable. Thus it is unknown whether a high energy electron is moving nearly perpendicular to, or nearly parallel to, the plane. Also, Boeuf and Marode¹¹ have shown that the distribution of electron velocities is not isotropic; the angular distribution of electron velocities is highly energy dependent. This result is confirmed by the highly disparate mean energy profiles of the forward and backward electron flux observed in the zero magnetic field simulations. The calculation of the energy distribution function therefore would require both simplifying assumptions regarding the trajectories of the electrons and additional computational efforts; consequently, it was not performed in the present work.

C. Results of the simulation

Simulations of the cathode region for He and He:N₂:CO₂ were performed with different magnetic field strengths between 0.0 T and 1.0 T, although the focus was on the 0.0 T and 0.1 T field cases. The results from the 0.0 T case serve as a point of reference, while the results from the 0.1 T case clearly display the effect of a magnetic field without a large perturbation of the discharge. Tables III.1 and III.2 present results from these simulations. Electrons were generally not propagated beyond the cathode fall distance. In order to establish the likely contribution of the electron flux to ionization beyond the cathode region (i.e. in the negative glow), a run was performed for each case in which the electrons were allowed to propagate indefinitely in space until their energy had dropped below the minimum ionization energy (15 eV). The differences between the ionization for the runs with this end condition and the runs with the $z=D_c$ end condition served to establish the probable occurrences of ionization beyond the cathode region ($z>D_c$). In some cases with strong magnetic fields, the requisite computation time was so long that a sufficient number of electrons could not be

propagated through the discharge to provide accurate values for this post- D_c ionization. No values are given for these cases. The trend from cases with weaker magnetic fields towards less post- D_c ionization should, however, continue. The Hall parameter given is based on the total number of collisions in the simulation, the total number of electrons emergent at $z=D_c$, and the average time of flight. Thus, it is an average for the entire cathode region. The He:N₂:CO₂ simulations involved 1 million collisions each, while the He simulations involved from 500 thousand to 1.3 million collisions, with the number increasing with magnetic field strength.

Electron flux in the non-magnetised cathode region

The passage of electrons through the He cathode region was computed for the non-magnetised case and the distribution of the flux of electrons was recorded throughout the region (Fig. III.4). It is evident that as the electron flux proceeds through the region, the initially narrow range of energies is broadened by the combination of large energy gains in the high field region for some electrons and large energy losses through collisions for others. Distinct groups, "cohorts", of electrons with zero, one, or two collisions are also visible at the high energy end of the distribution. These cohorts persist in the forward flux to the very end of the cathode region.

One of the observations made from forward scattering models (i.e. ones in which all electrons maintain the same direction of travel) has been the presence of a large cohort of collisionless 'beam' electrons. Although a cohort of such electrons is observed in the forward flux in the full scattering model, assumption of forward scattering produced a cohort 3.5 times as large. The forward scattering model had a beaming component of 2.5% of the electron flux, while the full scattering had a beaming component of 0.6%. Carman and Maitland¹⁴ reported a 5% beaming component in their forward scattering simulation at normal cathode fall (150 V). Gill and Webb²⁰ measured a beaming component of 1-3% with cathode falls of 200 V and higher. It seems likely that a value for the beaming component measured at

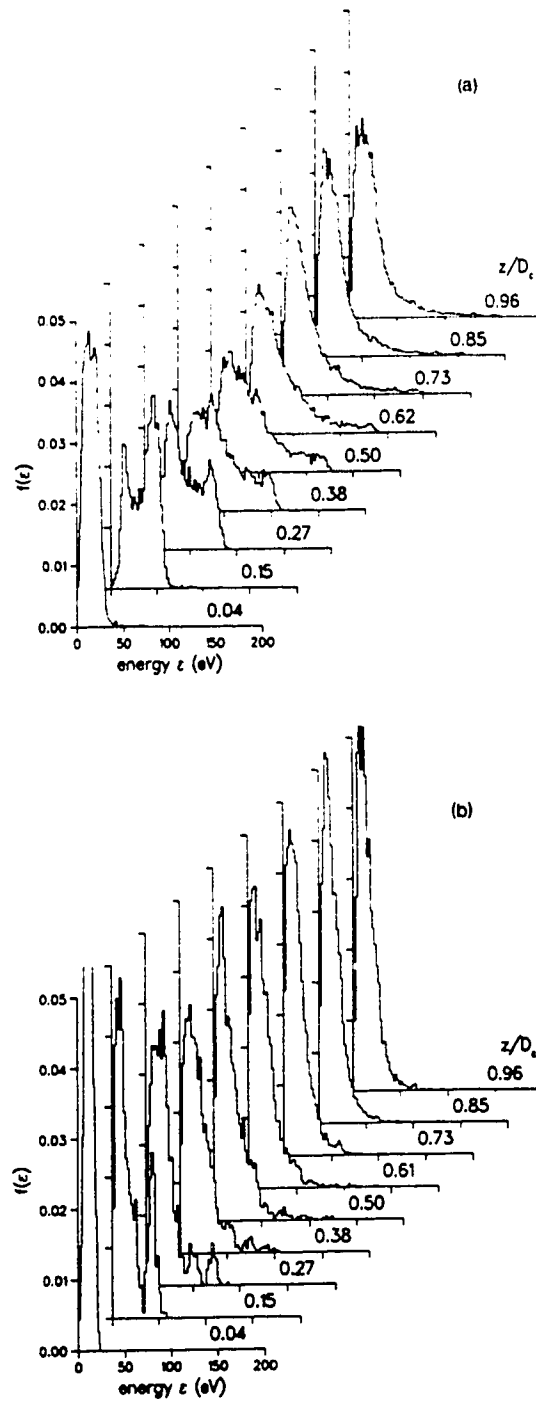


Fig. III.4 The energy density of the electron flux (EDEF) in the He cathode region (Full scattering): (a) forward flux and (b) reverse flux.

150 V might agree well with the lower, full scattering estimate reported here.

In the reverse flux, the high energy cohorts decay rapidly. This follows from the fact that as fewer collisionless electrons persist in the cathode region, fewer are available to collide and be transferred to the reverse flux. Also, as the collisionless electrons attain higher energies, forward scattering predominates and fewer collisions result in retrograde electrons. The reverse flux EDEF, then, has a narrower distribution of electron energies than the forward flux and contains very few high energy electrons relative to that of the forward flux.

The mean energy of the electron flux in the electric field direction (Fig. III.5) rises to a maximum at approximately $z/D_c = 0.35$ for both the forward and reverse flux. The difference in energy between forward and reverse flux is due to the large numbers of electrons in the forward flux which have lost little energy through inelastic collisions. The degree to which the electron population is collisionally dominated at any point in the cathode region is thus inversely proportional to the difference in mean energy between forward and reverse flux.

Boeuf and Marode¹¹ found the mean energy of the electron energy probability distribution function to also peak between $z/D_c = 0.3$ and 0.4 with a value of 35 eV and to display a minimum shortly before $z = D_c$ of 10 eV. This corresponds to 44 eV and 25 eV, respectively, for the forward electron flux and 22 eV and 16 eV for the reverse electron flux. If the heavier weighting given to low energy electrons in calculating the probability distribution function were applied to the mean energy curves presented here, they would be lowered considerably.

The evolution of the EDEF in the He:N₂:CO₂ cathode region (Fig. III.6) occurs differently than in the He discharge. In particular, the distinct cohorts of electrons with the same energy are not seen to progress through the region. Instead, a much smoother high energy tail forms almost at the outset and then rapidly diminishes. This lack of energy cohorts can be attributed to the diversity, probability, and relatively low onset energies of inelastic collisions in the laser mixture. The relatively large numbers of collisions per electron

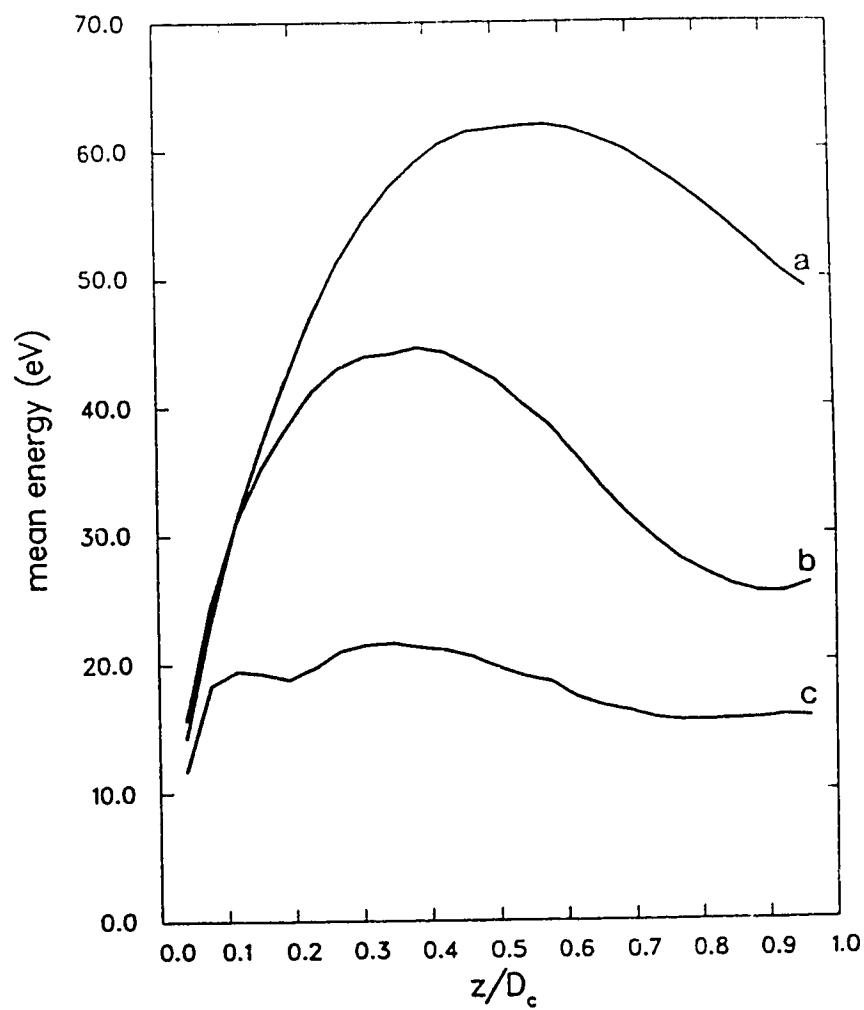


Fig. III.5 The mean energy of the He cathode region EDEF:(a) forward scattering;(b) full scattering, forward flux; and (c) full scattering, reverse flux.

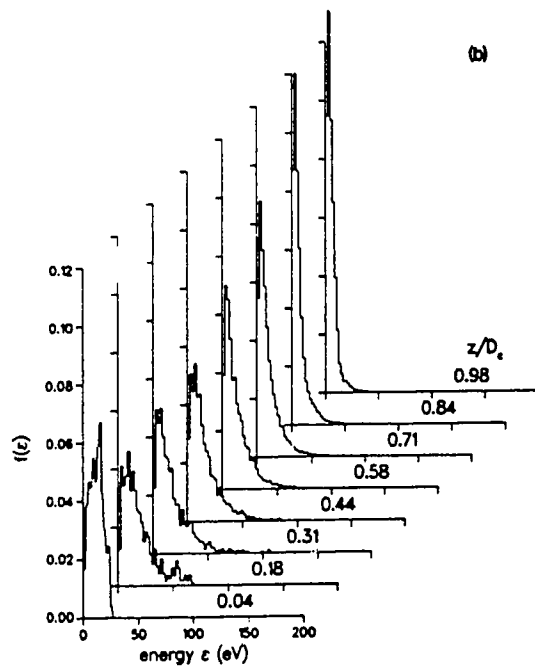
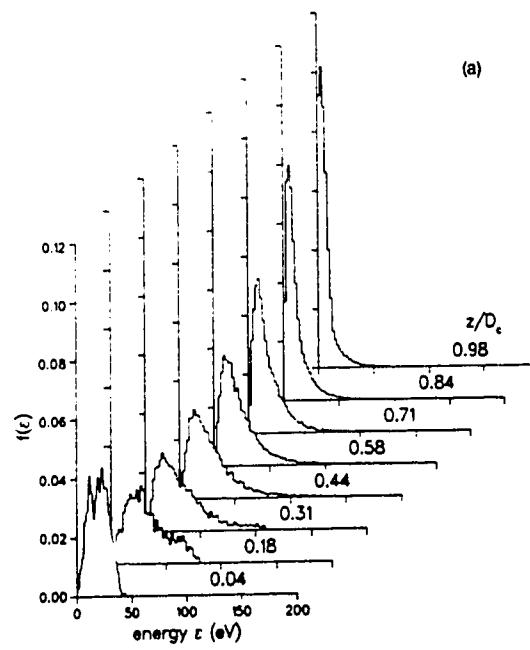


Fig. III.6 The evolution of the EDEF in the He:N₂:CO₂ cathode region: (a) forward flux and (b) reverse flux.

strengthens the effect of the diversity by dramatically increasing the number of combinations of energy losses each electron sustains. As a result, electron energies are more rapidly homogenised and the EDEFs for forward and reverse fluxes are more alike than in the He cathode region. The mean energy profile for the He:N₂:CO₂ mixture (Fig. III.7) reflects the relative unimportance of the high energy electrons in the flux: the maximum mean energy is approximately 10 eV less than that for He albeit the potential drop is greater for the mixture. As well, the difference in mean energy between forward and reverse flux at $z=D_c$ is less than 2 eV, compared with 10 eV for He.

The effective pressure concept in a magnetised cathode region

The effect of a magnetic field upon the positive column of the normal glow discharge includes the mimicking of greater number density or higher pressure,¹⁹ or, alternatively, an equivalent reduced electric field.²¹ This was used earlier in this paper to estimate the degree of perturbation of the cathode region by the magnetic field. In order to test the validity of the concept of an equivalent pressure to the cathode region, comparison was made of simulations with a) 30 Torr pressure and no magnetic field, b) 30 Torr pressure and 0.1 T magnetic field, and c) a "reduced" pressure and 0.1 T magnetic field. The reduced pressure was obtained by specifying a lower pressure according to Eqn. (2) (27.6 Torr for Ne:N₂:CO₂ and 26.1 Torr for He) while retaining the cathode fall distance for 30 Torr. If the effective pressure concept were valid in the cathode region, case 'c' would provide results identical with case 'a' but not with case 'b'.

The results that were obtained indicate that in the cathode region the electric field varies too rapidly for an equivalent pressure to be valid. For z/D_c less than approximately 0.2, the electron motion appears to be almost ballistic, with the acceleration between collisions dominant, while for z/D_c greater than 0.5, the electron motion is more drift-like. Thus, an equivalent pressure which might be appropriate to one regime would not be so for the other. The mean energy profiles of the forward flux corresponding to the cases 'a', 'b', and 'c'

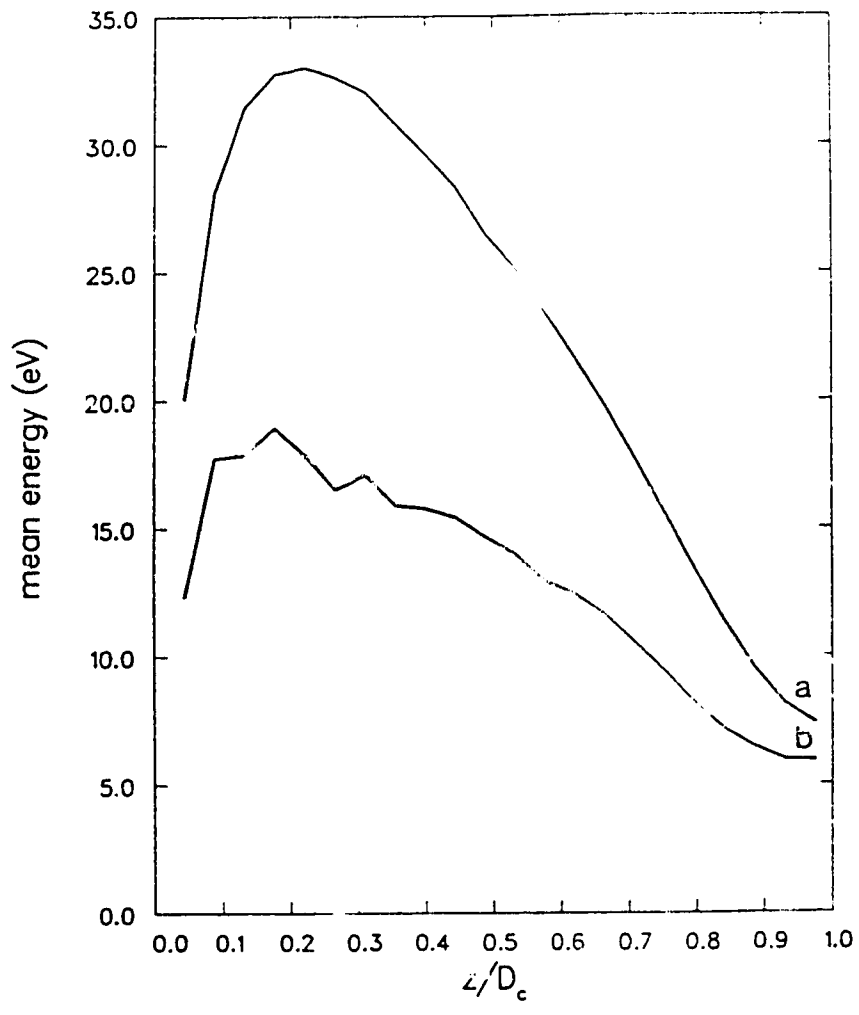


Fig. III.7 The mean energy of the EDEF in the He:N₂:CO₂ cathode region: (a) forward flux and (b) reverse flux.

above (Fig. III.8) clearly show the interaction of pressure and electric and magnetic fields.

The path taken by an electron in the crossed constant electric and magnetic fields is the combination of the circular motion arising from the Lorentz force and the linear motion due to the $E \times B$ drift. For the case where the electron has no initial velocity, this combination results in a cycloidal trajectory. The formula for the radius of the cycloid-defining circle²¹ is

$$r = E / \omega_{ce} B \quad (6)$$

Electrons with non-zero initial velocity follow similar trajectories.

The portion of the cathode region in which the mean energy of the EDEF of the forward flux is increasing shows that both pressure and magnetic field effects limit the motion of the electrons (Fig. III.8). The mean energy in case 'b' has the lowest maximum (32.4 eV at $z/D_c = 0.213$). The pressure and magnetic field chosen by the application of Eqn. (2) are not, however, equivalent. The energy in case 'c' is able to rise more quickly than in case 'a' because the cycloids induced in case 'c' by the crossed E and B fields have very large radii compared to the mean free paths: $\lambda/r = 0.067$ for case 'b' (i.e. β is small). Thus the reduction of the pressure in case 'c' results in an increased forward electron displacement (even with the deflection of the trajectory due to the magnetic field) over that found in case 'a'.

In the latter portion of the cathode region the reduction in electric field strength results in the cycloidal radii of electrons being of the order of the mean free path (i.e. β approaches order unity). At $z/D_c = 0.6$, $\lambda/r = 0.937$ for case 'b', while due to lower pressure, $\lambda/r = 1.02$ for case 'c'. There is a tendency, then, for the magnetic field to "trap" the high energy electrons (with large λ) and prevent them from advancing in the z-direction. The effect of collisions on high energy electrons is to randomise their cycloidal trajectories and effectively allow them to advance. Thus, paradoxically, the electrons in case 'b' exit the cathode region with more collisions and less energy than the non-magnetised case 'a', but with more collisions and *greater* energy than those in case 'c'. Case 'c' electrons have more

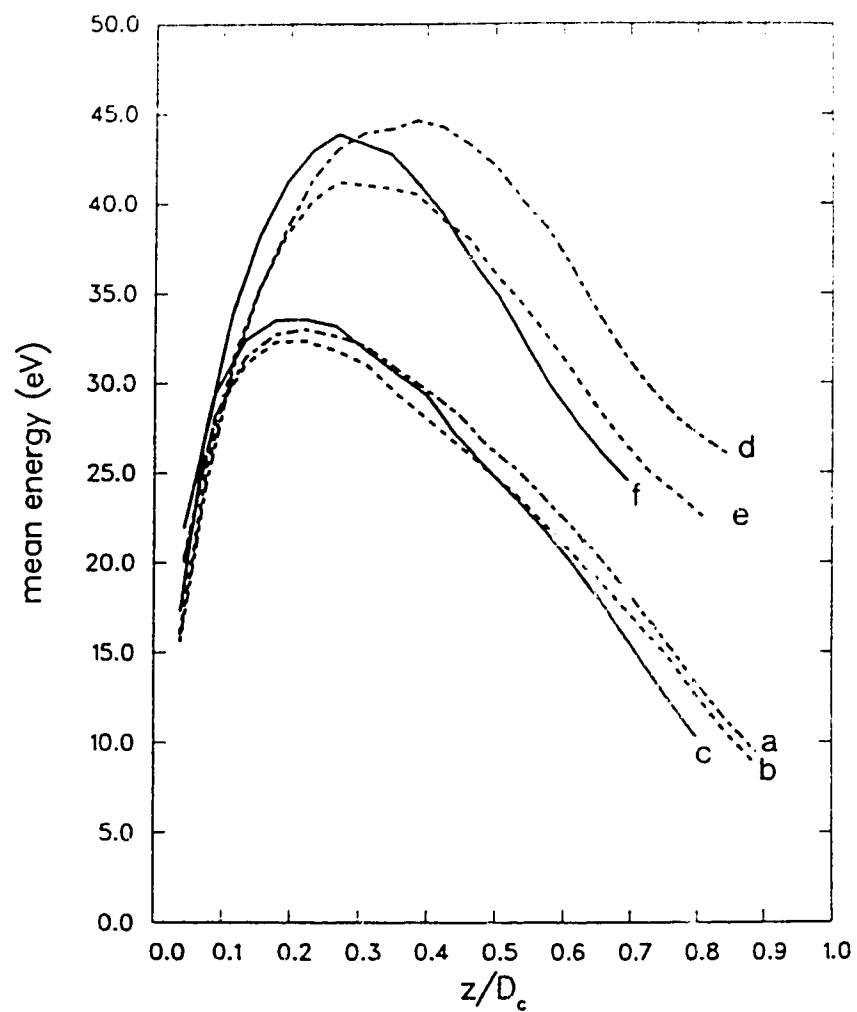


Fig. III.8 The mean energy of the EDEF in the He:N₂:CO₂ cathode region (forward flux): (a) 30 Torr and 0 T, (b) 30 Torr and 0.1 T, and (c) 27.6 Torr and 0.1 T; and in the He cathode region (forward flux): (d) 30 Torr and 0 T, (e) 30 Torr and 0.1 T, and (f) 26.1 Torr and 0.1 T.

collisions than case 'a' electrons. In the latter portion of the cathode region, then, an effective pressure less than that specified by Eqn. (2) would, in fact, be produced by the magnetic field, as counted by total collisions. However, an effect of pressure greater than that specified by Eqn. (2) would be produced, as measured by equilibration.

The evolution of the mean energy of the EDEF in He shows characteristics similar to those in He:N₂:CO₂, although the electrons in case 'f' have more collisions than in case 'd' and fewer than in case 'e'. As seen in Fig. III.8, the effects of a 0.1 T field on the He cathode region are more pronounced than for the He:N₂:CO₂ mixture.

In the initial portion of the cathode region, then, the equivalent pressure model underestimates the effective pressure exerted by the crossed electric and magnetic fields. In the latter portion it overestimates it. This suggests that the equivalent pressure model does not apply over the entirety of this region of the discharge: the required assumption of constant drift is too grossly violated. Thus it is impossible to account for all the effects on electron dynamics of the application of magnetic fields to the cathode region by this means.

Electron flux in the magnetised cathode region

The differential effect of a magnetic field on the electrons of different energies in the cathode region is illustrated by the EDEF of the forward flux. The cohort of collisionless, high energy electrons prominent in the non-magnetised He cathode region (Fig. III.4) is greatly reduced in the magnetised case (Fig. III.9). The exponential attrition of a cohort of size N at the rate α is described by the equation

$$N(z) = N(0)\exp(\alpha z). \quad (7)$$

The rate of attrition of the cohort of collisionless electrons is directly proportional to the path length of the electrons with that energy in the z -direction. Therefore, any difference in attrition rates between the magnetised and non-magnetised cases is attributable to the transverse motion due to the magnetic field. In the non-magnetised cathode region, the rate

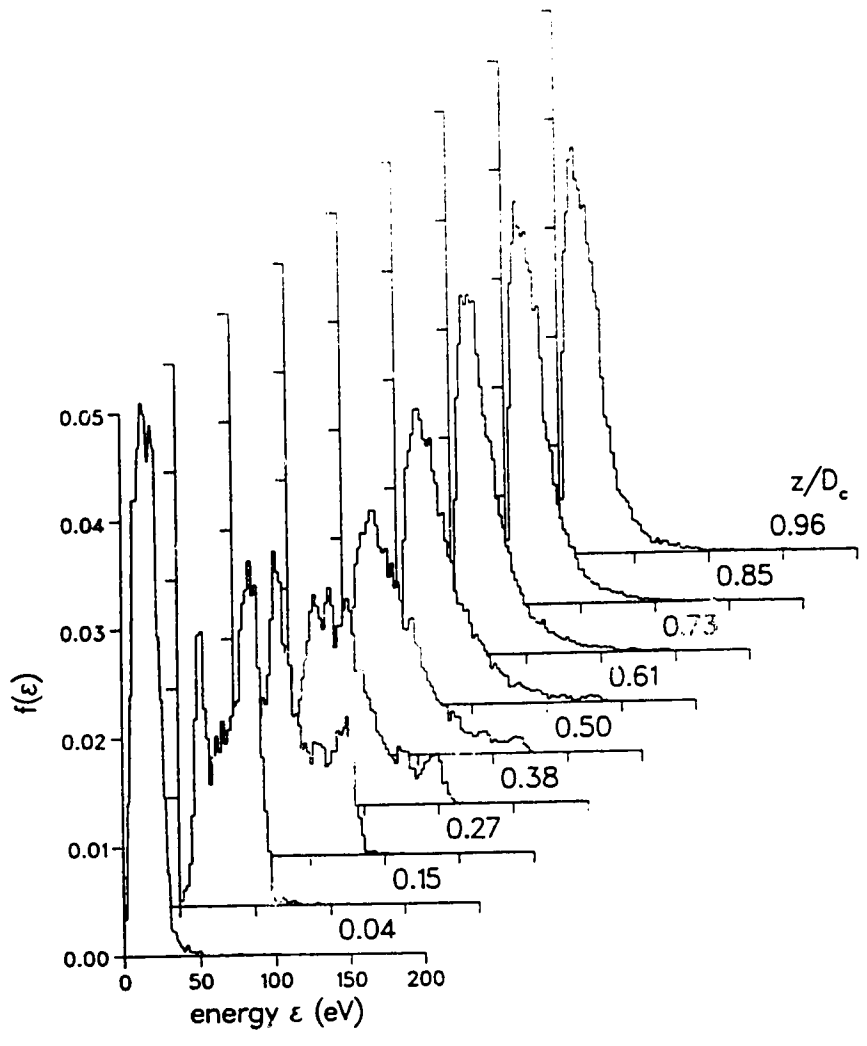


Fig. III.9 The evolution of the EDEF of the forward flux in the He cathode region at 30 Torr and 0.1 T.

of attrition of the collisionless electron cohort is an approximately constant $\alpha = -4.3/D_c$ (Fig. III.10). In the magnetised region $\alpha = -6.0/D_c$ overall, but there are two distinct regimes. For $z/D_c = 0$ to 0.38 , α is approximately the same as the non-magnetised cathode region, while for $z/D_c > 0.38$, $\alpha = -6.6/D_c$. This change in attrition rate indicates the passage from a regime where magnetic effects are not important to one where they are. It is clear that the enhanced collisionality of the magnetised cathode region applies disproportionately to the highest energy electrons. This may be seen from the values for p' computed above using Eqn. (2). These are supposed to account for the enhancement of collisions by the magnetic field, but do not account for the 50% increase in the attrition rate of the highest energy electrons.

The enhanced collisionality of the higher energy electrons in the latter portion of the cathode region can also be seen in the EDEF of the forward flux for the He:N₂:CO₂ mixture (Fig. III.11). Even in the non-magnetised case, no cohort of collisionless electrons remains at $z=D_c$. By $z/D_c=0.44$, the tendency for the electrons in the magnetised cathode region to collide more frequently than those in the non-magnetised region has resulted in a narrower distribution with a higher peak. However, while there are slightly fewer high energy electrons in the magnetised case, the highest energy electrons have the same energy in both cases (140 eV). (In the case with the equivalent pressure compensation (not shown), the EDEF at the same z/D_c shows less narrowing and the highest energy electrons possess an energy of 150 eV.) Near the end of the cathode region (Fig. III.12) ($z/D_c=0.98$), the EDEF for the magnetised case (Fig. III.12) shows that the highest energy electrons do not appear in the same relative quantities that they do in the non-magnetised case. This indicates the energy selective nature of the magnetic enhancement of collision frequency. A logarithmic scale has been used to emphasise the high energy tail of the distribution.

A comparison of the EDEFs of the reverse flux of both He and He:N₂:CO₂ reveals little change under the influence of the magnetic field, particularly in the case of He:N₂:CO₂. This is consistent with the argument that the magnetic field preferentially influences the high energy electrons.

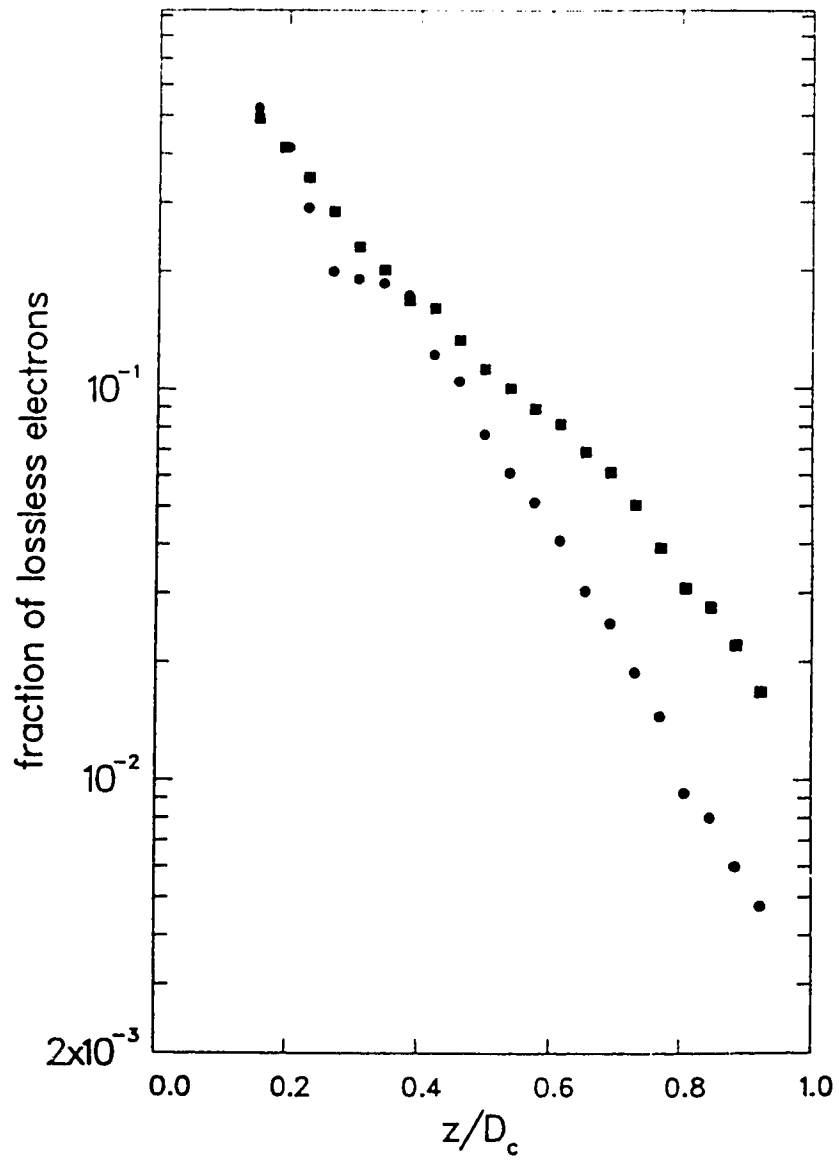


Fig. III.10 The attrition of the cohort of collisionless electrons in the He cathode region. The closed squares represent the 0 T case and the closed circles represent the 0.1 T case.

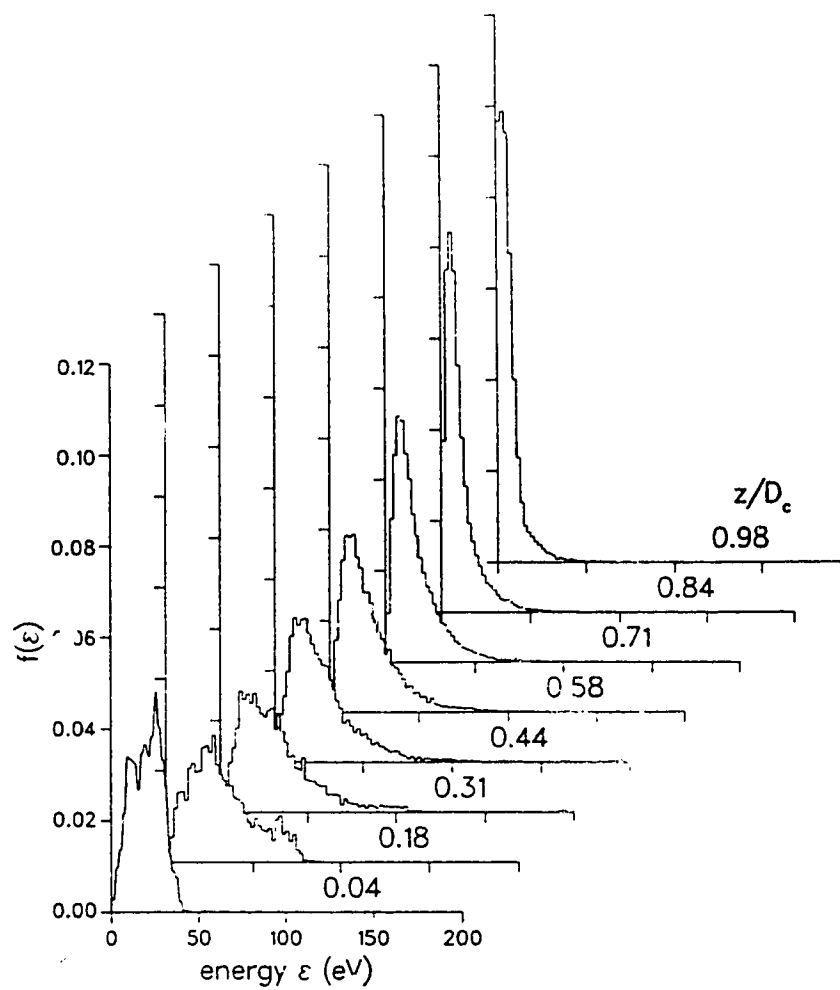


Fig. III.11 The evolution of the EDEF of the forward flux in the He:N₂:CO₂ cathode region at 30 Torr and 0.1 T.

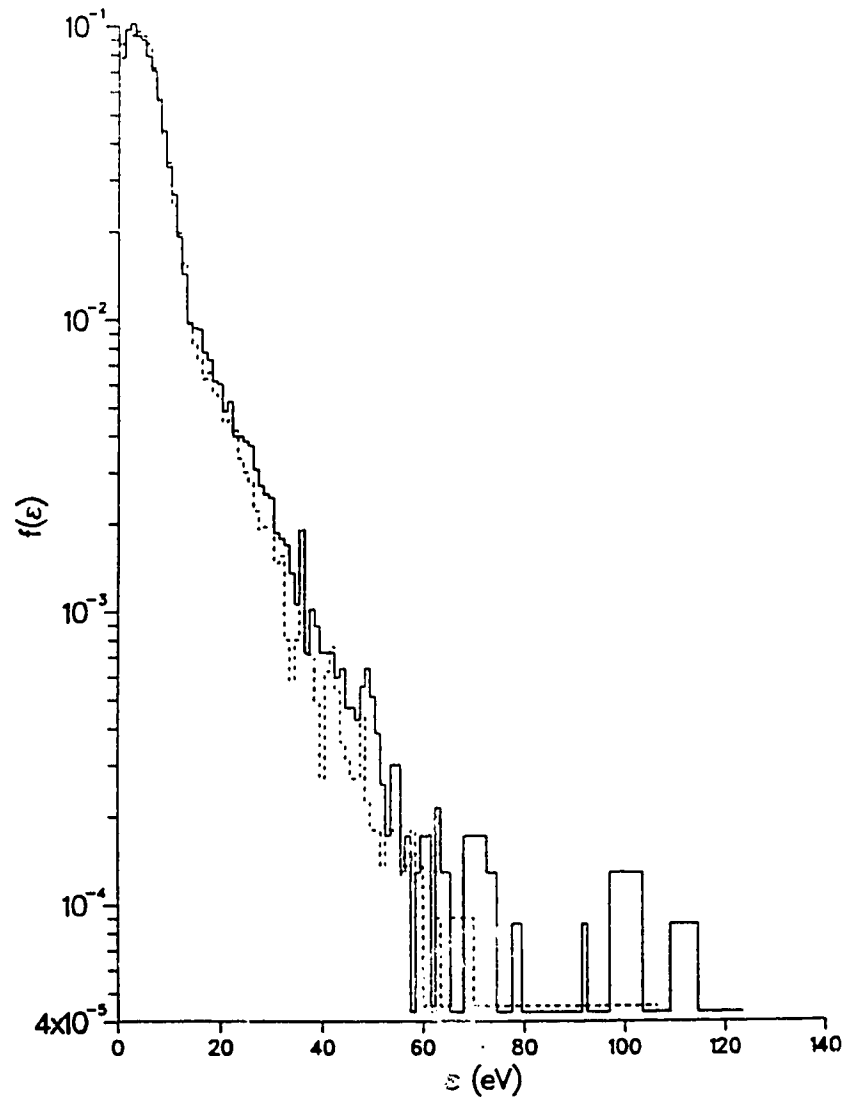


Fig. III.12 The EDEF for forward flux at $z/D_c = 0.98$ in the He:N₂:CO₂ cathode region (the dashed line represents the EDEF for 0.1 T).

The corollary effect of the magnetic field's enhancement of the collision rates of high energy electrons is increased heating of the gas in the cathode region. The energy deposited by electrons can be calculated by tabulating the collision losses per electron (in eV) as it propagates through the plane $z/D_c = 1.0$. This energy contributes to heating of the cathode region and line radiation, most of which is re-absorbed by the gas. The ionic current also deposits energy in the gas. However, complete thermodynamic calculations for the cathode region involve considerations, such as the cathode material and photo-ionization, which are beyond the scope of this paper. The energy deposited, according to Tables III.1 and III.2, then, is that deposited by electrons alone. Energy deposition over the entire cathode region is increased only 2% by the 0.1 T magnetic field in He:N₂:CO₂. This accords well with the experimental observation that thermal instabilities are suppressed, rather than enhanced, by magnetic fields.

Efficiency of the magnetised cathode region

One of the most important issues in the cathode region from the practical standpoint of laser technology is the amount of electron current generated at the cathode. The magnetic field, by changing the energy distribution of the electron flux, is a potential candidate for improving cathode performance. Tables III.1 and III.2 show that, in fact, magnetic fields of 0.1 T do improve the electron multiplication factors (the ratio of electrons emitted from the cathode to those observed at the end of the cathode region) by up to 16% for He and 5% for He:N₂:CO₂. The results show that this is the best that can be achieved in a normal glow for the planar geometry and collisional ionization mechanism assumed in this simulation. Figures III.13 and III.14 show the growth of the electron avalanches in the two gases and display the mechanisms responsible for this minor improvement in cathode efficiency. As shown in Fig. III.13, the electron multiplication factor given in Table III.1 for the non-magnetised case includes the reduction of the electron flux by the reabsorption of electrons by the cathode. (The reflections into the cathode are possible since the electrons are given an initial energy

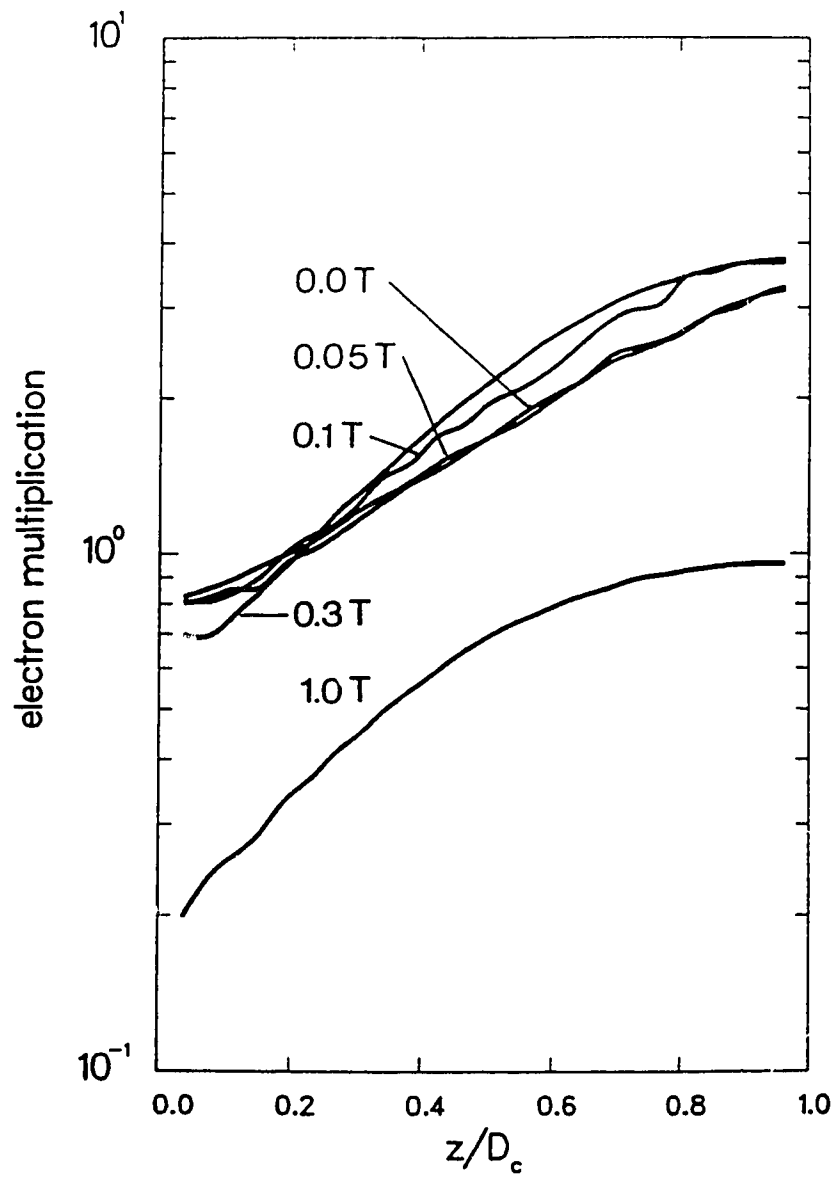


Fig. III.13 The growth of the electron avalanche in the He cathode region for various magnetic fields.

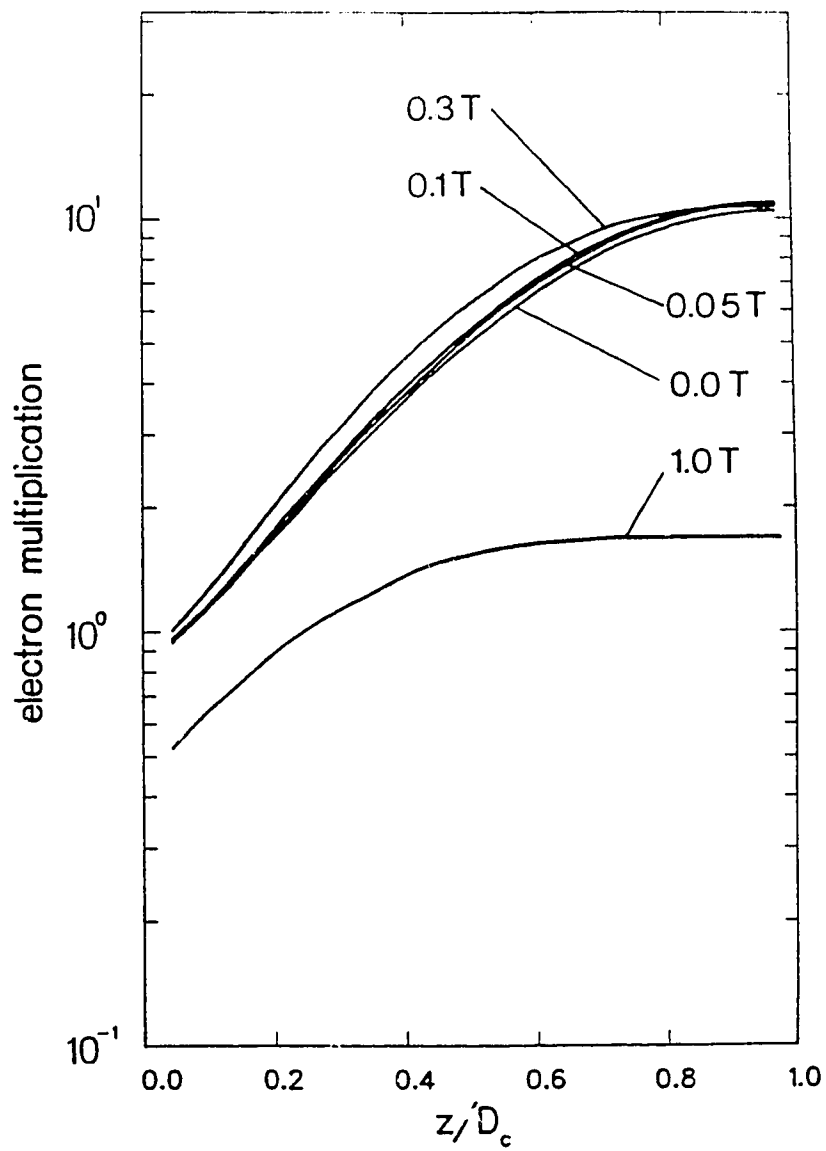


Fig. III.14 The growth of the electron avalanche in the He:N₂:CO₂ cathode region for various magnetic fields.

Table III.i Propagation of electrons in the cathode region of magnetised He normal glow discharges (30 Torr, 600 K). The electron multiplication is normalised to the initial number of electrons.

Magnetic Field (T)	Initial Electrons	Electron Multiplier ($z=D_c$)	Electron Multiplier ($z>D_c$)	Mean Collision Frequency (GHz)	Mean Time of Flight (ns)	Hall Parameter	Energy Deposited (eV)
0.0	4000	3.39	0.38	31.05	1.16		29.90
0.05	4000	3.53	0.84	31.18	1.26	0.492	30.50
0.10	4000	3.93	0.56	30.94	1.555	0.568	32.73
0.1 (26.1 Torr)	4000	3.90	0.09	26.65	1.468	0.660	32.11
0.3	2203	4.09	0.07	30.61	3.757	1.724	37.73
1.0	1148	1.76	----	32.93	15.53	5.434	51.82

Table III.2 Propagation of electrons in the cathode region of magnetised He:N₂:CO₂ normal glow discharges (30 Torr, 600 K). The electron multiplication is normalised to the initial number of electrons.

Magnetic Field (T)	Initial Electrons	Electron Multiplication ($z=D_c$)	Electron Multiplication ($z>D_c$)	Mean Collision Frequency (GHz)	Mean Time of Flight (ns)	Hall Parameter	Energy Deposited (eV)
0.0	1491	10.56	0.80	41.81	1.570	0.0	53.49
0.05	1405	11.00	0.51	40.85	1.639	0.215	53.35
0.1	1307	11.08	0.23	41.15	1.735	0.427	54.64
0.1 (27.6 Torr)	1473	11.30	0.006	38.20	1.625	0.460	52.54
0.3	817	10.81	-----	39.43	2.974	1.338	64.81
1.0	1036	7.24	-----	25.93	22.40	6.783	128.15

uniformly distributed between 0 and 10 eV and so can overcome the opposing electric potential.) The cases with strong magnetic fields tend to have increased cathode reabsorption due to the curved paths of the electrons, but also higher ionization rates. Such a combination of opposing trends must lead to an optimal condition. The increased electron growth rate is a result of the more rapid equilibration in the magnetised cathode region. Thus, as the magnetic field increases, the total energy available to emitted electrons is given up through collisions sooner in the cathode region. This results in the early flattening in the growth-curve of the electron flux under the strongest magnetic fields. Since the stronger magnetic fields may cause the cathode region parameters to be altered, this extrapolation to very strong fields (such as 1.0 T) must be treated cautiously. Stronger magnetic fields further reduce the electron flux at the cathode through increased absorption. This loss is not compensated by the enhanced electron production of the remainder of the cathode fall. The cathode reabsorption effect is not dependent on the perturbation assumption under which this analysis takes place because it occurs so close to the cathode. In Fig. III.13, the electron multiplication for 0.3 T can be seen to be already declining, due to cathode reabsorption. Optimal electron multiplication must take place for a magnetic field between 0.1 and 0.3 T. In the He:N₂:CO₂ cathode region, the effects of a magnetic field are again not as dramatic as in He. The growth in electron flux peaks between 0.05 and 0.1 T, with the electron reabsorption at the cathode not playing a role even with fields of 0.3 T. The decrease in reabsorption *vis a vis* He is due probably to more inelastic collisions reducing the kinetic energy of electrons below the value at which they might still return to the cathode. The effect of the magnetic field in general is not as important in the He:N₂:CO₂ mixture as in He because the EDEF does not have the large numbers of collisionless electrons to be harnessed for ionization which the He discharge does.

Electron production beyond the cathode region is normalised to the number of initial electrons, and is given in Tables III.1 and III.2. The observed sensitivity to the magnetic field shows the effect of a magnetic field on the number of high energy electrons beyond the cathode region. The increased post-D_c production in the 0.05 and 0.1 T He cases indicates an

optimal magnetic field for an electric field reversal. Such a reversal may also be present, for fields less than 0.05 T, in the He:N₂:CO₂ mixture. It is not possible to identify exactly where ionization takes place on the basis of these results. Specifically, in these simulations so few sufficiently energetic electrons persist past $z=D_c$ that an accurate estimate of their spatial distribution is unobtainable. Also, to ensure the termination of a simulation, a field reversal could not be introduced into the model of the cathode region. However, in a self-sustained, high pressure discharge (30 Torr) typical of CO₂ lasers, significant ionization of the bulk does not occur due to electrons emitted from the cathode. Essentially all the ionization occurs near the cathode. This suggests that a potential minimum may exist in the vicinity of the negative glow in these self-sustained, high pressure devices.

D. Conclusions

Previous investigations into the effects of transverse magnetic fields in CO₂ lasers have concentrated on the dispersal of incipient current instabilities. This study has investigated the effects of transverse magnetic fields on the EDEF in the cathode region and on ionization in the cathode region.

The principle effect of a strong magnetic field on the He:N₂:CO₂ cathode region is to promote collisions. A straightforward application of an effective pressure model to account for the magnetic deflection fails to account for the energy dependence of the electron molecule collision cross-sections, especially those of the highest energy electrons. These electrons, which have long mean free paths, are impeded by looping trajectories. As a result, the stronger the magnetic field, the fewer the highest energy electrons able to escape the cathode region. Their energy is expended in inelastic collisions and increased ionization in the cathode region. The increased heating of the cathode region is of minor importance.

Two results pertinent to glow discharge performance have been presented. First, there is a magnetic field strength which provides the greatest multiplication of charge carriers in and beyond the cathode region. This multiplication can be significant, depending on the gas

involved. Second, the magnetic field causes ionizations to occur in a confined region close to the cathode. This can lead to a local potential minimum in the negative glow for some values of magnetic field strength. Together, these results could, in effect, reduce the cathode fall of the discharge. The implication for CO₂ laser design is that the application of modest strength transverse magnetic fields to the cathode region can both stabilise the discharge and improve its electrical efficiency.

REFERENCES

- [1] H.J.J Seguin, C.E. Capjack, D. Antoniuk, K.A. Nam, Appl. Phys. Lett., **37**, 130 (1980).
- [2] C.E. Capjack, D.M. Antoniuk, H.J.J. Seguin, J. Appl. Phys., **52**, 4517 (1981).
- [3] D.M. Antoniuk, C.E. Capjack, H.J.J. Seguin, J. Appl. Phys., **55**, 708 (1984).
- [4] D.M. Antoniuk, H.J.J. Seguin, C.E. Capjack, Appl. Phys. B, **35**, 155 (1984).
- [5] R. Razdan, C.E. Capjack, H.J.J. Seguin, J. Appl. Phys. **57**, 4954(1985).
- [6] R. Razdan, C.E. Capjack, H.J.J. Seguin, Appl. Optics **25**, 2915(1986).
- [7] A.E.D. Heylen, C.L. Dargan, Int. J. Electron., **35**, 433 (1973).
- [8] V.A. Seguin, H.J.J. Seguin, C.E. Capjack, S.K. Nikumb, Appl. Phys. B, **43**, 127 (1987).
- [9] R.A. Gottscho, A. Mitchell, G.R. Scheller, Y.-Y. Chan, D.B. Graves, Phys. Rev. A, **40**, 6407 (1989).
- [10] Tran Ngoc An, E. Marode, P.C. Johnson, J. Phys. D **10**, 2317(1977).
- [11] J.P. Boeuf, E. Marode, J. Phys. D **15**, 2169(1982).
- [12] M. Ohuchi, T. Kubota, J. Phys. D **16**, 1705(1983).
- [13] S. Hashiguchi, M. Hasikuni, Jap. J. Appl. Phys. **27**, 1010(1988).
- [14] R.J. Carman, A. Maitland, J. Phys. D **20**, 1021(1987).
- [15] R.J. Carman, J. Phys. D **22**, 55(1989).
- [16] K.H. Schoenbach, H. Chen. G. Schaefer, J. Appl. Phys., **67**, 154 (1990).
- [17] M. Surendra, D.B. Graves, G.M. Jellum, Phys. Rev. A, **41**, 1112 (1990).
- [18] A. von Engel, *Ionised Gases* (Oxford University Press, London, 1965), p. 229.
- [19] H.A. Blevin, S.C. Haydon, Austral. J. Phys., **340** (1958).
- [20] P. Gill, C.E. Webb, J. Phys. D **10**, 299(1977).
- [21] A.E.D. Heylen, IEE Proc., **127**, Pt. A, 221 (1980).

IV. Magnetic laser discharge stabilisation - scaling to high pressure systems

2

A. Introduction

Pulsed, high pressure glows have long been utilised in TEA geometries for the extraction of intense optical radiation from CO₂ and excimer laser systems. Historically such discharges have been characterised by short discharge running times and low recurrence rates. However, in recent years there has been a growing demand in the area of industrial materials processing for lasers that can simultaneously deliver both high peak and high average power. Laser developers have sought to satisfy this requirement by an extension to higher repetition rates and pulse-stretching in these high pressure discharge devices. Higher repetition rates have been achieved through incorporation of gas-transport concepts into TEA laser designs. Also some success in pulse stretching has been obtained with electron beam pumped devices.¹ However, stretched-pulse performance in lasers utilising glow discharge pumping has proven to be a formidable task. High pressure glows which feature elevated electrical energy deposition are also characterised by a relatively short stable running interval. Thus, an initially uniform and distributed glow is soon observed to collapse into a constricted arc. This critical glow-to-arc transition time is strongly dependent upon the level of excitation imposed, but relatively insensitive to the method of preionisation. Typical stable discharge operation times are a few microseconds in CO₂ lasers and only a few tens of nanoseconds in excimer systems.^{2,3}

It has been documented that magnetically induced $\mathbf{J} \times \mathbf{B}$ forces within the space charge sheaths of a glow can be employed to extend the threshold for glow-to-arc transitions in low and medium pressure CW discharges. The investigation reported here examines the feasibility of extending these magnetic stabilisation concepts to high pressure, pulsed glows. A simplified analytical model will be developed with the help of a large Monte Carlo simulation code to

¹A version of this chapter has been accepted for publication. Capjack, C.E., Labun, A.H., Seguin, H.J.J., and Bilida, W.D., J. Appl. Phys.

give a scaling law for the magnetic field that is required to affect discharge stability as a function of gas pressure.

B. Instability mechanisms

Various instability mechanisms can become manifest in laser gas discharges as documented by extensive theoretical and experimental work.^{4,18} The more common of these include attachment-induced ionisation and thermal instabilities as well as streamer formation. In the first mechanism, electron attachment results in the creation of striations or ionisation waves throughout the plasma volume. Although this process is essentially independent of pressure or electric power density, it is strongly dependent upon electron temperature. In the case of normal TEA discharges, the electron temperature in the overvoltaged plasma is sufficiently high that this instability does not pose a problem.

Streamer formation is more important in high E/N discharges where large ionisation coefficients produce copious electron avalanches.⁵ When the space charge fields of such an avalanching head become comparable to the applied electric field, subsidiary electrons are initiated through photoionisation, which in turn create a conducting filamentary channel. Since the sequence of events involved in streamer formation proceeds in times much shorter than mobility-restricted electron transit times, this process will not be considered here.

Thermal instabilities result from localised gas heating and usually lead to discharge constriction. Heating of the plasma occurs whenever the power transferred to the vibrational modes of a molecule decays into translational energy. This process is very pressure dependent. In general, the limit to the electric power density that a plasma can sustain without becoming unstable can be determined from a consideration of each of the mechanisms outlined above. However, for the experimental conditions of interest in this study, thermal processes dominate. Thus, the only mechanism addressed in this paper is the effect of a profiled magnetic field on thermal instabilities.

C. Magnetic discharge stabilisation concept

Magnetic stabilisation of thermal instability modes involves the generation of a transverse discharge velocity^{6,7} within the ion and electron sheaths near the cathode surface. The transverse discharge velocity is defined as the speed at which electron regenerative processes are displaced laterally by $\mathbf{J} \times \mathbf{B}$ forces. Such a magnetic stabilisation process is depicted in Fig. IV.1 where the effect of a transverse magnetic field is to displace the electron avalanche in the $\mathbf{E} \times \mathbf{B}$ direction. In this figure, the cathode is located in the plane $y = 0$, the avalanching electron trajectory is shown by a dashed line, and the ion trajectory is given by the dotted line. The cathode fall region is located between $y = 0$ and $y = d_c$. The corresponding ion trajectories to the cathode surface are unaffected by the magnetic field because the ion Hall parameter β_i is typically < 1 . This transverse flow serves to disperse any localised nonuniformities in current density which may arise throughout the discharge cross section. The magnetic field requirements are determined by the condition that the transverse velocity be sufficiently large that any discharge nonuniformities are swept at a distance much larger than the instability scale length in a time interval less than the instability growth time. A minimum magnetic field requirement that results from this condition is derived in the following sections.

D. Scaling law for the transverse discharge velocity

An estimate for the transverse discharge velocity is obtained by using the following simplifying assumptions: (i) the ion Hall parameter is < 1 so that $v_{iy} = \mu_i E_y$ and (ii) the time taken by an electron avalanche to travel a distance y in the cathode fall region is $<$ ion transit return time ($\tau_i(y)$). With these approximations the discharge velocity can be expressed as

$$v_{ir} = \int_0^{d_c} \frac{D(y)N(y)}{\tau_i(y)} dy / \int_0^{d_c} N(y) dy \quad (1)$$

where $D(y)$ is the deflection of an electron avalanche starting at $x = 0$, $N(y)$ represents the

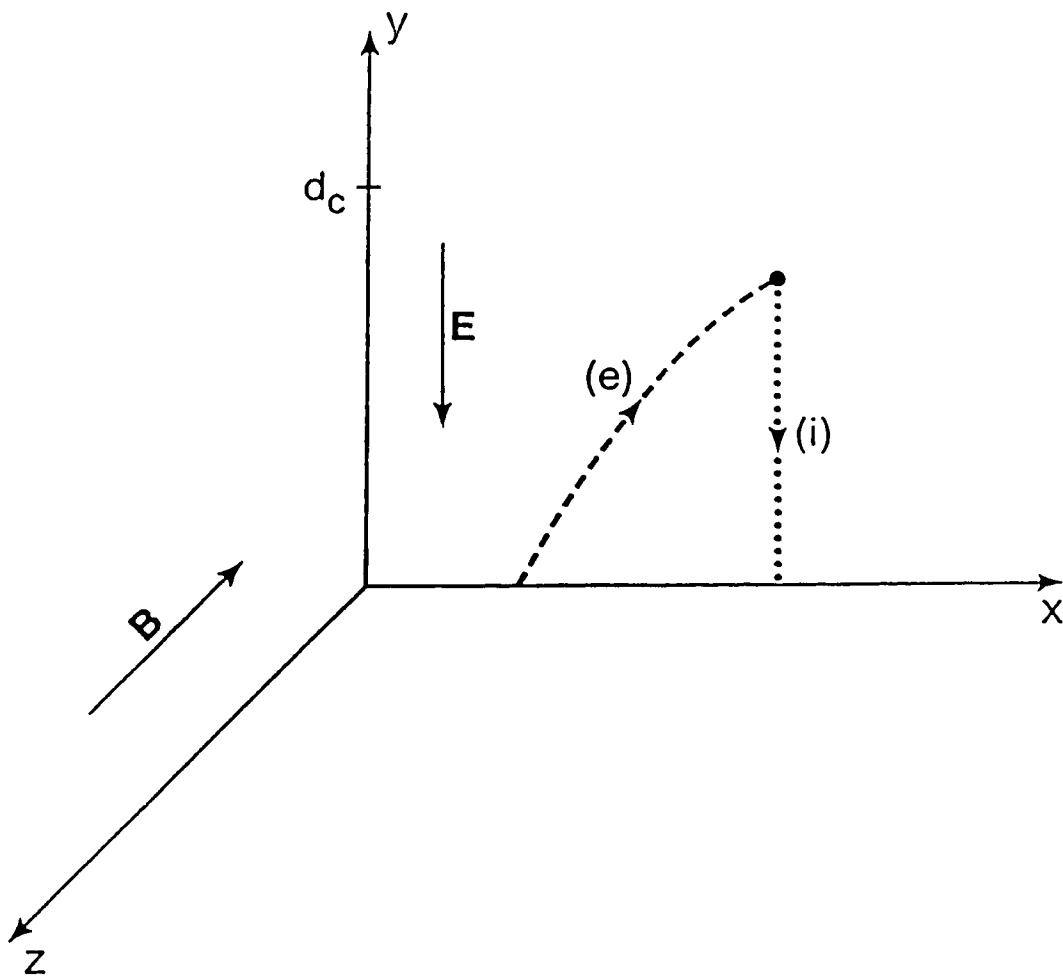


Fig. IV.1 Geometry of a magnetised cathode glow discharge region.

distribution of ionising collisions and $\tau_f(y)$ is the time taken by an ion created at y to return to the cathode and d_c is the cathode fall distance. Approximate expressions for each of the quantities in Eq. (1) are now developed.

The first term to be evaluated in Eq. (1) is the lateral displacement (in the x -direction) of the ionising collisions. A description of the dynamics of a magnetised cathode fall region is complicated by the nonequilibrium nature of this region. One successful approach has been the use of Monte Carlo codes as reported by Razdan *et al.*⁶ and Labun *et al.*⁸ As mentioned earlier, the gas medium is assumed to be weakly ionised (fractional ionisation is typically 10^{-7}) and the neutral flow velocities are assumed to be much less than the charged particle velocities. In this limit, the electron mobilities in the directions parallel to the electric field and perpendicular to the magnetic field (μ_{\parallel}) and transverse to both the electric and magnetic fields (μ_{\perp}) are given by⁹

$$\mu_{\parallel} = \frac{\mu_e}{1 + \beta_e^2} \quad \mu_{\perp} = \frac{-\mu_e \beta_e}{1 + \beta_e^2} \quad (2)$$

where $\mu_e = -e/\nu_{en}m$ is the electron mobility, β_e is the electron Hall parameter; ν_{en} is the electron collision frequency for momentum transfer (assuming only collisions with neutrals). By using Eq. (2), the lateral deflection (in the x -direction) of an electron avalanche in a transverse magnetic field can be approximated as

$$D(y) = \int_0^y \beta_e i' w \, dw \quad (3)$$

Although Eq. (3) appears to be simple, its evaluation is complicated because of the non-equilibrium nature of the cathode fall region. However, it will be shown that if a fixed laser gas mixture is considered (in this case a CO₂ laser mixture comprised of He:N₂:CO₂ in the ratio [20:8:2]), then a single Monte Carlo simulation⁸ may be used to determine the spatial dependence of parameters such as β_e , the electron energy, and the avalanche growth for arbitrary gas pressures. The argument to be developed is subject to the condition that the magnetic pressure \ll kinetic pressure.

The electric field strength within the cathode fall region is assumed to have a linear dependence given by $E(y) = (2V_c/d_c)(1 - y/d_c)$ where V_c is the cathode fall potential. The cathode fall potential is independent of pressure and is taken as¹⁰ 150 V for He, 215 V for N₂, and 450 V for CO₂. For the assumed gas mixture, $V_c = 187$ V. The pressure-cathode fall distance product is independent of pressure and is set to¹⁰ 1.3×10^{-2} m.Torr for He, 4.2×10^{-2} m.Torr for N₂, and 4.0×10^{-2} m.Torr for CO₂. For the assumed gas composition, $pd_c = c_1$ where the constant $c_1 = 2.25 \times 10^{-2}$ m.Torr.

An important parameter in laser discharges is the ratio E/N where N is the neutral gas density and E the electric field strength. It can be shown that the electron energy distribution function is related to the value of E/N in an equilibrium discharge.¹¹ By using the calculated value of V_c and noting that pd_c is constant

$$E_{av}/N = \frac{1.04 \times 10^{-25}}{c_1} V_c T(^{\circ}\text{K}) \quad (\text{V m}^3) \quad (4)$$

where $E_{av}/N = V_c/d_c N$. Equation (4) suggests that as a first approximation, the value of E/N in the cathode region of a glow discharge can be regarded as being independent of pressure. The implications of $pd_c = \text{constant}$ and E/N being independent of pressure is that the electron energy distribution and the relative electron avalanche growth in the cathode fall region are also independent of pressure. Thus the Monte Carlo simulations by Labun *et al.*⁸ in which the electron mean energy and ionisation production are obtained at a particular gas pressure may be used to approximate the dynamics occurring in cathode regions at arbitrary pressures. Results are given in Fig. IV.2 for a 30 Torr laser gas mixture with magnetic field strengths of 0 and 0.1 Tesla. The assumed gas temperature in the cathode fall region is 600°K. The results in Fig. IV.2 show a weak dependence upon the magnetic field strength; thus in the following analysis the electron energy distribution and ionisation growth will be approximated by the results for which $B = 0$.

The calculation of the electron Hall parameter within the cathode region requires information regarding the electron energy and the electron mean free path. Values for the

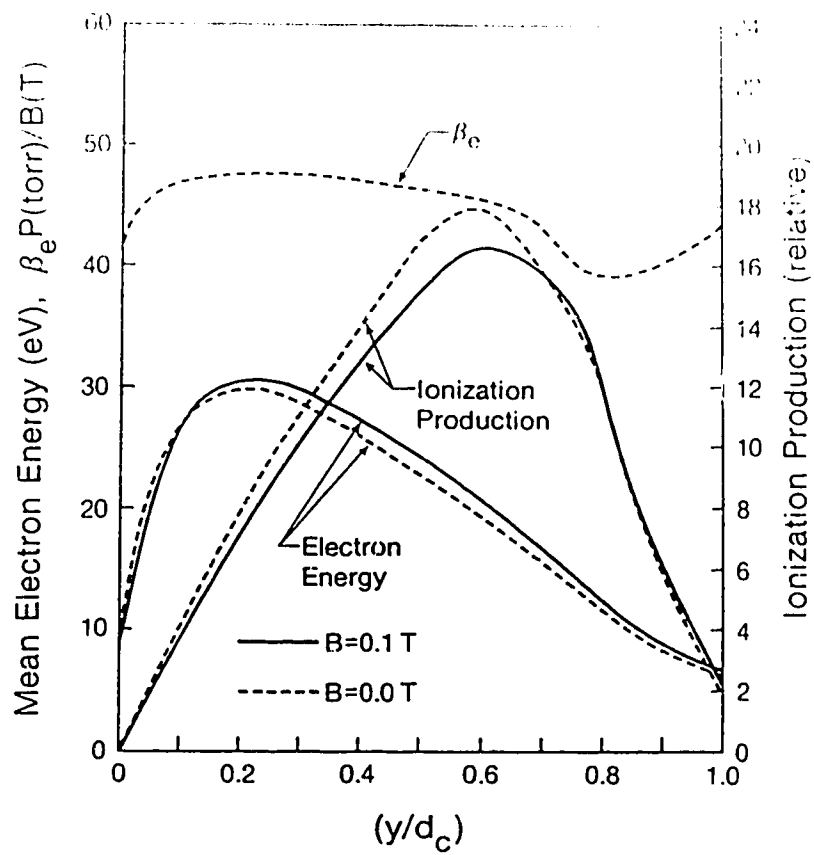


Fig. IV.2 Monte Carlo simulation results for the average electron energy and ionisation distributions and β_e ($B=0\text{ T}$) for a [20:8:2] laser mix.

electron mean free paths in CO₂, N₂, and He were taken from Labun *et al.*⁶ and were adjusted to account for differential scattering effects^{6,12} in calculating the momentum transfer collision frequency. The resulting temperature dependence of the electron Hall parameter is given in Fig. IV.3 over a temperature range of 1 to 60 eV for a He:N₂:CO₂ mixture with proportions [20:8:2].

The plot of β_e given in Fig. IV.2 has been calculated by using the energy dependence of β_e given in Fig. IV.3 and the average electron energy distribution given in Fig. IV.2. The lateral deflection of the electron avalanche $D(y)$ shown in Fig. IV.4 was calculated by using Eq. (4). Also included in Fig. IV.4 are the Monte Carlo simulation results for the mean values of the lateral displacement of the ionisation events within the cathode region. In the simulation, a 30 Torr gas mixture [20:8:2] and a 0.1 T magnetic field have been assumed. The results in this figure show that the use of an electron mobility calculated for "average energy" electrons has resulted in an underestimate of the actual displacement of ionisation events. This is expected since electrons involved in ionisations typically have energies much higher than average. They are therefore more prone to "forward scattering" which in effect translates to a larger mean free path and hence a higher effective value of β_e . Unfortunately, "single particle" effects are not well described by a fluid description of the cathode region. For example, with the above discharge parameters the Langevin equation¹³ predicts maximum electron energies of less than 3 eV in the cathode region. The utility of the results given by Figs. IV.2 to IV.4 and Eq. (3) is that the avalanche deflection $D(y)$ shows a (B/p) scaling with the magnetic field strength and the gas pressure. This will be used in the development of a scaling law for the transverse discharge velocity.

The spatial dependence of $N(y)$ in Eq. (1) was obtained by a spline fit to the ionisation production curve in Fig. IV.2. The remaining term in Eq. (1) is the ion transit time $\tau_i(y)$. By using the assumed linear dependence for $E(y)$ this may be shown to be

$$\tau_i(y) = \frac{-d^2}{2\mu_i V_c} \ln\left(1 - \frac{y}{d}\right) \quad (5)$$

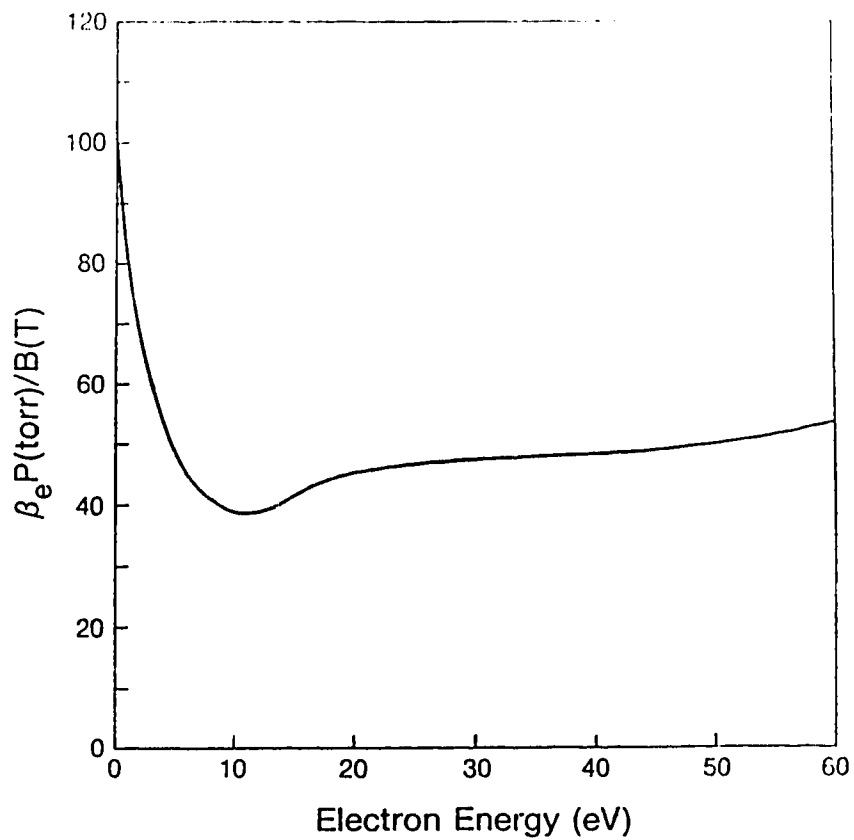


Fig. IV.3 Electron Hall parameter as a function of electron energy for a 30 Torr laser mixture of He:N₂:CO₂ in the proportions [20:8:2].

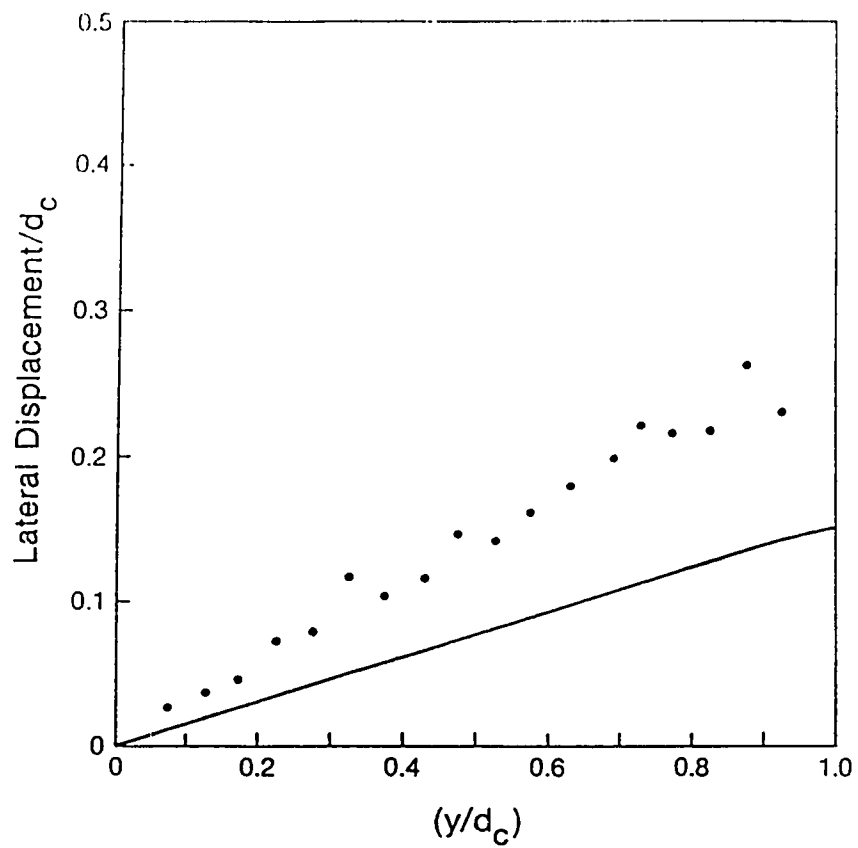


Fig. IV.4 The lateral displacement of the electron avalanche according to Eq. (3). The dots are Monte Carlo results. The magnetic field strength is 0.1 T.

where μ_i is the ion mobility. In the following analysis μ_i will be approximated by a weighted value based upon the fractional distribution of ionising collisions between the three species involved. The results from the Monte Carlo simulations indicate that approximately 12% of the ionising collisions involved He, 65% involved N_2 , and 23% involved the CO_2 molecule when a [20:8:2] laser mix was used. Values used for the various ion mobilities were taken from von Engel¹⁴ and Ellis *et al.*^{15,16} The value used in Eq. (5) for μ_i is 0.53 m²/Vs for a [20:8:2] laser mix at a pressure of 1 Torr.

By substituting Eqs. (3) and (5) into Eq. (1), the transverse discharge velocity can be expressed as

$$v_{tr} = \frac{-4.0 \times 10^5 B}{p} \int_0^1 \frac{Y N(Y)}{\ln(1-Y)} dY / \int_0^1 N(Y) dY \quad (6)$$

or

$$v_{tr} = c_{tr} \frac{B}{p} \text{ (m/s)} \quad (7)$$

where $c_{tr} = 2.7 \times 10^5$, $Y = (y/d_c)$, B is the magnetic field strength in Tesla, p is the pressure in Torr, and the spatial dependence of the ionisation $N(y)$ is approximated by a spline fit to the ionisation curve (for $B = 0$) in Fig. IV.2.

It is interesting to compare the value of v_{tr} that is obtained using Eq. (7) with that found using the Monte Carlo code described by Labun *et al.*⁸ For the case of a laser mix of He: N_2 : CO_2 with ratios [20:8:2] at a total pressure of 30 Torr and a magnetic field strength of 0.1 T, Eq. (7) predicts a transverse velocity of 900 m/s. The simulation results predict a velocity of 1700 m/s. As explained earlier, the discrepancy is due to the underestimate of the lateral deflection of the electron avalanche when a fluid description is used to describe electron behaviour. If the value of the constant c_{tr} is adjusted to 5.1×10^5 in order to make Eq. (7) agree with the Monte Carlo results for these particular operating conditions, Eq. (7) will then give excellent agreement with the Monte Carlo simulations over a wide range of magnetic field strengths and gas pressures. This is shown in Table IV.1.

The simple expression given by Eq.(7) is seen to accurately duplicate the results obtained from computationally intensive Monte Carlo simulations and also give a scaling law for the transverse discharge velocity within a magnetised cathode fall region. Data sets that have been used to give the adjusted value for c_{ir} for various gas mixtures are denoted by an asterisk in Table IV.1. Table IV.2 summarises the value to be used for c_{ir} for other standard laser gas mixtures.

Magnetic discharge stabilisation is expected to be effective if within an instability growth time^{4,18} τ_d , the regenerating electron avalanche is laterally displaced a distance much larger than either the instability transverse scale length or the discharge gap distance. If this distance is denoted by L_d , the discharge can be assumed to be stabilised if $v_{ir}\tau_d \gg L_d$. By using Eq. (7) in this relationship, the required magnetic field strength is given by

$$B \gg \frac{p L_d}{c_{ir} \tau_d} \quad (8)$$

An estimate for the instability formation time τ_d can be obtained from Haas⁴ and Nighan and Wiegand.¹⁸ Plots of τ_d as a function of total gas pressure and electrical power loading are given in Nighan and Wiegand¹⁸ for a laser gas composition in proportions [0.60:0.35:0.05].

An indication of how large the inequality in Eq. (8) must be in order for discharge stability to be assured can be obtained by an examination of the low pressure magnetic stabilisation experiments performed by Seguin *et al.*¹⁷ When He:N₂:CO₂ mixtures in the amounts 20:8:2 Torr were used, stable discharges were obtained when magnetic field strengths of 0.05 T were used. By assuming an instability formation time of 1 ms and a 0.01 m scale length,¹⁸ magnetic stabilisation is seen to be effective when $B \approx 85 p L_d / (c_{ir} \tau_d)$.

E. Required magnetic field – scaling law

An approximate pressure scaling law for the required magnetic field can be determined by an examination of the various terms in Eq. (8). First there is an explicit dependence upon the pressure p . The pressure dependence of τ_d can be inferred by an examination of Fig. 3 in

Table IV.1 Comparison of v_{tr} obtained from Monte Carlo and fluid model (Eq. (7)) predictions.

Mixture [CO ₂ :N ₂ :He]	Pressure (Torr)	Magnetic Field (Tesla)	v_{tr} (m/s) (Monte Carlo)	v_{tr} (m/s) (Eq. (7))
[20:8:2]	30	0.1	1.71x10 ³	1.71x10 ^{3*}
	90	0.3	1.71x10 ³	1.71x10 ³
	30	0.3	5.03x10 ³	5.13x10 ³
	90	0.1	5.82x10 ²	5.70x10 ²
[8:1:1]	30	0.1	2.40x10 ³	2.40x10 ^{3*}
	90	0.3	2.40x10 ³	2.40x10 ³
	30	0.3	7.88x10 ³	7.20x10 ³
	90	0.1	6.74x10 ²	8.00x10 ²
[12:7:1]	20	0.1	2.06x10 ³	2.06x10 ^{3*}
	200	0.5	0.98x10 ³	1.03x10 ³
[3:1:1]	30	0.1	1.06x10 ³	1.06x10 ^{3*}
	90	0.1	3.53x10 ²	3.53x10 ²

Table IV.2 Values of c_{tr} for various CO₂ laser mixtures.

Mixture He:N ₂ :CO ₂	c_{tr}
[20:8:2]	5.1×10^5
[8:1:1]	7.2×10^5
[12:7:1]	4.1×10^5
[3:1:1]	3.2×10^5

Nighan and Wiegand.¹⁸ The purpose for using a higher gas pressure in a laser discharge is so that larger power loading may be sustained. The results in the cited figure suggest an inverse pressure dependence for τ_d . If L_d is approximated as constant, the pressure scaling for the required magnetic field strength is given by

$$B \propto p^2 \quad (9)$$

The pressure scaling given by Eq. (9) unfortunately implies that the extension of the magnetic discharge scaling concept to higher pressure gas mixtures will be an experimentally challenging task because of the large magnetic field strengths that will be required. This difficulty has recently been confirmed in the experiments performed by Bilida¹⁸ where an attempt was made to magnetically stabilise high pressure laser gas discharges. In these experiments, a laser gas composition of [74:14:12] was used at total pressures ranging from 250 to 500 Torr. The maximum available magnetic field strength was 0.4 T. Based upon the successful low pressure experiments of Seguin *et al.*¹⁷ where magnetic field strengths of 0.05 T were used with 30 Torr mixtures, Eq. (9) suggests that magnetic field strengths of at least 3.5 Tesla would be required. The null results obtained in the high pressure experiments¹⁸ are therefore consistent with the scaling suggested by Eq. (9).

F. Conclusions

The magnetic discharge stabilisation technique is based upon the generation of a transverse discharge velocity within the cathode sheath region of a glow discharge which serves to disperse any localised nonuniformities in the current density in a time less than the discharge instability time. A pressure scaling law for this velocity has been obtained by combining results from a Monte Carlo simulation of a magnetised cathode sheath region with expressions for the electron mobilities in a partially ionised gas in the presence of crossed electric and magnetic fields. An important argument in this development is that both the pressure-cathode fall distance product and the value of E/N (in the cathode region) are

independent of pressure (to first order). This enabled the determination of the spatial dependence of quantities such as the electron Hall parameter, the electron energy distribution, and the avalanche growth for discharges at an arbitrary pressure from a single Monte Carlo simulation. The expression for the transverse discharge velocity has a simple (B/p) dependence which is in excellent agreement with the results obtained from complex Monte Carlo simulations for a wide range of discharge conditions.

Magnetic discharge stabilisation is expected to be effective when the lateral displacement of the regenerative electron avalanches within an instability formation time is much larger than the transverse instability scale length or the discharge gap distance. By noting that the instability time varies inversely with pressure (if the power loading is also increased), the required magnetic field is seen to scale as the pressure squared. Unfortunately, the implication of this strong pressure scaling is that the magnetic stabilisation technique is best suited to low or medium pressure laser gas discharges. For higher pressure systems, the cost and complexity of producing a very strong cathode magnetic field may render the approach impractical, unless very strong permanent magnets can be obtained.

REFERENCES

- [1] D.B. Cohn, H. Komine, IEEE J. Quantum Electron. **QE-19**, 786 (1983).
- [2] I. Okuda, Y. Owadano, T. Kasai, Y. Matsumoto, A. Yaoita, M. Tanimoto, F. Nemoto, S. Komeiji, M. Yano, Proc. of the 6th Intl. Conf. on High Power Particle Beams, Beam '86, 1986, Kobe, Japan.
- [3] K. Veda, H. Nishioka, H. Takuma, SPIE **710**, Excimer Lasers and Optics, 7 (1986).
- [4] R. Haas, Phys. Rev. A **8**, 1017 (1973).
- [5] G.A. Mesyats, Yu.I. Bychkov, V.V. Kremnev, Soviet Physics Uspekhi **15**, 282 (1972).
- [6] R. Razdan, C.E. Capjack, H.J.J. Seguin, J. Appl. Phys. **57**, 4954(1985).
- [7] R. Razdan, C.E. Capjack, H.J.J. Seguin, Appl. Phys. Lett. **48**, 1513 (1986).
- [8] Chapter III of this thesis.
- [9] N.A. Krall, A.W. Trivelpiece, *Principles of Plasma Physics*(McCraw-Hill, New York, 1973),p.329.
- [10] A. von Engel, *Ionised Gases* (Oxford University Press, London, 1965), p. 229.
- [11] W.J. Witteman, *The CO₂ Laser* (Springer Verlag, New York, 1987).
- [12] T.W. Shyn, Phys. Rev. **22**, 916 (1980).
- [13] B.S. Tanenbaum, *Plasma Physics*, (McGraw-Hill, NewY York, 1967).
- [14] A. von Engel, *Electric Plasmas: Their Nature and Uses* (Taylor and Francis Inc., New York, 1983),p. 133.
- [15] H.W. Ellis, E.W. McDaniel, Atomic Data and Nuclear Data Tables **22**, 179 (1978).
- [16] H.W. Ellis, R.Y. Pal, E.W. McDaniel, Atomic Data and Nuclear Data Tables **17**, 177 (1976).
- [17] V.A. Seguin, H.J.J. Seguin, C.E. Capjack, Appl. Optics **24**, 1265 (1985).
- [18] W.D. Bilida, M.Sc. Thesis, The University of Alberta, 1989.

V. A spark channel plasma electrode for a CO₂ laser gas discharge.

A. Introduction

High power transverse discharge carbon dioxide lasers excited by dc glow discharges presently achieve an electrical (wallplug) efficiency of approximately 10%. Unfortunately, this value is considerably lower than their quantum efficiency of 40%. Much of the inefficiency in these devices is due to the electrical sheath potentials (falls) surrounding the electrodes. In these discharges, the pumping current must pass through all regions of the glow, namely the cathode fall region, the positive column, and the anode fall region. The cathode fall for planar electrodes is typically 150 to 200 V,¹ while the anode fall is somewhat less. Even greater sheath potentials are incurred in many modern lasers which do not employ planar electrodes. For example, in the non-self-sustained PIE (Photo-initiated, Impulse-enhanced, Electrically-excited) high power laser featuring multi-element pin-type electrodes, cathode and anode falls are typically in the range of 300 V to 420 V.^{2,3} Since the total discharge voltage in such devices is usually around 2000 V, it follows that a substantial fraction of the electrical drive power is wasted in these small electrode sheaths. Such power deposition contributes to gas heating and instability, but unfortunately not to optical output.

The relatively large power loss in the electrode sheaths of the PIE laser prompted an investigation aimed at enhancing the overall efficiency of this type of device, through a reduction in cathode and anode falls. The technique chosen for negating these potentials was the generation of a **plasma electrode**. A plasma electrode is a high density plasma layer immediately adjacent to a metal electrode surface which effectively eliminates the normal space charge sheaths.⁴ Such a plasma layer therefore acts as a "virtual electrode" and a source of charge carriers for discharge current. This paper presents the results of a preliminary experiment in a gas laser discharge system fitted with such a plasma electrode device. The data

¹A version of this chapter has been accepted for publication: A.H. Labun, H.J.J. Seguin, C.E. Capjack, Appl. Phys. B.

suggest that the cathode and anode falls of the pumping glow discharge can indeed be minimised, if not completely eliminated, using this approach. The improvements documented in this investigation for a non-self-sustained CO₂ laser plasma may also be applicable to other types of dc excited gas lasers.

The cathode fall region

In a self-sustained glow, ions and electrons which carry current are produced primarily in the cathode fall region. In effect, the cathode fall maintains the dc discharge current through electron impact ionisation of the bulk gas. Specifically, electrons are emitted from the cold cathode surface through the mechanisms of ion bombardment (at rates of about 1 emitted electron per 20 incident ions) and the photoelectric effect. These free electrons are then accelerated by the large electric field in the region, due to the net positive space charge created by the relatively immobile ions near the cathode surface. As they proceed through the cathode sheath, electrons collide with neutral species, occasionally ionising them. Due to avalanching of this ionisation, the number of free electrons grows rapidly. Thus, the current in the discharge undergoes a transition from being ion-dominated near the cathode surface to being electron-dominated near the boundary of the cathode fall region. In the positive column, the discharge current is primarily an electron current. Although little additional ionisation occurs in this most important region of self-sustained laser plasmas, charge carriers are generated throughout the positive columns of externally ionised discharges. Such is the case with the PIE discharge, in which the positive column is irradiated with ultraviolet radiation.⁵ This process results in copious electron production throughout the inter-electrode volume. Experiment has shown that although external ionisation can greatly reduce the positive column voltage by increasing the bulk conductivity, the cathode fall itself is not significantly affected by the degree of external ionisation.⁶ In particular, measurements of the cathode falls on pin electrodes in PIE discharges over a wide range of ionisation levels did not reveal any reduction due to ionisation.³ Thus, the picture of the cathode fall region

presented above is valid for both self-sustained and externally ionised systems.

It can be shown that the cathode region of a glow discharge is an inefficient ioniser. The reason for this is that the probability of an ionising collision, at the energies attained by the electrons between collisions, is lower than the probability of an inelastic collision. This result can be derived from the maximum mean energy of the electron flux in the cathode glow. In a 20:8:2 (He:N₂:CO₂) mix the value is typically around 33 eV.⁷ Based on electron-neutral collision cross-sections for this mixture, the probability of an ionising collision with that energy is 8%, while the probability of an inelastic collision is 11%.

In contrast to the above, it is found that the electron energy in a transient, high voltage arc is much higher than that in a glow, due to the greater accelerating potentials present. Also, electron-neutral collisions at higher energies favour ionisation. For example, a 100 eV electron has a 27% ionisation probability but only a 25% inelastic collision probability. Thus, collisional ionisation is more efficient in a high voltage arc than in a glow. The enhanced ultraviolet (UV) emission from high energy collisions also contributes to the ionisational efficiency of such arcs. It follows that in principal, the charge carrier production function of the cathode fall region could be performed by a high voltage arc, with a net saving in power consumption.

The PIE excitation process

In the PIE excitation approach of interest here, the high frequency repetitive application of sequential photo- and electron impact ionisation events are used to create and maintain an extended volume laser plasma appropriate for CO₂ vibrational pumping. A special "volume" pulser provides high frequency, high voltage impulses across the discharge gap (typically 5 kHz, ≈20 kV across 10 cm, rising at 200 GV/s). This generates a diffuse corona which photoionises the inter-electrode region and subsequently avalanches the resultant free electrons throughout the volume; thereby further increasing the electron density. Persistence of these repeated, impulse ionisation events is sufficient to support a continuous,

non-self-sustained glow. The electrodes commonly used in the PIE approach consist of many individually ballasted pins which provide excellent UV irradiation of the inter-electrode volume. This unique excitation technique creates an exceptionally stable and uniform gain medium suitable for high-quality beam extraction. A consequence of the pin geometry is that large electric fields are required to concentrate the current onto the limited pin surface area. This results in an increased energy loss, which in turn detracts from the overall system efficiency attainable with the PIE excitation technique.

The plasma electrode concept

Plasma electrodes are well known in pulsed discharges, examples of which include high-density plasmas formed by arcs of various kinds, including sliding discharges,^{8,9,10,11} vacuum surface breakdown,¹² and explosive filaments.¹³ In recent years, lasers featuring auxiliary high voltage discharges serving in the role of plasma electrodes have been developed. The overall energy requirements of these devices have been similar to those with conventional electrodes. Specifically, Gorkovskii *et al.*¹¹ developed a transversely-excited atmospheric (TEA) CO₂ laser with plasma cathode and anode. The device featured a laser chamber with a 150 mm X 150 mm cross-section and a maximum discharge potential of 240 kV, an energy deposition of 200 J/atm, and a maximum current density of 20 A/cm². Plasma sheets were generated by 70 kV pulses impressed across the surfaces of two planar electrodes (800 mm long). The plasma sheets consumed only 15% of the principal discharge energy and also served to ionise the volume. By means of these plasma electrodes, energy deposition into the discharge could be optimised for efficient laser operation while still maintaining excellent discharge stability and homogeneity. Since the main discharge was developed from an existing high-density plasma in contact with the metal electrodes, it exhibited no cathode fall. Thus, the instabilities mechanisms normally associated with the cathode were minimised.¹⁰ In pulsed TEA lasers, such as the one just described, the extremely high discharge potential makes the energy saving realised by eliminating the cathode and anode falls of little consequence.

However, the improved discharge characteristics and stability attained have provided more than ample motivation for incorporating plasma electrodes in these devices.

Reports of plasma electrodes have been very rare in continuous discharges; indeed, the only reported case has been the plasma jet laser developed by McLeary, Beckwith, and Gibbs.¹⁴ The most extensively investigated pulsed plasma electrode, the sliding discharge, is not amenable to continuous operation. In this context, and from a power consumption standpoint alone, it would not be feasible to continuously maintain a plasma sheet of extended area. Moreover, due to rapid ablation of the dielectric material covering the electrodes, an electrode lifetime of only 10^4 shots has been projected.¹¹ This detrimental effect is, however, unavoidable, since the ablation process appears essential for the generation of the spectral characteristics of an efficient sliding discharge.¹⁵ It follows that practical plasma electrodes, suitable for operation in continuous discharges, must feature short duration, high-voltage, free-space arcs in order to negate the deleterious erosion effects associated with continuous operation.

The plasma electrode technique described in this paper is based on the PIE technique described above. However, the PIE excitation is concentrated in a much smaller region in order to generate high current density transient arcs. Thus, just as repetitive PIE impulses can sustain an extended volume continuous glow, the same process can be adapted to create a much higher electron density in a limited region. For instance, Tholl¹⁶ reported 100% ionisation in an expanding spark channel in 460 Torr H_2 . The ionisation fraction diminished to only 70% after 3 μs of channel expansion. An extrapolation of this ionisation persistence to lower pressure suggests that the repetitive formation of transient arcs at a frequency of several kilohertz might indeed create an effective plasma electrode for a continuous laser discharge.

B. Plasma electrode operation

The plasma electrode experiments described here were conducted in a transverse discharge gas transport laser chamber fitted with a slow gas purge. A 35:14:1 Torr He:N₂:CO₂ mixture was used. Because of geometrical factors discussed later in this paper the normal level of UV irradiation of the discharge by the volume pulser was reduced. Thus, since CO₂ strongly absorbs UV radiation¹⁷, only a low CO₂ partial pressure permitted adequate external ionisation. Studies were also carried out in N₂ at 50 Torr. Gas flow velocity was 20 m/s. The plasma electrode was created by a double-pin electrode consisting of two water-cooled 3.2 mm diameter stainless steel rods, each terminated by a short transverse 3.2 mm stainless steel pin with blunt tips. These were in turn attached to 10.0 mm diameter steel sleeves surmounted by ceramic caps (Fig. V.1). The steel rods were mounted in a water-cooled cylindrical Delrin block. The spark under study was developed between the tips of the transverse rods. Since no deterioration of the pins was observed after extended periods of operation, an indefinite lifetime adequate for cw operating conditions is projected. An inductor connected both elements of the electrode to the dc power supply, thereby allowing dc current to be drawn through both ends of the plasma electrode spark. A standard fluid-ballasted multi-element structure¹⁸ served as the opposing electrode, and a fixed inter-electrode gap of 9.0 cm was used throughout the study (Fig. V.2).

The drive circuit used to create the plasma electrode in this investigation was a modification of that used in the normal PIE excitation technique.⁵ From Fig. V.3 the electrical system consisted of three parts: the dc sustainer; the volume pulser, which ionised the discharge; and the plasma electrode pulser. In this investigation the volume pulser and the plasma electrode pulser operated independently and were not synchronised. The pulsers operated in the following manner. During the inter-pulse period when the thyratrons were non-conductive, capacitors C₁ and C₂ charged to the input power supply potential. When the thyratrons were triggered, these capacitors discharged rapidly, inducing impulses in the floating portions of the circuit via high-speed pulse transformers. These two pulses rose at

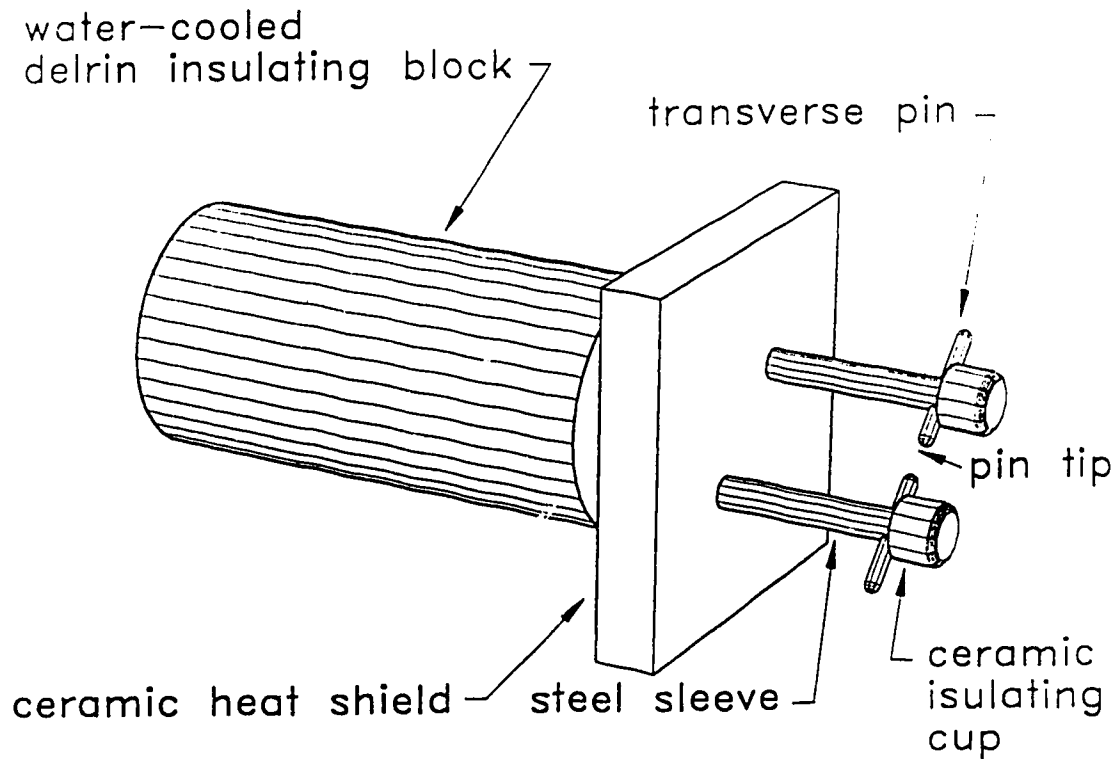


Fig. V.1 The double-pin electrode, with transverse pins fixed to two rods connected through the water-cooled Delrin block to the pulser circuits. The spark channel between the pin tips acts as a plasma electrode.

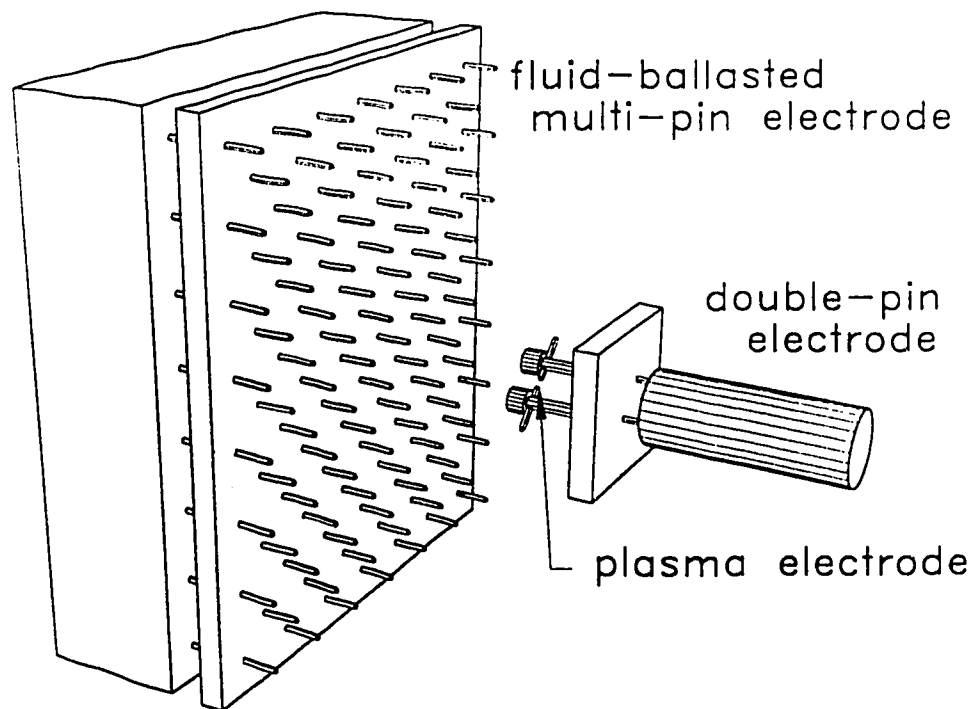
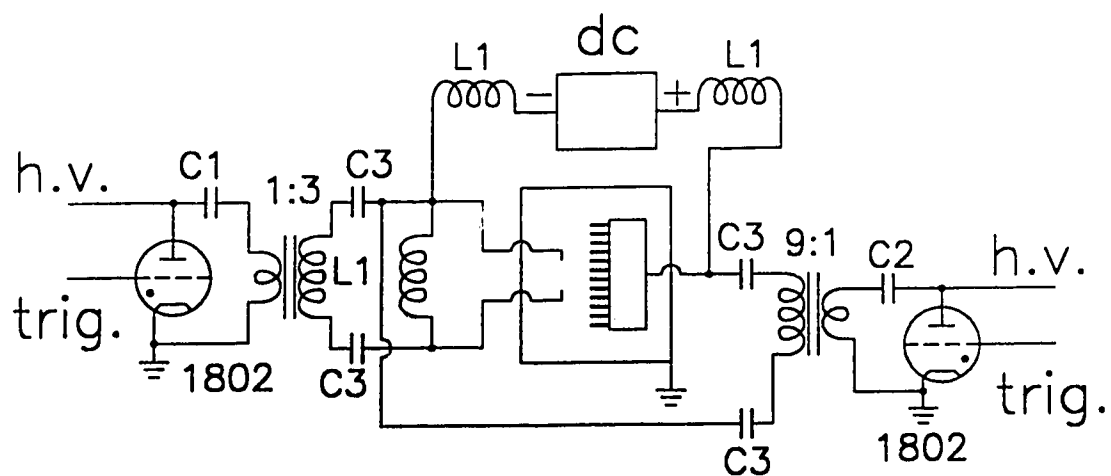


Fig. V.2 The discharge geometry. The positive column extends from the double-pin electrode to a broad region on the ballasted multi-pin electrode.



plasma
electrode
pulser

$$\begin{aligned} L1 &= 200 \mu \text{ H} \\ C1 &= 12 \text{ nF} \\ C2 &= 10 \text{ nF} \\ C3 &= 10 \text{ nF} \end{aligned}$$

volume
pulser

Fig. V.3 Discharge circuit schematic.

approximately 200 GV/s. The frequency of the volume pulser f_{PIE} was fixed at 5 kHz, while that of the plasma electrode pulser f_{pe} was varied. The pulse energy of the plasma electrode pulser was kept constant at all frequencies.

C. DC potential reduction measurements

As indicated previously, the principal goal in this investigation was to determine whether the cathode fall V_c and the anode fall V_a of a continuous discharge could be eliminated by means of plasma electrodes. Clearly, the simplest method of observing these potentials would be to place a probe near the double-pin electrode and observe the change when the plasma electrode was activated. When this was attempted, however, the probe shorted out the PIE corona. It thus became necessary to infer the changes in V_c and V_a from measurements of the dc power supply potential V_{tot} and current I . These inferences of changes in V_c and V_a were complicated by effects due to the pin electrode geometry and the PIE external ionisation process. A clear understanding of the influence of these factors on V_{tot} is necessary for interpretation of the data.

Potentials in externally ionised discharges

The relation of V_{tot} to the potentials of various regions within the discharge is given by

$$V_{tot} = V_c + V_{pc} + V_a + V_{bal} \quad (1)$$

where V_c is the cathode fall, V_{pc} is the positive column voltage, V_a is the anode fall, and V_{bal} is the potential across the fixed ballast resistance. The value of V_{pc} will be shown to be highly dependent on a number of discharge parameters. This often results in V_{pc} changing when V_c or V_a change. Therefore, in order to determine correctly what effect the plasma electrode has on V_c and V_a on the basis of measurements of changes in the supply potential δV_{tot} , it is necessary to properly account for variations in V_{pc} .

In a one-dimensional dc glow discharge of area A and length l , the value of V_{pc} depends on the conductivity σ , which in turn depends upon the gas density N and the electron density n_e :

$$V_{pc} = l \times I / (A \times \sigma(N, n_e)). \quad (2)$$

In terms of the quantities observed in this experiment,

$$V_{pc} = l \times I / (A \times \sigma(p, I, P_{PIE})). \quad (3)$$

The pressure p and the volume pulser power P_{PIE} together determine n_e , such that n_e increases with increasing P_{PIE} and decreases with increasing p . All three factors affect N , since I and P_{PIE} heat the gas and thereby reduce its density. Thus, V_{pc} is sensitive to several discharge parameters. This stands in contrast to V_c and V_a : their values are constant within the normal glow regime. The only exception occurs if the maximum normal glow current density is exceeded. In this case, V_c does increase, in the so-called abnormal glow.

Data collection

The experimental method used to obtain δV_{tot} was as follows. After the initial establishment of a fixed reference dc current I_{ref} at a given pulser power P_{PIE} , the plasma electrode was switched on. This action resulted in an immediate increase in I . V_{tot} was then decreased to re-establish I_{ref} . After this, the plasma electrode was switched off, and again I_{ref} was re-established by increasing V_{tot} .

Measurements were made of the reduction in the dc power supply potential δV_{tot} achieved by operating a plasma cathode in N_2 (Fig. V.4)¹⁹ and $He:N_2:CO_2$ (Fig. V.5) discharges. The value of δV_{tot} was seen to increase with f_{pe} over the range $0 < f_{pe} < 9$ kHz. No further change in δV_{tot} was observed for $f_{pe} > 9$ kHz. Consequently, this value of δV_{tot} was presumed to be the maximum obtainable by means of the plasma cathode, for a given P_{PIE} . The maximum δV_{tot} observed in Fig. V.5 (300 V) agrees with the value of V_c in the

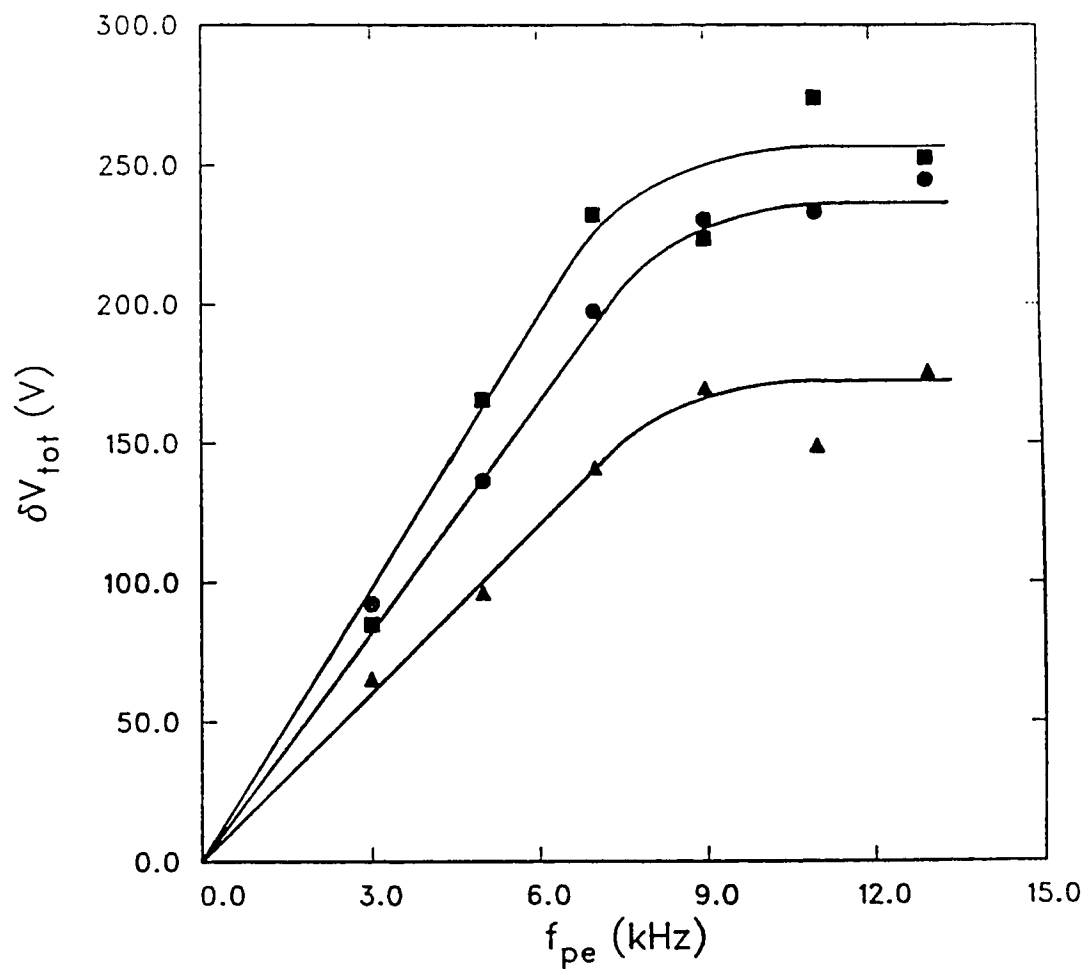


Fig. V.4 The overall potential reduction δV_{tot} vs. the plasma electrode frequency f_p for the N_2 plasma cathode. The closed squares represent data for $P_{PIE}=625$ W and $I=69$ mA, the closed circles represent data for 675 W and 54 ma, and the closed triangles represent data for 725 W and 89 mA, respectively.

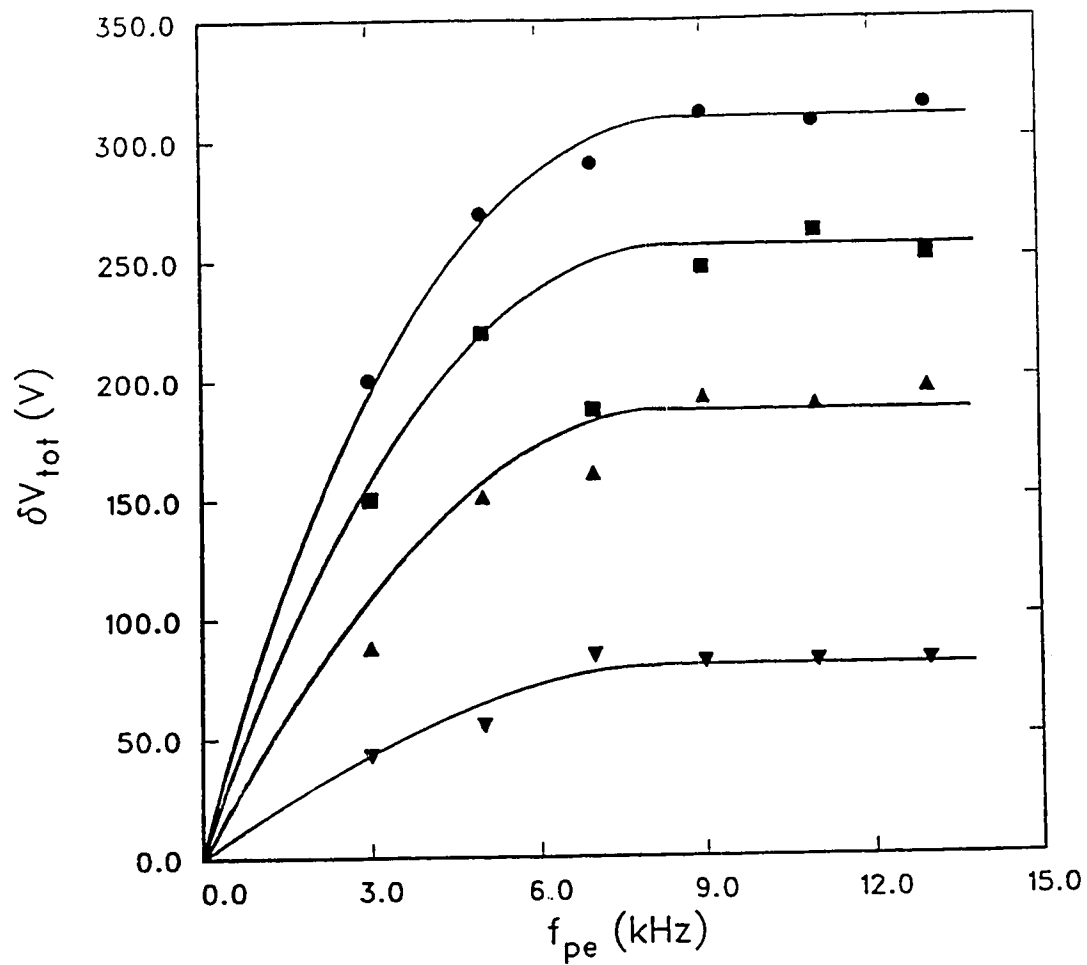


Fig. V.5 The overall potential reduction δV_{tot} vs. the plasma electrode frequency f_p for the He:N₂:CO₂ plasma cathode. The closed circles represent data for $P_{PIE}=216$ W, the closed squares represent data for 234 W, the closed triangles represent data for 282 W, and the inverted closed triangles represent data for 340 W, while $I=69$ mA for each case.

abnormal glow regime when measured with an electrostatic probe on a conventional multi-pin electrode.³

The values of δV_{tot} observed in the mixture for the plasma anode case (Fig. V.6) followed trends similar to those exhibited by the plasma cathode. Indeed, the largest potential reduction achieved was approximately 420 V. This value corresponds well with the maximum value of V_a ,³ measured previously on a multi-pin electrode array. These results suggest that an overall dc power supply potential reduction of 600-700 V can be attained in a transverse discharge laser fitted with both plasma cathodes and anodes.

Variation in δV_{tot} with P_{PIE} is clearly due to the degree of external ionisation of the inter-electrode volume. In the case of the He:N₂:CO₂ plasma cathode discharge, a value of $P_{PIE}=216$ W was barely adequate to permit significant dc current flow, while $P_{PIE}=360$ W resulted in a much higher degree of ionisation than that normally used in laser operation. As expected, the highly ionised discharge volume displayed a much lower V_{tot} and thus V_{pc} than the slightly ionised discharge (Fig. V.7). The same trend was displayed in the He:N₂:CO₂ plasma anode case. However, the lower efficiency of the volume pulser's ionisation process in this system polarity resulted in lower bulk conductivity and thus correspondingly higher values of V_{tot} . The simultaneous reductions of V_{tot} and δV_{tot} with P_{PIE} meant that the overall discharge potential during plasma electrode operation, $V_{tot} - \delta V_{tot}$, was approximately constant for the range of P_{PIE} investigated. As explained below, it is believed that δV_{tot} arises from the combination of a reduction in V_c and a simultaneous increase in V_{pc} . This phenomenon cannot be explained by the one-dimensional analysis presented above, since it is due to a two-dimensional effect associated with the physical geometry of pin electrodes.

Ionisation effects and pin electrodes

Although pin electrodes have been shown to provide excellent photo-ionisation for the PIE discharge, they tend to operate in the abnormal glow when emitting large cathode currents. This is a consequence of the non-uniform electrical fields associated with the

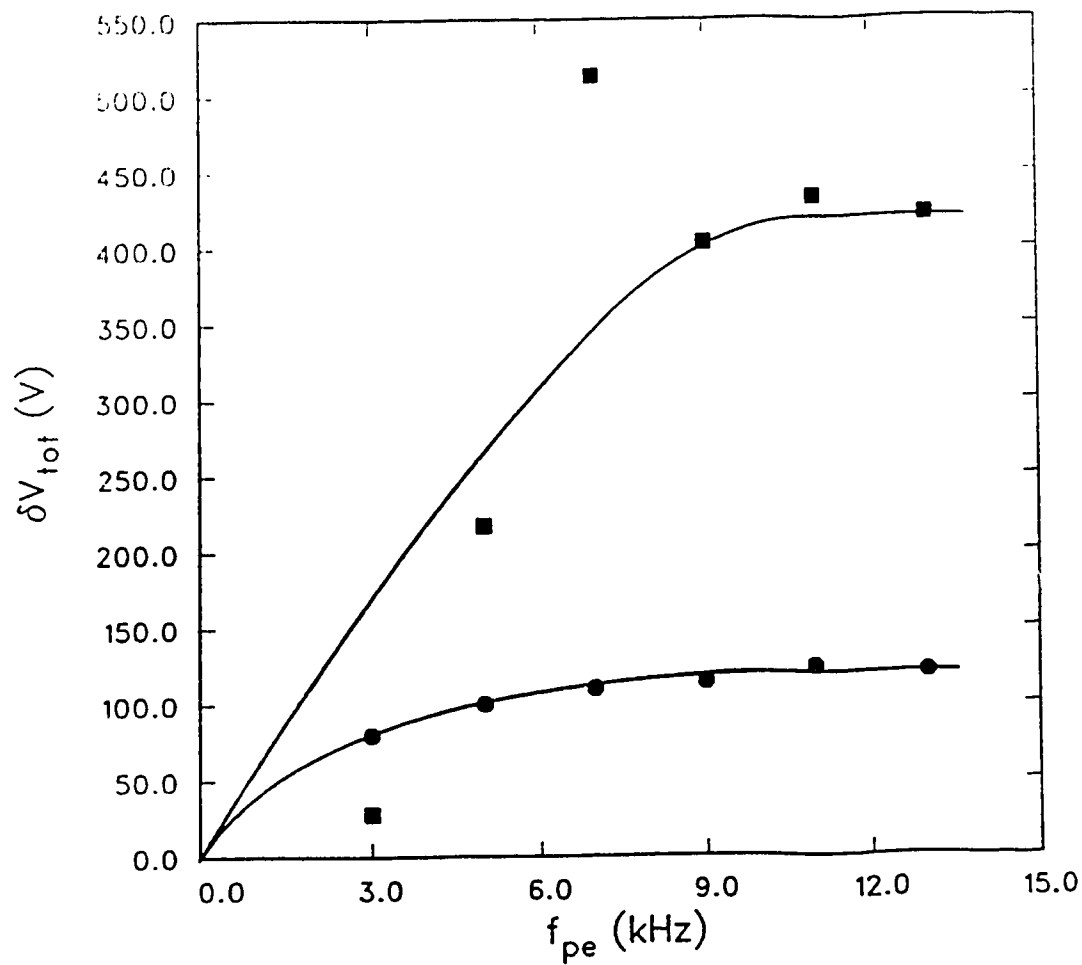


Fig. V.6 The overall potential reduction δV_{tot} vs. the plasma electrode frequency f_p for the He:N₂:CO₂ plasma anode. The closed squares represent data for $P_{PIE} = 295$ W and the closed circles represent data for 370 W. $I = 26$ mA for each case.

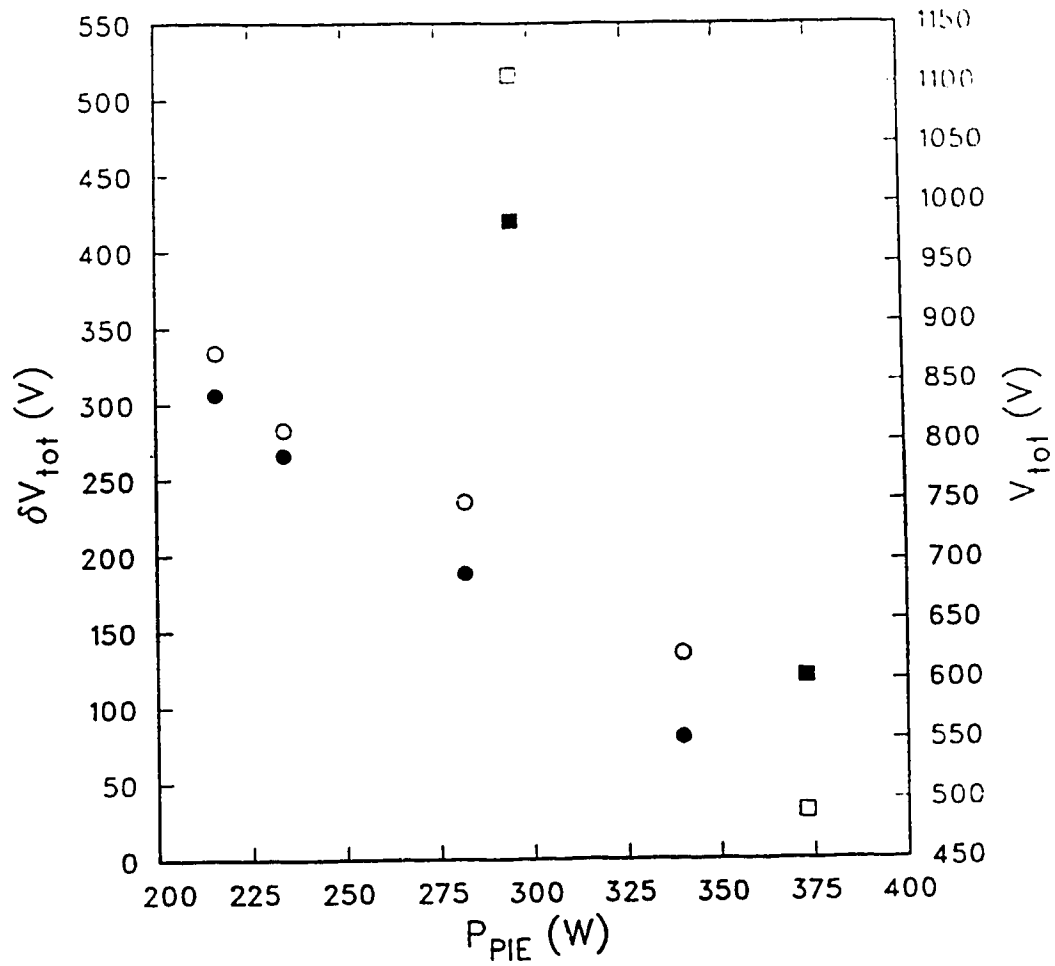


Fig. V.7 V_{tot} and δV_{tot} vs. P_{PIE} for the He:N₂:CO₂ plasma electrode. The closed circles represent data for δV_{tot} for the plasma cathode and the closed squares represent data for the plasma anode. The open circles represent data for V_{tot} for the plasma cathode and the open squares represent data for V_{tot} for the plasma anode.

geometry of the pins within the discharge. Since the electric field along the relatively long flux lines emanating from the shafts of the pins is weaker than that along the short flux lines emanating from the tips (Fig. V.8), current is emitted from the shafts only when the discharge is heavily loaded. The bright glow of the current emission region is observed to extend down the pin shaft as progressively greater currents are drawn from the pin. In spite of its more complex geometry, the double-pin electrode of Fig. V.1 does not differ essentially in its behaviour from that of a simple pin. At the currents being drawn in this investigation, the glowing emission region also extended down the 10.0 mm diameter sleeves of the double-pin electrode, indicating that the area near the tip was insufficient for these currents.

When P_{PIE} is low, the ionisation density is also low, so the region of high electrical conductivity is concentrated near the pin tips, where the corona effect is strongest (Fig. V.8(a)). Under this condition, current in a moderately ionised discharge tends to be emitted from the tips and flow along the discharge axis. Consequently, a strong E -field is required to maintain the resultant high axial current density. In this situation, the pin tip will likely operate in the abnormal glow.

On the other hand, when P_{PIE} is large and there is a great deal of ionisation, current is more easily emitted from the pin shafts and is thus diffused over a wide cross-sectional area (Fig. V. 8(b)). Thus, in a two-dimensional discharge, large values of P_{PIE} reduce V_{pc} in two ways: by increasing σ , as in a one-dimensional discharge, and by reducing current density through an expansion of the region available for conduction.

One effect of the plasma electrode is to concentrate current emission onto the spark channel. For this reason, no glow was observed on the shafts of the double-pin electrode during the plasma electrode operation. This situation corresponds to the low ionisation-density situation outlined above, where a large current density from a small emission area required a strong E -field. Thus, when the plasma electrode is operating in a moderately ionised regime, there is little additional current concentration onto the pin tips and correspondingly little effect on V_{pc} . Therefore, the change in the dc power supply potential is due primarily to a

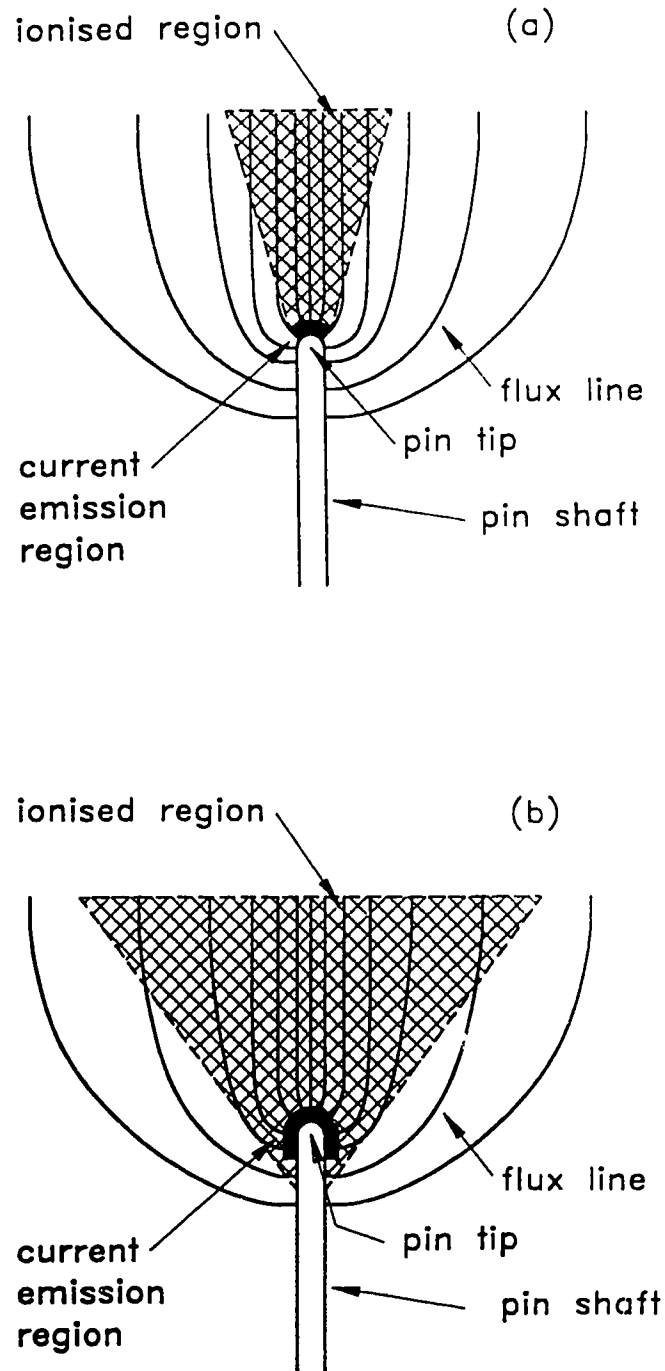


Fig. V.8 The externally ionised glow discharge for a pin cathode. In (a) P_{PIE} is much less than in (b), resulting in a narrower conductive zone.

reduction in the cathode fall, i.e. $\delta V_{tot} \approx V_c$. But when the plasma is operating in a strongly ionised regime, current concentration onto the pin tip requires an increase in V_{pc} , so that $\delta V_{tot} \approx V_c \cdot \delta V_{pc}$. Thus, the overall potential reductions observed in highly ionised discharges were markedly smaller than those in moderately ionised discharges (Fig. V.7). These results constitute persuasive evidence that the cathode fall has indeed been eliminated by the plasma cathode. It is also apparent that the greatest benefit of the plasma cathode is derived in discharges having moderate levels of ionisation and a sufficient dc current loading to be operating in the abnormal glow regime.

Plasma electrode frequency effects

The recorded increase in δV_{tot} with frequency is believed to be a consequence of the transience of the plasma electrode spark channels. Specifically, the regions of complete ionisation eventually relax, thereby terminating the plasma electrode effect. Thus, a shorter interval between plasma electrode impulses results in a higher average degree of ionisation on the double-pin electrode and concomitant improved performance. However, other mechanisms may also be involved. Since the impulses from the PIE pulser, as well as those from the plasma electrode pulser, affect ionisation in the discharge, some degree of coupling may occur. Indeed, Karlov *et al.*¹⁰ synchronised the TEA laser pulse with their plasma electrode pulse, delaying the laser pulse slightly, and so allowing photo-ionisation to occur before imposing a large accelerating field. They were thus able to advantageously "breed" electrons through high energy collisions between neutral atoms and the photo-electrons created in the inter-electrode volume by the sliding discharge. Since in this investigation the two pulsers were not synchronised, a higher f_{pe} would be expected to result in a greater probability of impulse coincidence and a concomitant enhanced conductivity. According to the experiment described in the next section, the plasma electrode improved discharge performance even when there was no external ionisation. Also, the degree of ionisation in the positive column appeared unaffected by the plasma electrode. In the light of these observations, it is clear that coupling

of PIE and plasma electrode impulses cannot account for the large increase in $\delta V'_{tot}$ with f_{pe} .

D. Discharge conductivity tests

A possible alternative to the hypothesis presented in this paper -- that the plasma electrodes reduced V'_{tot} by eliminating the electrode sheaths -- would be that the plasma electrode merely acted as an auxiliary photo-ionisation source and reduced V'_{pc} by enhancing the bulk conductivity σ .

Although visual observations suggested that a single spark plasma cathode did not ionise the volume, further and more definitive experiments were undertaken in order to settle the issue. A first test was to operate the discharge without the PIE volume pulser (i.e. a "self-sustained" discharge). Under this condition only a barely measurable dc current (i.e. 2 mA) could be drawn through the discharge. Also, when the plasma cathode was activated, still only a very small dc current was recorded (i.e. 14 mA). Moreover, the current which was drawn created a "rooster tail" plume of excited gas as it was blown downstream by the flowing gas. This gas transport feature is a well-known characteristic of a self-sustained dc discharge.

The possible indirect effect of the plasma cathode on the positive column of the PIE discharge was more difficult to assess. For instance, it is conceivable that even a small degree of photoionisation generated by the plasma cathode could result in a substantially increased σ , due to the avalanching effect of the PIE impulses. Alternatively, power dissipated by the arc might heat the positive column sufficiently that a concomitant increased σ could explain the observed reduction in V'_{tot} .

The hypothesis that σ was unaffected by the plasma cathode was validated by measurements of the conductivity within the positive column. Specifically, the floating conductivity probe circuit of Fig. V.9 was developed to directly measure any conductivity changes transverse to the electric field. Two T-shaped 0.7 mm diameter copper wires with 1 cm long cross pieces made of the same wire were held 0.7 cm apart in a plane transverse to

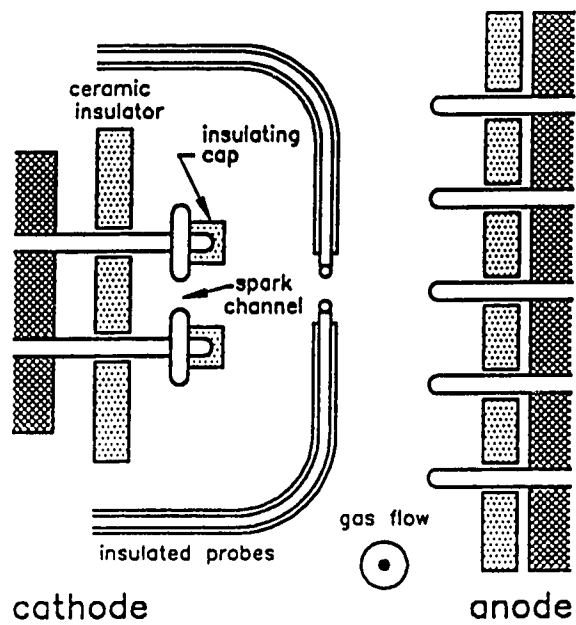


Fig. V.9 The conductivity probe. The current drawn between two probes is proportional to the conductivity at the mid-point of the discharge volume.

the discharge, some 5 cm from the plasma cathode. A 300 V battery was connected across the probes, with an AVO ammeter (50 ohm internal resistance) and a low-pass filter in the circuit. In this manner, current measured by the ammeter was proportional to the local plasma conductivity. Data were collected by operating the N_2 discharge in the following sequence:

1. a standard dc current was obtained with the plasma cathode off,
2. the plasma cathode was then turned on and the resultant (higher) stable dc current was recorded,
3. the dc power supply potential was next reduced to again obtain the standard dc current, and
4. the plasma cathode was finally switched off and the (lower) stable dc current was recorded.

Thus, a number of dc operating points with and without the plasma cathode were obtained over a range of frequencies, as illustrated in Fig. V.4. In this manner, Fig. V.10 displaying probe current versus a "bulk conductivity" σ_{bulk} was derived. The value of this conductivity was derived using the potential drop across the entire discharge circuit except the cathode region:

$$\sigma_{bulk} = (V_{tot} - V_c) / I. \quad (4)$$

The fixed value of V_c in (4) was the maximum shown in Fig. V.4 for the corresponding value of P_{PIE} . Probe current was plotted for two different magnitudes of P_{PIE} (675 W and 725 W). Transverse conductivities for the case when the plasma cathode was operating were computed in two different ways: by (4), which attributes δV_{tot} in Fig. V.4 to a positive column potential reduction, and by (5), which attributes it to a frequency dependent cathode fall reduction:

$$\sigma_{bulk} = (V_{tot} - V_c(f_{pe})) / I. \quad (5)$$

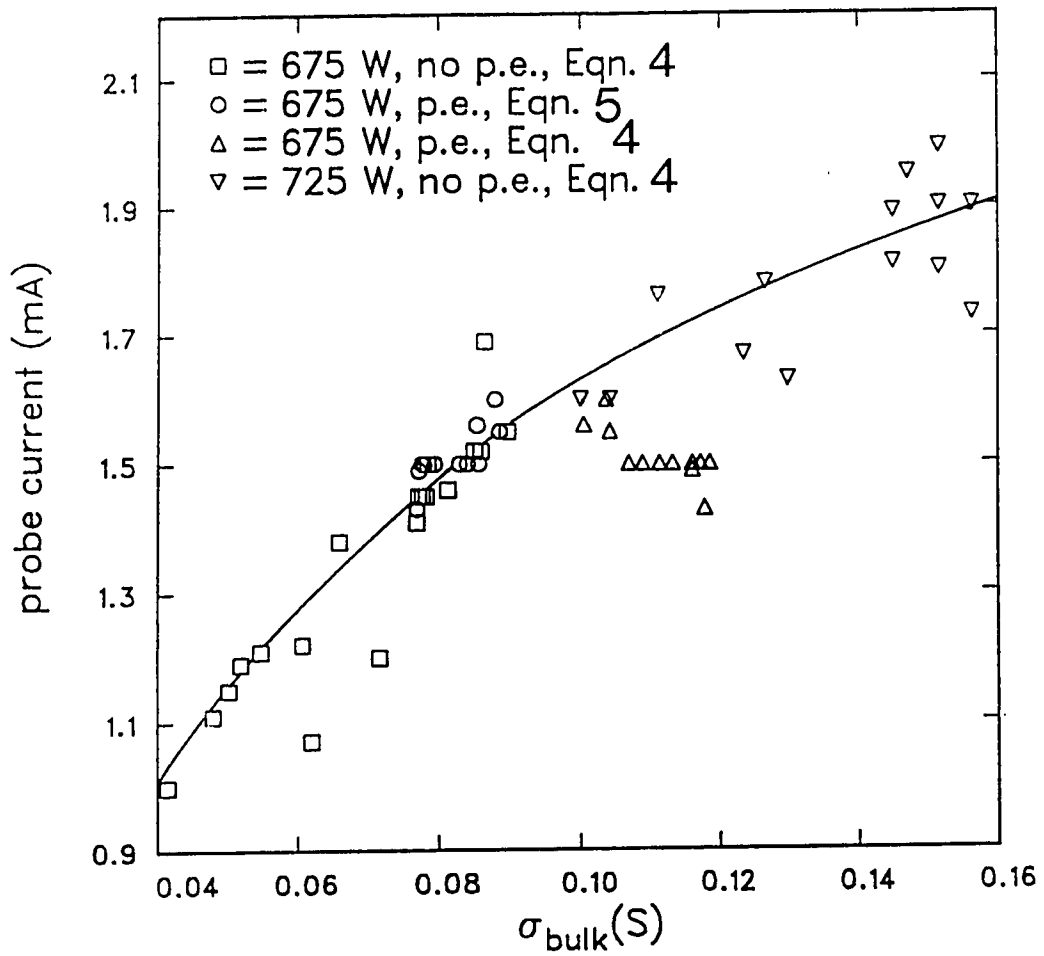


Fig. V.10 The probe current vs. the bulk conductivity with and without the plasma cathode.

The open circles conform to the probe characteristic.

As depicted in Fig. V.10, the probe current correlates well with bulk conductivity. It is also evident that plasma cathode data fit the calibration well when calculated assuming a cathode fall reduction hypothesis (5). However, agreement is not achieved when calculated by a bulk conductivity reduction hypothesis (4), and therefore, it seems clear that a reduction in cathode fall was wholly responsible for δV_{tot} . Since the spark channel does not influence σ when it is a cathode, it should also exhibit a negligible effect as an anode. Thus, it may be concluded that dc potential reductions observed during the operation of the plasma electrode are an immediate consequence of reductions in electrode sheath potentials.

E. Efficiency considerations

It is clear from the data reported herein that the power consumed in both the volume ionisation and in plasma electrode pulsers used in the maintenance of the PIE discharge was far in excess of the useful dc vibrational pumping power subsequently deposited into the positive column. However, it should be emphasised that this undesirable situation is largely an artefact of the particular experimental system used and not characteristic of the "normal" PIE excitation technique. Indeed, it has been well documented that the PIE non-self-sustained excitation process typically consumes less than 1% of the overall discharge power in high power laser configurations.^{20,21}

The specific reasons why these proof-of-concept experiments involving a plasma electrode did not approach this level of efficiency stem from the fact that the experiments with the small double-pin electrode module were conducted on apparatus initially designed for two large opposing 200-pin electrode array modules taken from an existing 30 kW PIE laser. Thus, whereas in normal usage there is a sufficient number of pins to sustain about 4 A of discharge current, in these tests the current-carrying capacity of only two pins was investigated. However, the value of P_{PIE} necessary to ionise the volume did not decrease proportionately. In fact, since the capacitive coupling between the double-pin electrode and the 200-pin electrode was now much smaller than that normally experienced between two

opposing 200-pin electrodes, the electrical impulse had a greater propensity to be transmitted to the metal vacuum chamber walls rather than through the discharge. Thus, the volume ionisation power ratio $P_{PIE}/(V_{tot} \times I)$ of 1% in standard PIE lasers was artificially inflated in this experiment by a 100-fold decrease in I and a simultaneous increase in P_{PIE} .

Now that the basic concept of a plasma electrode has been verified, further work will be required to address the efficiency that can be achieved by the device. In this context, experiments presently underway suggest that with suitable design, a small plasma electrode arc can be established at each pin tip by the same pulser that is used for volume ionisation. If this process can be scaled throughout all the pins comprising the electrodes of a PIE laser, then indeed a major improvement in the system will be realised.

Clearly, the overall effectiveness of a plasma electrode in any laser will depend not only on the potential reduction achieved in the electrode sheaths but also on the efficiency of optical power extraction from the positive column. Thus, the values of E/N obtained with and without the plasma electrode are of paramount importance. Since these preliminary experiments did not attempt to establish values of E/N , the optimum regime for plasma electrode operation could not be ascertained. However, in past experiments it has been observed that a modest level of ionisation yields the best laser performance.²¹ From Fig. V.7, it is clear that the plasma electrode has the most beneficial effect on total power for moderate levels of ionisation. Moreover, according to the pin geometry considerations discussed above, the E/N ratio of the laser plasma is not affected by the plasma electrode in this moderate ionisation regime. This being the case, the maximum effectiveness of a plasma electrode utilized in a laser discharge would seem to be conveniently co-incident with optimal optical energy extraction.

F. Conclusions

A plasma electrode based upon the repetitive generation of a spark channel has been demonstrated in an externally ionised, non-self-sustained discharge. A high density spark channel can eliminate the cathode and anode sheath potentials inherent with conventional metal electrodes. The reduction achieved in the dc discharge potential can amount to 600-700 V. Furthermore, the plasma electrode can be operated in conjunction with a PIE discharge circuit, thereby allowing independent control of the E/N ratio in the laser gain medium. Initial measurements indicate that a plasma electrode is most effective at eliminating these electrode sheaths in the E/N regime compatible with optimal laser amplification. Consequently, it is highly probable that a significant improvement in overall laser efficiency can be affected with an appropriate plasma electrode design. However, considerable further investigation of the concept is required to realise a practical system.

REFERENCES

- [1] A. von Engel, *Ionised Gases* (Oxford University Press, London, 1965), p. 229.
- [2] V.A. Seguin, H.J.J. Seguin, C.E. Capjack, and S.K. Nikumb, *Appl. Phys. B*, **42**, 3374 (1987).
- [3] Chapter II of this thesis.
- [4] F. Chen, *Introduction to Plasma Physics and Controlled Fusion, Pt. 1* (Plenum Press, New York, 1984), p. 294.
- [5] H.J.J. Seguin, A.K. Nam, and J. Tulip, *Appl. Phys. Lett.*, **32**, 418 (1978).
- [6] B. Bletzinger, *IEEE J. Plasma Sci.*, **PS-12**, 227 (1984).
- [7] Chapter III of this thesis.
- [8] S.I. Andreev, I.M. Belousouva, P.N. Dashuk, D.Yu. Zaroslov, E.A. Zobov, N.V. Karlov, G.P. Kuz'min, S.M. Nikiforov, A.M. Prokhorov, A.N. Sidorov, L.L. Chelnokov, M.D. Yarysheva, *JETP Lett.*, **21**, 194 (1975).
- [9] S.I. Andreev, I.M. Belousouva, P.N. Dashuk, D.Yu. Zaroslov, E.A. Zobov, N.V. Karlov, G.P. Kuz'min, S.M. Nikiforov, and A.M. Prokhorov, *Sov. J. Quant. Elect.*, **6**, 931 (1976).
- [10] N.V. Karlov, G.P. Kuz'min, and A.M. Prokhorov, *Izv. Akad. Nauk SSSR, Ser. Fiz.*, **48**, 1430 (1984).
- [11] V.P. Gorkovskii, N.V. Karlov, I.O. Kovalev, B.M. Koval'chuk, G.P. Kuz'min, G.A. Mesyats, and A.M. Prokhorov, *Sov. J. Quant. Elect.*, **14**, 1253 (1984).
- [12] S. Humphries, Jr., M. Savage, and D.M. Woodall, *Appl. Phys. Lett.*, **47**, 468 (1985).
- [13] K. Watanabe, F.A. van Goor, and W.J. Witteman, *Appl. Phys. Lett.*, **54**, 2639 (1989).
- [14] R. McLeary, P.J. Beckwith, and W.E.K. Gibbs, *IEEE J. Quantum Electron.*, **QE-10**, 649 (1974).
- [15] D.Yu. Zaroslov, N.V. Karlov, G.P. Kuz'min, and D. McKen, *Sov. J. Quantum Electron.*, **8**, 1048 (1978).
- [16] H. Tholl, *Z. Naturforsch.* **22 a**, 1068 (1967).

- [17] D.C. McKen, H.J.J. Seguin, and J. Tulip, IEEE J. Quantum Electron., **QE-12**, 470 (1976).
- [18] H.J.J. Seguin, A.K. Nam, and J. Tulip, J. Appl. Phys., **49**, 4566 (1978).
- [19] A.H. Labun, H.J.J. Seguin, and C.E. Capjack, Appl. Phys. Lett., **58**, 2625 (1991).
- [20] A.D. Nath, H.J.J. Seguin, and Vern A. Seguin, IEEE J. Quantum Electron., **QE-22**, 268 (1986).
- [21] S.K. Nikumb, H.J.J. Seguin, V.A. Seguin, and H. Reshef, J. Phys. E: Sci. Instrum., **20**, 911 (1987).

VI. General Discussion and Conclusions

The electrode sheath potentials of dc excited transverse discharge lasers dissipate a significant fraction of the total power deposited within the glow discharge. Since this contributes a considerable inefficiency in these systems, it has been deemed worthwhile to study the physics of the sheath regions and perform experiments to explore how these potentials may be reduced. Results of these investigations are drawn here into a general discussion of electrode design for minimum potential drops at the electrodes.

In experiments with cathodes, the magnitude of V_c (including the potential drop near the cathode due to all factors) in the conventional PIE discharge was largely determined by the current density at the tip. However, when the external ionisation was increased such that current could pass through the *shaft* of the pin and not just the tip, the current density in the gas near the tip was drastically reduced. This reduced V_c in two ways: the current concentration potential was reduced and the abnormal glow potential was reduced to the normal glow potential. The degree of external ionisation necessary to achieve this on a pin geometry resulted in a bulk gas E/N much too low for effective laser amplification, however. Thus, the method of external ionisation of the plasma to reduce V_c from the abnormal glow is generally unacceptable. These two contributions to the overall cathode fall potential (the concentration potential and the abnormal glow potential) seem to be unavoidable side-effects of a pin electrode geometry.

There is also no evidence that the cathode fall can be reduced below its nominal planar electrode value of approximately 200 V by ionisation of the bulk. Although the source of external ionisation may produce many if not most of the charge carriers present in the bulk, the discharge remains a weakly ionised, quasineutral plasma with a large sheath potential. This must be the case to maintain the current balance at the gas/electrode interface. For example, in order to steadily draw a current I of positive ions to the cathode surface to maintain a given current, the same current I of electrons must be generated in the sheath based on a material-dependent rate of secondary emission from the cathode surface (about

10%). (Electron emission due to the photoelectric effect is neglected.) This implies a cathode potential large enough to impart ionising energy to the electrons and sustain an avalanche. Since the potential required is a function of *ratios* of bombarding ions and emitted electrons, it is unaffected by variations in free carrier density in the bulk, as long as the fundamental mechanisms (e.g. collisional ionisation) of the sheath are unchanged. This generally holds for ionisation densities which are low enough to leave the sheath dimension (on the order of the Debye length) more than a few mean free paths in width. Thus, ionisation of the bulk is not a viable technique for both eliminating sheath potentials and sustaining a glow discharge. However, approaches which favourably alter the statistics of electron multiplication in the sheath may be used to incur a radical reduction of V_c .

Two approaches to just such a statistical manipulation proceeded with varying degrees of success. One approach was implemented experimentally, while the other was simulated by a Monte Carlo computer code. Justification for these attempts was made on the basis of ionisation cross-sections, which grew more favourable for higher electron energies than normally found in CO₂ lasers, especially in the positive column.

By imposing a transverse magnetic field on the simulated cathode region, the trajectories of the highest energy electrons were forced transverse to the electrode. In fact, these electrons could not leave the cathode region without colliding. Since their collisions favoured ionisation, the total amount of ionisation in the cathode sheath was increased. Unfortunately for the goal of reducing V_c in CO₂ lasers, there are relatively few such high energy electrons in the He:N₂:CO₂ mixture. Therefore the effect was smaller for laser mixtures than in the case of He, which has relatively more high energy electrons. Another factor not accounted for was the effect of magnetic fields on the bulk of the discharge. In that region, the magnetic field effectively decreases the mobility in the discharge, increasing the electric field strength necessary to conduct current. One suspects that, overall, the value of the V_c reduction effect of magnetic fields is likely to be marginal. The true benefit of a transverse magnetic field near the cathode is derived from its stabilisation of thermal

instabilities. This stabilisation effect was studied at higher pressures using the Monte Carlo simulation and found to require very high magnetic fields at the pressures relevant to high power TEA CO₂ lasers.

The approach of lowering V_c (and V_a) by means of sparks was quite successful. Again, the ionisation statistics of the high-voltage arc are better than those for the glow and this is not due only to the electron-neutral collisions. The spark channel achieves approximately complete ionisation by very high fields, intense UV emission and photoionisation. Thermionic emission from hot electrode spots and perhaps sputtered metal ions may also contribute to lowering V_c . This then reduces both the dimension and potential of the electrode sheath to their minimum values; V_c is possibly on the order of ten volts. Such a low value for V_c would be undetectable by the methods employed in this study. The period during which this ionisation relaxes appears long enough to permit the laser's bulk discharge to exploit the depressed values of V_c and V_a . Experiment has shown that the electrodes are not damaged by sparking, over the course of an extended testing period. Nor does the arc engender instabilities in the dc discharge. Thus it appears that it may be possible to operate a cw discharge (not necessarily a PIE discharge) with a pulsed, spark-based plasma electrode to effectively reduce or even eliminate V_c and V_a .

The practicality of the plasma electrode in a laser system depends on three additional considerations beyond the scope of this thesis: the additional capital cost of an extra feature on the laser, the effect on laser performance (including efficiency), and the reliability of a plasma electrode in a "real" laser system. Currently, the plasma electrode is a highly inefficient device which must operate in isolation from other plasma electrodes, should any be present, since an array of parallel plasma electrodes sourced from a single power supply would tend to have only one plasma electrode conducting all the current. From observations not reported in Chapter V, it would appear, however, that it may be possible to create a spark on each pin of the PIE multi-pin electrode using the conventional PIE volume ionisation pulse. Each spark may act as a plasma electrode. Since the gas volume itself acts as a form of

ballast, there is no apprehension that only one or some of the pins would support these sparks. Incidentally, a laser with an array of such plasma electrodes would be *ipso facto* a PIE laser. It would be presumptuous to speculate on whether other practical schemes for supporting plasma electrodes can be devised for non-PIE lasers, although the beneficial effect of eliminating electrode sheath potentials is not limited to PIE lasers. However, the expensive thyratron pulser and power supply, as well as the increased complexity of the electrode design, mitigate against the adaptation of conventional, fairly cheap laser designs to a plasma electrode version of the same design without simultaneously taking advantage of the other benefits of the PIE excitation system.

As shown in Chapter V, a single plasma electrode did not influence the electron density (or conductivity) of the positive column. Conceivably, an array of such electrodes could do so. However, this could be compensated by controlling various input parameters to the pulses, such as pulse potential, frequency, and rise-time. Since the PIE discharge depends on the alteration of the electron density of the volume by corona on the electrodes, it is difficult to see that this would be a problem, much less an insurmountable one. If the laser's gain medium remained unaffected, certainly its electrode sheaths would be eliminated by a plasma electrode. The effect on the laser's overall efficiency would be determined by the fraction of the laser's total power expended in the sheaths, since it is assumed that the efficiency with which the laser converts power deposited into the positive column is unaffected by the plasma electrode. Considering only the dc discharge circuit (including ballast), a reasonable situation in a PIE laser would consist of a positive column potential of 1000 V, $V_a + V_c = 700$ V, and $V_{tot} = 2600$ V. Elimination of the electrode sheath potentials would mean multiplying the laser's efficiency by a factor of 1.37. If the laser's efficiency was already 10%, it would become 13.7%, an increase of 3.7%. Probably a maximum efficiency gain on the order of 5% is possible with a reduced degree of ballasting, depending on the power expended in the plasma electrode (which in a practical system would have to be very small for the concept to be worth implementing) and on other power expenditures in the

laser, which are generally minor. The author's contention is that an increase in efficiency of that magnitude would be significant.

Finally, is the plasma electrode reliable enough for an industrial environment? That would depend on details of its design, but it seems that the sparks do not affect a large enough electrode (such as the 3 mm stainless steel pins used in Chapter V).

The response of V_a to the various measures undertaken in this series of experiments differed in two respects from that of V_c . First, regardless of the degree of external ionisation, the anode current remained concentrated at the pin tip. Thus, V_a was relatively insensitive to the degree of ionisation, since there was no change in the current concentration in the gas, nor is there a transition from an 'abnormal' anode fall to a normal one. Second, V_a was very sensitive to the ratio of negative ions to electrons. If the degree of attachment increased, so did V_a . This resulted in V_a being very sensitive to f_p . The corresponding changes to E/N could be accommodated by changing P_{PIE} , with almost no overall power penalty. This method thus suggested the possibility of an over 100 V potential saving for the dc discharge. This would result in a multiplication of the efficiency of the discharge by a factor of about 1.05. The high frequency of pulses required (10 kHz) suggests that the elimination of negative ions must be performed *in situ* in the discharge: circulation of the gas through catalytic cells in another part of the laser will not provide rapid enough response. Thus, it appears that something like a PIE discharge is necessary to reduce V_a through elimination of the negative ions.

A. Conclusions

The results of experiments and numerical simulations have demonstrated the possibility of reducing or even eliminating the electrode sheath potentials of high power dc-discharge CO₂ lasers, particularly PIE CO₂ lasers. The use of a plasma electrode based on a repetitive spark channel can result in the virtual elimination of the sheaths. Increasing the pulse frequency of a PIE discharge from the usual 5 kHz to 10 kHz, and thereby lowering the

negative ion concentration, can result in a reduction of over 100 V in the anode sheath potential. As well, in numerical simulations, the superposition of a transverse magnetic field onto the cathode region increases electron emission from the cathode region, a circumstance which would likely lead to a reduced cathode sheath potential in a physical device. These three widely disparate approaches to sheath potential reduction are similar in that they exploit the improved ionisation efficiency of high energy electrons in the electrode region while retaining the superior vibrational pumping performance of a low E/N in the bulk. These techniques need further research and refinement before being implemented in practical industrial laser systems. It is hoped that the successful employment of these methods of electrode sheath potential reduction will enable dc laser designers to achieve still higher laser output powers.

VII. Appendix: A listing of the MAGSIM code.

```

C*****C
C*****C
C***** MONTE-CARLO SIMULATION OF ELECTRON SWARMS *****C
C***** IN CO2-LASERS *****C
C*****C
C
C          R E V I S I O N   F E B .   2 1 ,   1 9 8 8
C
C PREVIOUS REVISIONS TO R.R.'S SOURCE HAVE INCLUDED EXTRA LOOPING
C FOR TERTIARY IONS. THIS REVISION TABULATES THE ENERGY OF EACH
C ELECTRON PRODUCED IN THE DISCHARGE AT REGULARLY SPACED INTERVALS
C IN THE CODE IN THE ARRAY *POPBIN* AS ITS QUALITATIVE REVISION.
C AS WELL, THE ARRAY SIZE OF THE STATE VECTORS FOR THE VARIOUS IONS
C HAS BEEN INCREASED BECAUSE THE RUNS WE NOW DO CREATE TOO MANY IONS.
C   R E V I S I O N   M A Y   1 2 ,   1 9 8 8
C THIS REVISION(MAY) REINTRODUCES THE ATTACHMENT OF CO2 AND EXTENDS
C BEYOND THE CATHODE FALL DISTANCE. THIS IS TO MONITOR THE POST-
C CATHODE FALL DEPOSITION OF THE ENERGY OF THE ELECTRONS AND OBSERVE
C THE EFFECTS OF ATTACHMENT.
C REVISION SEPTEMBER 14,1988
C THE COLLISION GENERATION AND ENERGY BIN STORAGE MECHANISMS ARE
C BEING FORMED INTO SUBROUTINES TO ENHANCE READABILITY OF THE CODE
C AND SIMPLIFY FUTURE REVISION.
C
CCCCCCCCCCCCCCCCCCCCCCCCCCCCCCCCCCCCCCCCCCCCCCCCCCCCCCCCCCCCCCCC
C REVISION AUGUST 19,1990
C THE ION RETURN TIME FORMULA HAS BEEN CORRECTED TO GIVE A CORRECT VALUE FOR
C THE DISCHARGE VELOCITY.
C
C   ANDREW LABUN
C
C$$$$$$$$$$$$$$$$$$$$$$$$$$$$$$$$$$$$$$$$$$$$$$$$$$$$$$$$$$$$$$$$
C   MAIN PROGRAM:
C   PROGRAM MAGSIM
C DEFINE ALL THE VARIABLES AS DOUBLE PRECISION AND DIMENSION THE
C VARIOUS ARRAYS.
C
  IMPLICIT REAL(A - H,O - Z)
  REAL L(200), L1, L2, MU(19), ILEFT
  LOGICAL STAY
  INTEGER TOTNC, TOTNHE, TOTNN2, TOTNCO, TN1HE, TN2HE, TNIHE, TN1N2,
1     TN2N2, TN3N2, TN4N2, TN5N2, TN6N2, TNIN2, TN1CO2, TN2CO2,
2     TN3CO2, TN4CO2, TN5CO2, TN6CO2, TN7CO2, TNICO2, TNI,
3     TNACO2, TERTEL, HE1, N21, CO21, NFLAG, ENBIN,
4     POPBIN(0:125,1:200)
  DIMENSION SPHE(201,81), SPN2(201,81), SPCO2(201,81), QHE(200,4),
1     QN2(200,8), QCO2(200,10), XIHE(200), YIHE(200),
2     ZIHE(200), VXIHE(200), VYIHE(200), VZIHE(200),
3     ENIHE(200), XIN2(200), YIN2(200), ZIN2(200), VXIN2(200),
4     VYIN2(200), VZIN2(200), ENIN2(200), XICO2(200),
5     YICO2(200), ZICO2(200), VXICO2(200), VYICO2(200),
6     VZICO2(200), ENICO2(200), TIHE(200), TIN2(200),
7     X6N2(200), Y6N2(200), Z6N2(200), VX6N2(200), VY6N2(200),
8     VZ6N2(200), EN6N2(200), X7CO2(200), Y7CO2(200),
9     Z7CO2(200), VX7CO2(200), VY7CO2(200), VZ7CO2(200),
*     EN7CO2(200), TICO2(200), XNWHE(200), YNWHE(200),
1     ZNWHE(200), VXNWHE(200), VYNWHE(200), VZNWHE(200)
  DIMENSION XNWN2(200), YNWN2(200), ZNWN2(200), VXNWN2(200),
1     VYNWN2(200), VZNWN2(200), XNWCO2(200), YNWCO2(200),
2     ZNWCO2(200), VXNWCO(200), VYNWCO(200), VZNWCO(200),
3     TENBAR(125), INBAR(125), AENBAR(125)
C
C DEFINE ALL THE COMMON BLOCKS.
C

```

```

COMMON /EDATA/ DC, VC, B0, MU, PRESS, BEAM
COMMON /ARRAND/ DSEED
COMMON /XSEC/ SPHE, QHE, SPN2, QN2, SPCO2, QCO2
COMMON /CHE/ XIHE, YIHE, ZIHE, VXIHE, VYIHE, VZIHE, ENIHE, TIHE,
1 K1HE, K2HE, KIHE
COMMON /CN2/ XIN2, YIN2, ZIN2, VXIN2, VYIN2, VZIN2, ENIN2, TIN2,
1 X6N2, Y6N2, Z6N2, VX6N2, VY6N2, VZ6N2, EN6N2,
2 K1N2, K2N2, K3N2, K4N2, K5N2, K6N2, KIN2
COMMON /CCO2/ XICO2, YICO2, ZICO2, VXICO2, VYICO2, VZICO2, ENICO2,
1 X7CO2, Y7CO2, Z7CO2, VX7CO2, VY7CO2, VZ7CO2, EN7CO2,
2 TICO2, K1CO2, K2CO2, K3CO2, K4CO2, K5CO2, K6CO2, K7CO2,
3 KICO2, KACO2
COMMON /SECELS/
1 XNWHE, YNWHE, ZNWHE, VXNWHE, VYNWHE, VZNWHE, XNWN2, YNWN2, ZNWN2,
2 VXNWN2, VYNWN2, VZNWN2, XNWCO2, YNWCO2, ZNWCO2, VXNWCO, VYNWCO,
3 VZNWCO
C
C DEFINE THE DATA VALUES.
C
DATA EM /9.1D-31/, QE /-1.6D-19/
C
C DETERMINE THE NUMBER OF STU'S REMAINING TO THE 205
C USING CHKCPU WITH AN INITIAL DUMMY VALUE -99
C
C ILEFT=-99
C ILEFT=-99.0
C STAY=.TRUE.
C CALL CHKCPU(STAY, ILEFT)
C READ THE DATA VALUES FOR NE = NO. OF ELECTRONS
C PRESS = GAS PRESSURE IN TORR
C BO = MAG. FIELD IN TESLA
C TEMP = TEMPERATURE OF BULK GAS (DEGREES KELVIN)
C DSEED = RANDOM NO. SEED.
C DC = CATHODE FALL DISTANCE
C BEAM = ENERGY OF ELECTRONS LEAVING CATHODE (EV)
C
READ (1,*) NE, PRESS, B0, TEMP, DSEED, DC, BEAM, VC
C
C READ IN THE PARTIAL PRESSURES OF HE:N2:CO2.
C
READ (2,*) PRESHE, PRESN2, PRESKO
C
C DEFINE THE CATHODE FALL DISTANCE AND VOLTAGE (DC AND VC).
C
TOTPRE = PRESHE + PRESN2 + PRESKO
PRESHE = PRESHE / TOTPRE
PRESN2 = PRESN2 / TOTPRE
PRESKO = PRESKO / TOTPRE
C
DCHE = 13D-03
DCN2 = 42D-03
DCCO2 = 40D-03
DC = (PRESHE*DCHE + PRESN2*DCN2 + PRESKO*DCCO2) / PRESS
C
VCHE = 150.0
VCN2 = 215.0
VCCO2 = 450.0
VC = PRESHE * VCHE + PRESN2 * VCN2 + PRESKO * VCCO2
C
C NOW DETERMINE THE ACTUAL PRESSURES OF THE CONSTITUENT GASES.
C
PRESHE = PRESS * PRESHE
PRESN2 = PRESS * PRESN2
PRESKO = PRESS * PRESKO

```

```

C
C THE MEAN FREE PATH OF THE ELECTRON IS DETERMINED FOR ANY PRESSURE.
C
C   LHEI = PRESHE / (105.33D-8 * 760.)
C   LN2I = PRESN2 / (35.525D-8 * 760.)
C   LCO2I = PRESKO / (23.7D-8 * 760.)
C   L = 1.0 / (LHEI + LN2I + LCO2I)
C   L = 1.5216E-05
C
C WRITE THE HEADING FOR THE OUTPUT FILE.
C
C   IBO = B0 * 1.000001D4
C   IPRESS = PRESS
C   IDSEED = DSEED
C   DCMM = DC * 1000.00
C   WRITE (6,10) IBO, IPRESS, TEMP, IDSEED, NE, VC, DCMM, BEAM
10 FORMAT (7X, 'MONTE-CARLO SIMULATION OF ELECTRON SWARM FLOW IN ',
1   ' THE CATHODE FALL REGION', /, 15X, 'OF A LASER GAS',
2   ' DISCHARGE UNDER THE INFLUENCE OF', /, 25X, 'ELECTRIC',
3   ' AND MAGNETIC FIELDS', //, 9X, '--- ELECTRIC FIELD IS',
4   ' LINEARLY VARYING ACROSS THE CATHODE FALL REGION', /, 12X,
5   ' AND IS IN THE -Z', ' DIRECTION.', /, 9X,
6   '--- MAGNETIC FIELD IS EQUAL TO ', I5, ' GAUSS IN THE +X ',
7   'DIRECTION.', /, 9X, '--- PRESSURE IS ', I3, ' TORR.', /,
8   9X, '--- TEMP IS ', F7.2, ' DEGREES KELVIN', /,
9   9X, '--- DSEED IS ', I4, /, 9X, '--- TOTAL NO. OF PRIMARY',
*   ' ELECTRONS IS ', I4, /, 9X, '--- CATHODE FALL VOLTAGE = ',
1  F5.1, /, 9X, '--- CATHODE FALL DISTANCE = ', F7.4, ' MM.',
2  /, 9X, '--- ELECTRON BEAM ENERGY LEAVING CATHODE = ',
3  F5.2, ' EV.')
C
C READ IN THE CROSS-SECTIONAL DATA FROM UNIT 3 (FILES X-HE+X-HE1)
C NOTE THAT THE CROSS-SECTIONS FOR HE, N2 AND CO2 ARE ACTUALLY IN
C UNITS OF NQ (I.E. M.-INVERSE). N = NO. OF GAS MOLECULES P.U.
C VOLUME AND Q = ACTUAL CROSS-SECTION @ PRESSURE = 1 TORR AND
C TEMP. = 0 DEGREES C.
C
C   QHE(I,1) -----> TOTAL CROSS-SECTION
C   QHE(I,2) -----> EXCITATION ONSET 19.8 EV
C   QHE(I,3) -----> EXCITATION ONSET 21.5 EV
C   QHE(I,4) -----> EXCITATION ONSET 24.5 EV
C
C READ IN THE CROSS-SECTIONAL DATA FROM UNIT 4 (FILES X-N2+X-N21)
C   QN2(I,1) -----> TOTAL CROSS-SECTION
C   QN2(I,2) -----> VIBRATION EXCITATION
C   QN2(I,3) -----> EXCITATION ONSET 6.22 EV
C   QN2(I,4) -----> EXCITATION ONSET 7.39 EV
C   QN2(I,5) -----> EXCITATION ONSET 8.59 EV
C   QN2(I,6) -----> EXCITATION ONSET 11.1 EV
C   QN2(I,7) -----> EXCITATION ONSET 15.7 EV
C   QN2(I,8) -----> IONIZATION ONSET 25.5 EV
C
C READ IN THE CROSS-SECTIONAL DATA FROM UNIT 5 (FILES X-CO2+X-CO21)
C   QCO2(I,1) -----> TOTAL CROSS-SECTION
C   QCO2(I,2) -----> VIBRATION EXCITATION
C   QCO2(I,3) -----> EXCITATION ONSET 3.1 EV
C   QCO2(I,4) -----> EXCITATION ONSET 6.1 EV
C   QCO2(I,5) -----> EXCITATION ONSET 7.0 EV
C   QCO2(I,6) -----> EXCITATION ONSET 10.5 EV
C   QCO2(I,7) -----> EXCITATION ONSET 11.5 EV
C   QCO2(I,8) -----> IONIZATION ONSET 13.3 EV
C   QCO2(I,9) -----> DISS. ION. ONSET 25.0 EV
C   QCO2(I,10) -----> DISS. ATT. ONSET 3.0 EV
C

```

```

      DO 20 I = 1, 200
        READ (3,*) QHE(I,1), QHE(I,2), QHE(I,3), QHE(I,4)
      20 CONTINUE
C
C READ IN THE SCATTERING ANGLE DATA FROM UNIT 1 (FILE X-HE1).
C
      DO 30 I = 1, 101
        READ (3,*) (SPHE(I,J),J=1,81)
      30 CONTINUE
C
C
      DO 40 I = 1, 200
        READ (4,*) QN2(I,1), QN2(I,2), QN2(I,3), QN2(I,4), QN2(I,5),
      1 QN2(I,6), QN2(I,7), QN2(I,8)
      40 CONTINUE
C
C READ IN THE SCATTERING ANGLE DATA FROM UNIT 2 (FILE X-N21).
C
      DO 50 I = 1, 101
        READ (4,*) (SPN2(I,J),J=1,81)
      C      DO 45 J=1,81
      C        SPN2(I,J)=0.
      C 45 CONTINUE
      50 CONTINUE
C
C
      DO 60 I = 1, 200
        READ (5,*) QCO2(I,1), QCO2(I,2), QCO2(I,3), QCO2(I,4),
      1 QCO2(I,5), QCO2(I,6), QCO2(I,7), QCO2(I,8), QCO2(I,9),
      2 QCO2(I,10)
      60 CONTINUE
C
C READ IN THE SCATTERING ANGLE DATA FROM UNIT 5 (FILE X-CO21).
C
      DO 70 I = 1, 101
        READ (5,*) (SPCO2(I,J),J=1,81)
      C      DO 65 J=1,81
      C        SPCO2(I,J)=0.
      C 65 CONTINUE
      70 CONTINUE
C
C COMPUTE THE MEAN FREE PATH FOR EACH ENERGY AT STANDARD TEMPERATURE
C
      DO 72 NM=1,200
        IF (NM.LE.100) THEN
          XXHE=QHE(NM,1)
          XXN2=QN2(NM,1)
          XXCO2=QCO2(NM,1)
          IF (XXHE.LT.1.) XXHE=1.
          IF (XXN2.LT.1.) XXN2=1.
          IF (XXCO2.LT.1.) XXCO2=1.
          TEMPHE=0.
          TEMPN2=0.
          TEMPCO=0.
          IF (PRESHE.GT.0.) TEMPHE=PRESHE*XXHE
          IF (PRESN2.GT.0.) TEMPN2=PRESN2*XXN2
          IF (PRESCO.GT.0.) TEMPCO=PRESCO*XXCO2
          L(NM)=1./(TEMPHE+TEMPN2+TEMPCO)
        ELSE
          L(NM)=L(100)
        ENDIF
      72 CONTINUE
C
      MU(1) = 0.83

```

```
MU(2) = 0.78
MU(3) = 0.71
MU(4) = 0.67
MU(5) = 0.62
MU(6) = 0.595
MU(7) = 0.555
MU(8) = 0.525
MU(9) = 0.5
MU(10) = 0.48
MU(11) = 0.35
MU(12) = 0.28
MU(13) = 0.25
MU(14) = 0.22
MU(15) = 0.2
MU(16) = 0.18
MU(17) = 0.17
MU(18) = 0.165
MU(19) = 0.16
C
C INITIALISE THE POPULATION RECORD BINS TO ZERO
C
      DO 76 N1=0,125
        DO 74 N2=1,200
          POPBIN(N1,N2)=0
      74 CONTINUE
      76 CONTINUE
C INITIALIZE THE VALUES OF TOTAL ENERGY, RADIUS, NO. OF COLLISIONS,
C NO. OF IONISATIONS, TIME AND Y.
C
      TOTEN = 0.0
      TOTX = 1.E-6
      TOTNC = 0.0
      TOTNHE = 0.0
      TOTNN2 = 0.0
      TOTNCO = 0.0
      TOTT = 0.0
      TOTY = 1.E-6
C
      TN1HE = 0.0
      TN2HE = 0.0
      TNIHE = 0.0
C
      TN1N2 = 0.0
      TN2N2 = 0.0
      TN3N2 = 0.0
      TN4N2 = 0.0
      TN5N2 = 0.0
      TN6N2 = 0.0
      TNIN2 = 0.0
C
      TN1CO2 = 0.0
      TN2CO2 = 0.0
      TN3CO2 = 0.0
      TN4CO2 = 0.0
      TN5CO2 = 0.0
      TN6CO2 = 0.0
      TN7CO2 = 0.0
      TNICO2 = 0.0
      TNACO2 = 0.0
C
      TOTVHE = 0.0
      TOTVN2 = 0.0
      TOTVCO = 0.0
C
```

```

      INEGHE = 0
      INEGN2 = 0
      INEGCO = 0
C
      NIPRI = 1
      KHEPRI = 0
      KN2PRI = 0
      KCOPRI = 0
C
      TERTEL = 0
C
      DO 80 IB = 1, 125
          TENBAR(IB) = 0.0
          INBAR(IB) = 0
      80 CONTINUE
C
      DO 960 I = 1, NE
C
C CHECK ON TIME REMAINING. IF INSUFFICIENT, JUMP TO EXIT ROUTINE
C
      CALL CHKCPU(STAY, ILEFT)
      IF (.NOT.STAY) GO TO 970
C INITIALISE THE NUMBER OF IONISED ELECTRONS, KI, TO ZERO.
C ALSO INITIALISE THE NO. OF COLLISIONS, NCOLL, TO ZERO.
C
      IBAR = 1
      NCOLL = 0
      NCOLHE = 0
      NCOLN2 = 0
      NCOLCO = 0
      TIME = 0.0
      ENPREV = 0.
      ACCLEN = 9.
C
      K1HE = 0
      K2HE = 0
      KIHE = 0
C
      K1N2 = 0
      K2N2 = 0
      K3N2 = 0
      K4N2 = 0
      K5N2 = 0
      K6N2 = 0
      KIN2 = 0
C
      K1CO2 = 0
      K2CO2 = 0
      K3CO2 = 0
      K4CO2 = 0
      K5CO2 = 0
      K6CO2 = 0
      K7CO2 = 0
      KICO2 = 0
      KACO2 = 0
C
C INITIALISE THE POSITION AND VELOCITY OF THE ELECTRON.
      CALL INIT(X, Y, Z, VX, VY, VZ, PRESHE, PRESN2, PRESCO, L)
      CALL ENERGY(VX, VY, VZ, VV, ENPREV)
      EN = ENPREV
C
C STORE THE THE ENERGY OF THE ELECTRON IN ENBAR WHENEVER Z IS AN
C INTEGER MULTIPLE OF 0.033 MM. FOR VALUES INBETWEEN SKIPPED BY Z SET
C ENBAR = 999. THESE VALUES WILL BE NEGLECTED WHEN COMPUTING

```

C ENERGY HISTOGRAMS.
 C A COMPLETE RECORD OF ELECTRON ENERGY AND NUMBER DISTRIBUTIONS IS
 C MADE BY RECORDING THE ELECTRON'S PRESENCE IN ONE OF THE ARRAY
 C ELEMENTS OF POPBIN (POSITION, ENERGY).

C
 CALL PRICOL(X, Y, Z, VX, VY, VZ, IBAR, ACCLN, ENPREV, POPBIN, TENBAR,
 1 INBAR, L, TEMP, TIME, EN, NCOLCO, NCOLHE, NCOLN2,
 2 NCOLL, PRESS, PRESHE, PRESN2, PRESO)
 137 TOTEN = TOTEN + EN
 TOTX = TOTX + X
 TOTNC = TOTNC + NCOLL
 TOTNHE = TOTNHE + NCOLHE
 TOTNN2 = TOTNN2 + NCOLN2
 TOTNCO = TOTNCO + NCOLCO
 TOTTT = TOTTT + TIME
 TIME = 0.
 TOTY = TOTY + Y

C
 TN1HE = TN1HE + K1HE
 TN2HE = TN2HE + K2HE
 TNIHE = TNIHE + KIHE

C
 TN1N2 = TN1N2 + K1N2
 TN2N2 = TN2N2 + K2N2
 TN3N2 = TN3N2 + K3N2
 TN4N2 = TN4N2 + K4N2
 TN5N2 = TN5N2 + K5N2
 TN6N2 = TN6N2 + K6N2
 TNIN2 = TNIN2 + KIN2

C
 TN1CO2 = TN1CO2 + K1CO2
 TN2CO2 = TN2CO2 + K2CO2
 TN3CO2 = TN3CO2 + K3CO2
 TN4CO2 = TN4CO2 + K4CO2
 TN5CO2 = TN5CO2 + K5CO2
 TN6CO2 = TN6CO2 + K6CO2
 TN7CO2 = TN7CO2 + K7CO2
 TNICO2 = TNICO2 + KICO2
 TNACO2 = TNACO2 + KACO2

C
 C THE FOLLOWING WRITE STATEMENTS ARE USED TO STORE THE POSITIONS
 C AND TIME OF ION FORMATION FOR USE LATER IN CALCULATING THE
 C HALL DRIFT VELOCITY.

C
 IF (KIHE .LT. 1) GO TO 140
 CALL VELHE(1, KIHE, INEGHE, YIHE, ZIHE, TIHE, TOTVHE)
 C
 140 IF (KIN2 .LT. 1) GO TO 150
 CALL VELN2(1, KIN2, INEGN2, YIN2, ZIN2, TIN2, TOTVN2)
 C
 150 IF (KICO2 .LT. 1) GO TO 160
 CALL VELCO2(1, KICO2, INEGCO, YICO2, ZICO2, TICO2, TOTVCO)
 C
 160 CONTINUE
 C
 170 IF (KIHE .EQ. 0) GO TO 181
 DO 180 J1 = 1, KIHE
 XNWHE(J1) = XIHE(J1)
 YNWHE(J1) = YIHE(J1)
 ZNWHE(J1) = ZIHE(J1)
 VXNWHE(J1) = VXIHE(J1)
 VYNWHE(J1) = VYIHE(J1)
 VZNWHE(J1) = VZIHE(J1)


```

180  CONTINUE
181  CONTINUE
C
C  FILL ARRAYS OF SECONDARY ELECTRONS WITH ZEROS  C
C
DO 185 J1= KIHE + 1, 200
  XNWHE(J1) = 0
  YNWHE(J1) = 0
  ZNWHE(J1) = 0
  VXNWHE(J1) = 0
  VYNWHE(J1) = 0
  VZNWHE(J1) = 0
185 CONTINUE
C
190  IF (KIN2 .EQ. 0) GO TO 210
DO 200 J1 = 1, KIN2
  XNWN2(J1) = XIN2(J1)
  YNWN2(J1) = YIN2(J1)
  ZNWN2(J1) = ZIN2(J1)
  VXNWN2(J1) = VXIN2(J1)
  VYNWN2(J1) = VYIN2(J1)
  VZNWN2(J1) = VZIN2(J1)
200  CONTINUE
C
210  IF (K6N2 .EQ. 0) GO TO 221
I1 = KIN2
DO 220 J1 = 1, K6N2
  I1 = I1 + 1
  XNWN2(I1) = X6N2(J1)
  YNWN2(I1) = Y6N2(J1)
  ZNWN2(I1) = Z6N2(J1)
  VXNWN2(I1) = VX6N2(J1)
  VYNWN2(I1) = VY6N2(J1)
  VZNWN2(I1) = VZ6N2(J1)
220  CONTINUE
221  CONTINUE
C
C  FILL ARRAYS OF SECONDARY ELECTRONS WITH ZEROES  C
C
DO 225 J1 = KIN2 + K6N2 +1, 200
  XNWN2(J1) = 0
  YNWN2(J1) = 0
  ZNWN2(J1) = 0
  VXNWN2(J1) = 0
  VYNWN2(J1) = 0
  VZNWN2(J1) = 0
225 CONTINUE
C
230  IF (KICO2 .EQ. 0) GO TO 250
DO 240 J1 = 1, KICO2
  XNWCO2(J1) = XICO2(J1)
  YNWCO2(J1) = YICO2(J1)
  ZNWCO2(J1) = ZICO2(J1)
  VXNWCO(J1) = VXICO2(J1)
  VYNWCO(J1) = VYICO2(J1)
  VZNWCO(J1) = VZICO2(J1)
240  CONTINUE
C
250  IF (K7CO2 .EQ. 0) GO TO 262
I1 = KICO2
DO 260 J1 = 1, K7CO2
  I1 = I1 + 1
  XNWCO2(I1) = X7CO2(J1)
  YNWCO2(I1) = Y7CO2(J1)

```

```

                ZNWCO2(I1) = Z7CO2(J1)
                VXNWCO(I1) = VX7CO2(J1)
                VYNWCO(I1) = VY7CO2(J1)
                VZNWCO(I1) = VZ7CO2(J1)
260    CONTINUE
262    CONTINUE
C
C    FILL ARRAYS OF SECONDARY ELECTRONS WITH ZEROES
C
C    DO 263 J1 = KICO2 + K7CO2 + 1, 200
        XNWCO2(J1) = 0
        YNWCO2(J1) = 0
        ZNWCO2(J1) = 0
        VXNWCO(J1) = 0
        VYNWCO(J1) = 0
        VZNWCO(J1) = 0
263    CONTINUE
C
        HE1 = 1
        N21 = 1
        CO21 = 1
        JN2 = KIN2 + K6N2
        JCO2 = KICO2 + K7CO2
        JHE = KIHE
        J1HE = 0
        J1N2 = 0
        J1CO2 = 0
C
265    CONTINUE
        NFLAG = 0
C
270    KII2HE = KIHE
        KII2N2 = KIN2 + K6N2
        KII2CO = KICO2 + K7CO2
        IF (KII2HE .LE. 0) THEN
            NFLAG = NFLAG + 1
            GO TO 350
        END IF
C
C-----C
C    NOW FOLLOW THE PATH OF THE IONISED ELECTRONS FROM HELIUM ATOMS.
C-----C
C
C    INITIALISE THE FOLLOWING VARIABLES TO KEEP TAG OF THE NO. OF
C    ELECTRONS EXCITED TO HIGHER LEVELS BY THE NEWLY IONISED ELECTRON.
C        KIIHE = INITIAL NO. OF IONISED ATOMS.
C        KIHE = TOTAL NO. OF IONISED ATOMS.
C        K1IHE = INITIAL NO. OF ATOMS EXCITED TO LEVEL 1.
C        K1HE = TOTAL NO. OF ATOMS EXCITED TO LEVEL 1.
C        K2IHE = INITIAL NO. OF ATOMS EXCITED TO LEVEL 2.
C        K2HE = TOTAL NO. OF ATOMS EXCITED TO LEVEL 2.
C
        DO 340 J1 = HE1, 200
C
        IF (ZNWHE(J1) .LE. 0) THEN
            IF (J1.EQ.HE1) THEN
                NFLAG = NFLAG + 1
            END IF
            GO TO 345
        END IF
C
        IF (J1.EQ.JHE + 1) J1HE = KIHE
C
        K1IHE = K1HE

```

```

      K2IHE = K2HE
      KIIHE = KIHE
C
      K1IN2 = K1N2
      K2IN2 = K2N2
      K3IN2 = K3N2
      K4IN2 = K4N2
      K5IN2 = K5N2
      K6IN2 = K6N2
      KIIN2 = KIN2
C
      K1ICO2 = K1CO2
      K2ICO2 = K2CO2
      K3ICO2 = K3CO2
      K4ICO2 = K4CO2
      K5ICO2 = K5CO2
      K6ICO2 = K6CO2
      K7ICO2 = K7CO2
      KIICO2 = KICO2
      KAICO2 = KACO2
C
      K1I1HE = K1IHE + 1
      K2I1HE = K2IHE + 1
      KII1HE = KIIHE + 1
C
      K1I1N2 = K1IN2 + 1
      K2I1N2 = K2IN2 + 1
      K3I1N2 = K3IN2 + 1
      K4I1N2 = K4IN2 + 1
      K5I1N2 = K5IN2 + 1
      K6I1N2 = K6IN2 + 1
      KII1N2 = KIIN2 + 1
C
      K1I1CO = K1ICO2 + 1
      K2I1CO = K2ICO2 + 1
      K3I1CO = K3ICO2 + 1
      K4I1CO = K4ICO2 + 1
      K5I1CO = K5ICO2 + 1
      K6I1CO = K6ICO2 + 1
      K7I1CO = K7ICO2 + 1
      KII1CO = KIICO2 + 1
      KAI1CO = KAICO2 + 1
C
      NCOLL = 0
      NCOLHE = 0
      NCOLN2 = 0
      NCOLCO = 0
C
C
C INITIALISE THE VALUES OF X, Y, Z, VX, VY AND VZ
C TO THE VALUES AT THE POINT OF IONISATION.
C
      X = XNWHE(J1)
      Y = YNWHE(J1)
      Z = ZNWHE(J1)
      VX = VXNWHE(J1)
      VY = VYNWHE(J1)
      VZ = VZNWHE(J1)
      TIME = TIHE(J1)
      IBAR = Z * 1000. * PRESS
      IF (IBAR.LT.1) IBAR = 1
C ELECTRON ENERGY AT IONISATION POINT
      CALL ENERGY(VX,VY,VZ,VWXYZ,ENPREV)
      ACCLEN = ENPREV

```

```

      EN = ENPREV
      CALL SECCOL(X, Y, Z, VX, VY, VZ, IBAR, ACCLN, ENPREV, POPBIN, TENBAR,
1         INBAR, L, TEMP, TIME, EN, NCOLCO, NCOLHE, NCOLN2,
2         NCOLL, PRESS, PRESHE, PRESN2, PRESKO)
317  TOTEN = TOTEN + EN
      TOTX = TOTX + X
      TOTNC = TOTNC + NCOLL
      TOTNHE = TOTNHE + NCOLHE
      TOTNN2 = TOTNN2 + NCOLN2
      TOTNCO = TOTNCO + NCOLCO
      TOTT = TOTT + TIME
      TIME = 0
      TOTY = TOTY + Y
C
      TN1HE = TN1HE + K1HE - K1IHE
      TN2HE = TN2HE + K2HE - K2IHE
      TNIHE = TNIHE + KIHE - KIIHE
C
      TN1N2 = TN1N2 + K1N2 - K1IN2
      TN2N2 = TN2N2 + K2N2 - K2IN2
      TN3N2 = TN3N2 + K3N2 - K3IN2
      TN4N2 = TN4N2 + K4N2 - K4IN2
      TN5N2 = TN5N2 + K5N2 - K5IN2
      TN6N2 = TN6N2 + K6N2 - K6IN2
      TNIN2 = TNIN2 + KIN2 - KIIN2
C
      TN1CO2 = TN1CO2 + K1CO2 - K1ICO2
      TN2CO2 = TN2CO2 + K2CO2 - K2ICO2
      TN3CO2 = TN3CO2 + K3CO2 - K3ICO2
      TN4CO2 = TN4CO2 + K4CO2 - K4ICO2
      TN5CO2 = TN5CO2 + K5CO2 - K5ICO2
      TN6CO2 = TN6CO2 + K6CO2 - K6ICO2
      TN7CO2 = TN7CO2 + K7CO2 - K7ICO2
      TNICO2 = TNICO2 + KICO2 - KIICO2
      TNACO2 = TNACO2 + KACO2 - KAICO2
C
      IF (KIHE .LT. KIIHE) GO TO 320
      CALL VELHE(KIIHE, KIHE, INEGHE, YIHE, ZIHE, TIME, TOTVHE)
C
320  IF (KIN2 .LT. KIIIN2) GO TO 330
      CALL VELN2(KIIIN2, KIN2, INEGN2, YIN2, ZIN2, TIN2, TOTVN2)
C
330  IF (KICO2 .LT. KIIICO) GO TO 340
      CALL VELCO2(KIIICO, KICO2, INEGCO, YICO2, ZICO2, TICO2,
1         TOTVCO)
C
340  CONTINUE
345  CONTINUE
C
      HE1 = J1
C
350  IF (KII2N2 .LE. 0) THEN
      NFLAG = NFLAG + 1
      GO TO 430
      END IF
C
-----C
C  NOW FOLLOW THE PATH OF THE IONISED ELECTRONS FROM NITROGEN ATOMS.  C
C-----C
C
C  INITIALISE THE FOLLOWING VARIABLES TO KEEP TAG OF THE NO. OF
C  ELECTRONS EXCITED TO HIGHER LEVELS BY THE NEWLY IONISED ELECTRON.
C      KII = INITIAL NO. OF IONISED ATOMS.
C      KI = TOTAL NO. OF IONISED ATOMS.

```

```

C      K1I = INITIAL NO. OF ATOMS EXCITED TO LEVEL 1.
C      K1 = TOTAL NO. OF ATOMS EXCITED TO LEVEL 1.
C      :           :
C      :           :
C
C      V           V
C      K6I = INITIAL NO. OF ATOMS EXCITED TO LEVEL 6.
C      K6 = TOTAL NO. OF ATOMS EXCITED TO LEVEL 6.
C
C      DO 420 J1 = N21, 200
C
C      IF (ZNWN2(J1) .LE. 0) THEN
C        IF (J1.EQ.N21) THEN
C          NFLAG = NFLAG + 1
C        END IF
C        GO TO 425
C      END IF
C
C      IF (J1.EQ.JN2 + 1) J1N2 = K1N2 + K6N2
C
C      K1IHE = K1HE
C      K2IHE = K2HE
C      KIIHE = KIHE
C
C      K1IN2 = K1N2
C      K2IN2 = K2N2
C      K3IN2 = K3N2
C      K4IN2 = K4N2
C      K5IN2 = K5N2
C      K6IN2 = K6N2
C      KIIN2 = KIN2
C
C      K1ICO2 = K1CO2
C      K2ICO2 = K2CO2
C      K3ICO2 = K3CO2
C      K4ICO2 = K4CO2
C      K5ICO2 = K5CO2
C      K6ICO2 = K6CO2
C      K7ICO2 = K7CO2
C      KIICO2 = KICO2
C      KAICO2 = KACO2
C
C      K1I1HE = K1IHE + 1
C      K2I1HE = K2IHE + 1
C      KII1HE = KIIHE + 1
C
C      K1I1N2 = K1IN2 + 1
C      K2I1N2 = K2IN2 + 1
C      K3I1N2 = K3IN2 + 1
C      K4I1N2 = K4IN2 + 1
C      K5I1N2 = K5IN2 + 1
C      K6I1N2 = K6IN2 + 1
C      KII1N2 = KIIN2 + 1
C
C      K1I1CO = K1ICO2 + 1
C      K2I1CO = K2ICO2 + 1
C      K3I1CO = K3ICO2 + 1
C      K4I1CO = K4ICO2 + 1
C      K5I1CO = K5ICO2 + 1
C      K6I1CO = K6ICO2 + 1
C      K7I1CO = K7ICO2 + 1
C      KII1CO = KIICO2 + 1

```

```

      KAI1CO = KAICO2 + 1
C
      NCOLL = 0
      NCOLHE = 0
      NCOLN2 = 0
      NCOLCO = 0
C
C
C INITIALISE THE VALUES OF X, Y, Z, VX, VY AND VZ
C TO THE VALUES AT THE POINT OF IONISATION.
C
      X = XNWN2(J1)
      Y = YNWN2(J1)
      Z = ZNWN2(J1)
      VX = VXNWN2(J1)
      VY = VYNWN2(J1)
      VZ = VZNWN2(J1)
      TIME = TIN2(J1)
C
      IBAR = Z * 1000. * PRESS
      IF (IBAR.LT.1) IBAR = 1
C ELECTRON ENERGY AT IONISATION POINT
      CALL ENERGY(VX,V.,VZ,VWXYZ,ENPREV)
      ACCLEN = ENPREV
      EN = ENPREV
      CALL SECCOL(X,Y,Z,VX,VY,VZ,IBAR,ACCLEN,ENPREV,POPBIN,TENBAR,
1          INBAR,L,TEMP,TIME,EN,NCOLCO,NCOLHE,NCOLN2,
2          NCOLL,PRESS,PRESHE,PRESN2,PRESKO)
397      TOTEN = TOTEN + EN
          TOTX = TOTX + X
          TOTNC = TOTNC + NCOLL
          TOTNHE = TOTNHE + NCOLHE
          TOTNN2 = TOTNN2 + NCOLN2
          TOTNCO = TOTNCO + NCOLCO
          TOTT = TOTT + TIME
      TIME = 0
      TOTY = TOTY + Y
C
      TN1HE = TN1HE + K1HE - K1IHE
      TN2HE = TN2HE + K2HE - K2IHE
      TNIHE = TNIHE + KIHE - KIIHE
C
      TN1N2 = TN1N2 + K1N2 - K1IN2
      TN2N2 = TN2N2 + K2N2 - K2IN2
      TN3N2 = TN3N2 + K3N2 - K3IN2
      TN4N2 = TN4N2 + K4N2 - K4IN2
      TN5N2 = TN5N2 + K5N2 - K5IN2
      TN6N2 = TN6N2 + K6N2 - K6IN2
      TNIN2 = TNIN2 + KIN2 - KIIN2
C
      TN1CO2 = TN1CO2 + K1CO2 - K1ICO2
      TN2CO2 = TN2CO2 + K2CO2 - K2ICO2
      TN3CO2 = TN3CO2 + K3CO2 - K3ICO2
      TN4CO2 = TN4CO2 + K4CO2 - K4ICO2
      TN5CO2 = TN5CO2 + K5CO2 - K5ICO2
      TN6CO2 = TN6CO2 + K6CO2 - K6ICO2
      TN7CO2 = TN7CO2 + K7CO2 - K7ICO2
      TNICO2 = TNICO2 + KICO2 - KIICO2
      TNACO2 = TNACO2 + KACO2 - KAICO2
C
      IF (KIHE .LT. KIIHE) GO TO 400
      CALL VELHE(KIIHE, KIHE, INEGHE, YIHE, ZIHE, TIHE, TOTVHE)
C
400      IF (KIN2 .LT. KIIIN2) GO TO 410

```

```

      CALL VELN2(K1IN2, KIN2, INEGN2, YIN2, ZIN2, TIN2, TOTVN2)
C
410  IF (K1CO2 .LT. K1I1CO) GO TO 420
      CALL VELCO(K1I1CO, K1CO2, INEGCO, Y1CO2, Z1CO2, T1CO2,
1      TOTVCO)
C
420  CONTINUE
425  CONTINUE
C
      N21 = J1
C
430  IF (K1I2CO .LE. 0) THEN
      NFLAG = NFLAG + 1
      GO TO 510
      END IF
C-----C
C-----C
C  NOW FOLLOW THE PATH OF THE IONISED ELECTRONS FROM CO2 ATOMS.  C
C-----C
C
C  INITIALISE THE FOLLOWING VARIABLES TO KEEP TAG OF THE NO. OF
C  ELECTRONS EXCITED TO HIGHER LEVELS BY THE NEWLY IONISED ELECTRON.
C      K1I = INITIAL NO. OF IONISED ATOMS.
C      KI = TOTAL NO. OF IONISED ATOMS.
C      K1I = INITIAL NO. OF ATOMS EXCITED TO LEVEL 1.
C      K1 = TOTAL NO. OF ATOMS EXCITED TO LEVEL 1.
C      :
C      :
C
C
C      V
C      V
C      K7I = INITIAL NO. OF ATOMS EXCITED TO LEVEL 7.
C      K7 = TOTAL NO. OF ATOMS EXCITED TO LEVEL 7.
C
C      " 500 J1 = CO2". 000
C
C  IF (ZNWC02(J1) .LE. 0) THEN
C  IF (J1.EQ.CO21) THEN
C      NFLAG = NFLAG + 1
C  END IF
C  GO TO 505
C  END IF
C  IF (J1.EQ.JCO2 + 1) J1CO2 = K1CO2 + K7CO2
C
C      K1IHE = K1HE
C      K2IHE = K2HE
C      K1IHE = KIHE
C
C      K1IN2 = K1N2
C      K2IN2 = K2N2
C      K3IN2 = K3N2
C      K4IN2 = K4N2
C      K5IN2 = K5N2
C      K6IN2 = K6N2
C      KIIN2 = KIN2
C
C      K1ICO2 = K1CO2
C      K2ICO2 = K2CO2
C      K3ICO2 = K3CO2
C      K4ICO2 = K4CO2
C      K5ICO2 = K5CO2
C      K6ICO2 = K6CO2
C      K7ICO2 = K7CO2

```

```

KIICO2 = KICO2
KAICO2 = KACO2

C
K1I1HE = K1IHE + 1
K2I1HE = K2IHE + 1
K7I1HE = K7IHE + 1

C
K1I1N2 = K1IN2 + 1
K2I1N2 = K2IN2 + 1
K3I1N2 = K3IN2 + 1
K4I1N2 = K4IN2 + 1
K5I1N2 = K5IN2 + 1
K6I1N2 = K6IN2 + 1
K7I1N2 = K7IN2 + 1

C
K1I1CO = K1ICO2 + 1
K2I1CO = K2ICO2 + 1
K3I1CO = K3ICO2 + 1
K4I1CO = K4ICO2 + 1
K5I1CO = K5ICO2 + 1
K6I1CO = K6ICO2 + 1
K7I1CO = K7ICO2 + 1
K7I1CO = K7ICO2 + 1
KAI1CO = KAICO2 + 1

C
NCOLL = 0
NCOLHE = 0
NCOLN2 = 0
NCOLCO = 0

C
C INITIALISE THE VALUES OF X, Y, Z, VX, VY AND VZ
C TO THE VALUES AT THE POINT OF IONISATION.
C
X = XNWCO2(J1)
Y = YNWCO2(J1)
Z = ZNWCO2(J1)
VX = VXNWCO(J1)
VY = VYNWCO(J1)
VZ = VZNWCO(J1)
TIME = TICO2(J1)

C
IBAR = Z * 1000. * PRESS
IF (IBAR.LT.1) IBAR = 1
C ELECTRON ENERGY AT IONISATION POINT
CALL ENEPGY(VX,VY,VZ,VWXYZ,ENPREV)
ACCLN = ENPREV
EN = ENPREV
CALL SECCOL(X, Y, Z, VX, VY, VZ, IBAR, ACCLN, ENPREV, POPBIN, TENBAR,
1      INBAR, L, TEMP, TIME, EN, NCOLCO, NCOLHE, NCOLN2,
2      NCOLL, PRESS, PRESHE, PRESN2, PRESKO)
477 TOTEN = TOTEN + EN
TOTX = TOTX + X
TOTNC = TOTNC + NCOLL
TOTNHE = TOTNHE + NCOLHE
TOTNN2 = TOTNN2 + NCOLN2
TOTNCO = TOTNCO + NCOLCO
TOTT = TOTT + TIME
TIME = 0
TOTY = TOTY + Y

C
TN1HE = TN1HE + KIHE - K1IHE
TN2HE = TN2HE + K2HE - K2IHE
TNIHE = TNIHE + KIHE - K7IHE

```



```

C
TN1N2 = TN1N2 + K1N2 - K1IN2
TN2N2 = TN2N2 + K2N2 - K2IN2
TN3N2 = TN3N2 + K3N2 - K3IN2
TN4N2 = TN4N2 + K4N2 - K4IN2
TN5N2 = TN5N2 + K5N2 - K5IN2
TN6N2 = TN6N2 + K6N2 - K6IN2
TNIN2 = TNIN2 + KIN2 - KIIN2

C
TN1CO2 = TN1CO2 + K1CO2 - K1ICO2
TN2CO2 = TN2CO2 + K2CO2 - K2ICO2
TN3CO2 = TN3CO2 + K3CO2 - K3ICO2
TN4CO2 = TN4CO2 + K4CO2 - K4ICO2
TN5CO2 = TN5CO2 + K5CO2 - K5ICO2
TN6CO2 = TN6CO2 + K6CO2 - K6ICO2
TN7CO2 = TN7CO2 + K7CO2 - K7ICO2
TNICO2 = TNICO2 + KICO2 - KIICO2
TNACO2 = TNACO2 + KACO2 - KAICO2

C
IF (KIHE .LT. KII1HE) GO TO 480
CALL VELHE(KII1HE, KIHE, INEGHE, YIHE, ZIHE, TIHE, TOTVHE)

C
480 IF (KIN2 .LT. KII1N2) GO TO 490
CALL VELN2(KII1N2, KIN2, INEGN2, YIN2, ZIN2, TIN2, TOTVN2)

C
490 IF (KICO2 .LT. KII1CO) GO TO 500
CALL VELCO2(KII1CO, KICO2, INEGCO, YICO2, ZICO2, TICO2,
1      TOTVCO)

C
500 CONTINUE
505 CONTINUE

C
CO21 = J1

C
510 IF (NFLAG .LT. 3) GO TO 265

C
KHEPRI = KHEPRI + JHE
KN2PRI = KN2PRI + JN2
KCOPRI = KCOPRI + JCO2
NIPRI = KHEPRI + KN2PRI + KCOPRI
TERTEL = TERTEL + HE1 + N21 + CO21 - 3 - J1HE - J1N2 - J1CO2

C
C THE FINAL POSITIONS AND VELOCITIES ARE TABULATED AFTER EVERY
C 100 PRIMARY ELECTRONS.

C
ICHECK = I / 500
ICHECK = ICHECK * 500
IF (I .NE. ICHECK .AND. I .NE. NE) GO TO 960

C
C COMPUTE THE AVERAGE VALUES OF ENERGY, RADIUS, NO. OF COLLISIONS,
C NO. OF IONISATIONS, TIME TAKEN TO CROSS THE CATHODE FALL AND THE
C E X B DRIFT.

C
960 CONTINUE
970 CONTINUE
TOTN = I + NIPRI - 1
IF (TOTN.LE.0) TOTN = 1
IF (TOTN.LE.0) TOTN = 1
AVGEN = TOTEN / TOTN
AVGNC = TOTNC / TOTN
AVGNHE = TOTNHE / TOTN
AVGNN2 = TOTNN2 / TOTN
AVGNCO = TOTNCO / TOTN

C

```

```

AVNIHE = TNIHE / TOTN
AVN1HE = TN1HE / TOTN
AVN2HE = TN2HE / TOTN
C
AVNIN2 = TNIN2 / TOTN
AVN1N2 = TN1N2 / TOTN
AVN2N2 = TN2N2 / TOTN
AVN3N2 = TN3N2 / TOTN
AVN4N2 = TN4N2 / TOTN
AVN5N2 = TN5N2 / TOTN
AVN6N2 = TN6N2 / TOTN
C
AVNICO = TNICO2 / TOTN
AVN1CO = TN1CO2 / TOTN
AVN2CO = TN2CO2 / TOTN
AVN3CO = TN3CO2 / TOTN
AVN4CO = TN4CO2 / TOTN
AVN5CO = TN5CO2 / TOTN
AVN6CO = TN6CO2 / TOTN
AVN7CO = TN7CO2 / TOTN
AVNACO = TNACO2 / TOTN
C
IF (TOTL.LE.2.E-10) TOTL= 2.E-10
AVGT = TOTL / TOTN
IF (TOTX.LE.0.) TOTX = 1.E-6
IF (TOTY.LE.0.) TOTY = 1.E-6
AVGX = TOTX / TOTN
AVGY = TOTY / TOTN
AVGV = DSQRT(2.*AVGEN*1.6D-19/EM)
AVGNU = AVGV / L(1)
HALL = 1.6D-19 * B0 / (EM*AVGNU)
DRIFTE = DC / AVGT
DRIFTX = AVGX / AVGT
DRIFTB = AVGY / AVGT
ALPHE = (ALOG((AVNIHE + 1.))) / DC
ALPN2 = (ALOG((AVNIN2 + 1.))) / DC
ALPCO2 = (ALOG((AVNICO + 1.))) / DC
C
DO 530 IB = 1, 125
  IF (INBAR(IB) .GE. 1) GO TO 520
  AENBAR(IB) = 999.
  GO TO 530
520  AENBAR(IB) = TENBAR(IB) / INBAR(IB)
530  CONTINUE
C
C
WRITE (6,540)
540  FORMAT (//, 19X, 'RESULTS OF MONTE-CARLO SIMULATION', /,
1     19X, 33('-'), //, 2X, 91('_'))
C
WRITE (6,550)
550  FORMAT (//, 8X, '# OF ELECT.', 8X, 'B0 (GAUSS)', 8X,
1     'PRESS (TORR)', 8X, 'PARTIAL PRESS HE:N2:CO2')
WRITE (6,560) I - 1, IBO, PRESS, PRESHE, PRESN2, PRESO
560  FORMAT (T11, I4, T30, I5, T50, F5.1, T70, F5.1, ':', F4.1, ':',
1     F4.1)
WRITE (6,570)
570  FORMAT (//, 8X, 'TOT# COL', 10X, ' TOT# HE', 10X, ' TOT# N2',
1     11X, 'TOT# CO2')
WRITE (6,580) TOTNC, TOTNHE, TOTNN2, TOTNCO
580  FORMAT (T10, I6, T29, I6, T47, I6, T65, I6)
WRITE (6,590)
590  FORMAT (//, 10X, 'AVG# COL', 11X, ' AVG# HE', 9X, ' AVG# N2',
1     11X, 'AVG# CO2')

```

```

WRITE (6,600) AVGNCO, AVGNHE, AVGN2, AVGNCO
600 FORMAT (T10, 1PE11.4, T29, E11.4, T47, E11.4, T65, E11.4)
WRITE (6,610)
610 FORMAT (//, 4X, 'COLLISION DISTRIBUTION FOR HELIUM', /,
1      4X, 33('-'))
WRITE (6,620)
620 FORMAT (//, 10X, 'TOT# 1', 12X, 'TOT# 2', 11X, 'TOT# ION')
WRITE (6,630) TN1HE, TN2HE, TNIHE
630 FORMAT (T10, I5, T29, I5, T47, I5)
WRITE (6,640)
640 FORMAT (//, 10X, 'AVG# 1', 13X, 'AVG# 2', 12X, 'AVG# ION')
WRITE (6,650) AVN1HE, AVN2HE, AVNIHE
650 FORMAT (T10, 1PE11.4, T29, E11.4, T47, E11.4)
WRITE (6,660)
660 FORMAT (//, 4X, 'COLLISION DISTRIBUTION FOR NITROGEN', /,
1      4X, 35('-'))
WRITE (6,670)
670 FORMAT (//, 9X, 'TOT# 1', 13X, 'TOT# 2', 12X, 'TOT# 3', 12X,
1      'TOT# 4')
WRITE (6,580) TN1N2, TN2N2, TN3N2, TN4N2
WRITE (6,680)
680 FORMAT (/, 9X, 'TOT# 5', 13X, 'TOT# 6', 12X, 'TOT# ION')
WRITE (6,630) TN5N2, TN6N2, TNIN2
WRITE (6,690)
690 FORMAT (//, 10X, 'AVG# 1', 13X, 'AVG# 2', 12X, 'AVG# 3', 12X,
1      'AVG# 4')
WRITE (6,600) AVN1N2, AVN2N2, AVN3N2, AVN4N2
WRITE (6,700)
700 FORMAT (/, 10X, 'AVG# 5', 13X, 'AVG# 6', 12X, 'AVG# ION')
WRITE (6,650) AVN5N2, AVN6N2, AVNIN2
WRITE (6,710)
710 FORMAT (//, 4X, 'COLLISION DISTRIBUTION FOR CARBON-DIOXIDE', /,
1      4X, 41('-'))
WRITE (6,720)
720 FORMAT (//, 9X, 'TOT# 1', 13X, 'TOT# 2', 12X, 'TOT# 3', 12X,
1      'TOT# 4', 10X, 'TOT# 5')
WRITE (6,730) TN1CO2, TN2CO2, TN3CO2, TN4CO2, TN5CO2
730 FORMAT (T10, I5, T29, I5, T47, I5, T65, I5, T81, I5)
WRITE (6,740)
740 FORMAT (/, 9X, 'TOT# 6', 13X, 'TOT# 7', 11X, 'TOT# ION', 10X,
1      'TOT# ATCH')
WRITE (6,580) TN6CO2, TN7CO2, TNICO2, TNACO2
WRITE (6,750)
750 FORMAT (//, 10X, 'AVG# 1', 13X, 'AVG# 2', 12X, 'AVG# 3', 12X,
1      'AVG# 4', 10X, 'AVG# 5')
WRITE (6,760) AVN1CO, AVN2CO, AVN3CO, AVN4CO, AVN5CO
760 FORMAT (T10, 1PE11.4, T29, E11.4, T47, E11.4, T65, E11.4, T81,
1      E11.4)
WRITE (6,770)
770 FORMAT (/, 10X, 'AVG# 6', 13X, 'AVG# 7', 12X, 'AVG# ION', 10X,
1      'AVG# ATCH')
WRITE (6,600) AVN6CO, AVN7CO, AVNICO, AVNACO
WRITE (6,780)
780 FORMAT (//, 27X, 'SWARM PARAMETERS (ALL AVERAGED)', /, 27X,
1      31('_'), //, 6X, 'TIME OF FLIGHT', 4X, 'FINAL ENERGY',
2      ' (EV)', 6X, 'VELOCITY', 10X, 'XFINAL(M)', 7X, 'YFINAL(M)')
WRITE (6,760) AVGT, AVGEN, AVGV, AVGX, AVGY
WRITE (6,790)
790 FORMAT (/, 10X, 'ALPHA-HE', 11X, 'ALPHA-N2', 10X, 'ALPHA-CO2')
WRITE (6,650) ALPHE, ALPN2, ALPCO2
WRITE (6,800)
800 FORMAT (/, 10X, 'DRIFT-E', 12X, 'DRIFT-X', 11X, 'DRIFT-B')
WRITE (6,650) DRIFTE, DRIFTX, DRIFTB
WRITE (6,810)

```

```

810  FORMAT (//, 9X, 'COLL. FREQ', 10X, 'HALL PAR', 7X,
1      'MEAN FREE PATH')
C
      WRITE (6,650) AVGNU, HALL
      WRITE (6,820) KHEPRI, KN2PRI, KCOPRI, NIPRI
820  FORMAT (/, 2X, 91('_'), //, 8X, 'TOTAL NO. OF PRIMARY HE ',
1      ' IONISATIONS = ', I5, /, 8X, 'TOTAL NO. OF PRIMARY',
2      ' N2 IONISATIONS = ', I5, /, 8X, 'TOTAL NO. OF',
3      ' PRIMARY CO2 IONISATIONS = ', I5, /, 8X, 44('-'), /,
4      8X, 'TOTAL NO. OF PRIMARY IONISATIONS', 5X, '= ', I5, /,
5      8X, 44('-'))
C
C WRITE DOWN THE AVERAGE TRANSVERSE DISCHARGE VELOCITY OF THE
C INDIVIDUAL GAS IONS AND THE OVERALL DISCHARGE VEL.
C
      TNIHE = TNIHE - INEGHE
      TNIN2 = TNIN2 - INEGN2
      TNICO2 = TNICO2 - INEGCO
      TNI = TNIHE + TNIN2 + TNICO2
C
      WRITE (6,830) TNIHE, TNIN2, TNICO2, TNI
830  FORMAT (//, 8X, 'TOTAL NO. OF HE IONS =', I5, /, 8X,
1      'TOTAL NO. OF N2 IONS = ', I5, /, 8X,
2      'TOTAL NO. OF CO2 IONS = ', I5, /, 8X, 30('-'), /, 8X,
3      'TOTAL NO. OF ALL IONS = ', I6, /, 8X, 30('-'))
C
      WRITE (6,834) TERTEL
834  FORMAT (//, 8X, 'TOTAL NO. OF TERTIARY IONISATIONS = ', I5)
C
      IF (TNIHE .GT. 0) GO TO 840
      AVGVHE = 0.0
      GO TO 850
840  AVGVHE = TOTVHE / TNIHE
850  IF (TNIN2 .GT. 0) GO TO 860
      AVGVN2 = 0.0
      GO TO 870
860  AVGVN2 = TOTVN2 / TNIN2
870  IF (TNICO2 .GT. 0) GO TO 880
      AVGVCO = 0.0
      GO TO 890
880  AVGVCO = TOTVCO / TNICO2
890  IF (TNI .GT. 0) GO TO 900
      AVGV = 0.0
      GO TO 910
900  AVGV = (TOTVHE + TOTVN2 + TOTVCO) / TNI
910  WRITE (6,920) AVGVHE, AVGVN2, AVGVCO, AVGV
920  FORMAT (//, 8X, 'AVERAGE VELOCITY OF HE IONS = ', E11.4, /,
1      8X, 'AVERAGE VELOCITY OF N2 IONS = ', E11.4, /, 8X,
2      'AVERAGE VELOCITY OF CO2 IONS = ', E11.4, /, 8X, 44('-'),
3      /, 8X, 'AVERAGE VELOCITY OF GAS MIXTURE = ', E11.4, /,
4      8X, 44('-'))
C
      WRITE (6,930)
930  FORMAT (//, 3X, 'THESE ARE THE ENERGY LEVELS AT VARIOUS ',
1      ' POSITIONS IN THE CATHODE FALL REGION', /, 5X, 'E2', 6X,
2      'E4', 6X, 'E6', 6X, 'E8', 5X, 'E10', 5X, 'E12', 5X,
3      'E14', 5X, 'E16', 5X, 'E18', 5X, 'E20')
C
      WRITE (6,940) (AENBAR(IB), IB=1,80)
940  FORMAT (8(10(2X,F6.2),/))
      WRITE (6,950) (INBAR(IB), IB=1,80)
950  FORMAT (/, 3X, 'THESE ARE THE NO. OF ELEMENTS OVER ',
1      ' WHICH AVERAGING WAS DONE', 8(/, 10(2X,I6)))
C

```

```

      IF (AVGNHE .EQ. 0.0) GO TO 941
      AVN1HE = 100*AVN1HE/AVGNHE
      AVN2HE = 100*AVN2HE/AVGNHE
      AVNIHE = 100*AVNIHE/AVGNHE
C
941 IF (AVGNN2 .EQ. 0.0) GO TO 942
      AVN1N2 = 100*AVN1N2/AVGNN2
      AVN2N2 = 100*AVN2N2/AVGNN2
      AVN3N2 = 100*AVN3N2/AVGNN2
      AVN4N2 = 100*AVN4N2/AVGNN2
      AVN5N2 = 100*AVN5N2/AVGNN2
      AVN6N2 = 100*AVN6N2/AVGNN2
      AVNIN2 = 100*AVNIN2/AVGNN2
C
942 IF (AVGNCO .EQ. 0.0) GO TO 943
      AVN1CO = 100*AVN1CO/AVGNCO
      AVN2CO = 100*AVN2CO/AVGNCO
      AVN3CO = 100*AVN3CO/AVGNCO
      AVN4CO = 100*AVN4CO/AVGNCO
      AVN5CO = 100*AVN5CO/AVGNCO
      AVN6CO = 100*AVN6CO/AVGNCO
      AVN7CO = 100*AVN7CO/AVGNCO
      AVNICO = 100*AVNICO/AVGNCO
C
943 AVNEHE = 100.0 - (AVN1HE + AVN2HE + AVNIHE)
      AVNEN2 = 100.0 - (AVN1N2 + AVN2N2 + AVN3N2 + AVN4N2
1          + AVN5N2 + AVN6N2 + AVNIN2)
      AVNECO = 100.0 - (AVN1CO + AVN2CO + AVN3CO + AVN4CO
1          + AVN5CO + AVN6CO + AVN7CO + AVNICO)
C
      WRITE(6,951) AVNEHE, AVN1HE, AVN2HE, AVNIHE, AVNEN2, AVN1N2,
1          AVN2N2, AVN3N2, AVN4N2, AVN5N2, AVN6N2, AVNIN2,
2          AVNECO, AVN1CO, AVN2CO, AVN3CO, AVN4CO, AVN5CO,
3          AVN6CO, AVN7CO, AVNICO
951 FORMAT(1X, ' ', 91X, ' ', /, 10X, 'PERCENTAGE COLLISIONS WITH HELIUM',
1          /, 5X, 4 (F7.3, 2X), /, 10X, 'PERCENTAGE COLLISIONS WITH N2',
2          /, 5X, 8 (F7.3, 2X), /, 10X, 'PERCENTAGE COLLISIONS WITH CO2',
3          /, 5X, 9 (F7.3, 2X))
      WRITE(6,955)
      IBAR = 1/(1000 * PRESS)
955 FORMAT(/, 1X, 'ELECTRON ENERGY DISTRIBUTIONS AT THE POSITIONS', 1X,
1          'NOTED ABOVE (EVERY ', F9.4, ' M AND 1 EV).')
      DO 959 K=0, 4
          WRITE(6,956) (K*10+M, M=1, 10)
956 FORMAT(12X, 10(I2, 5X))
          DO 958 II=200, 1, -1
              WRITE(6,957) II, (POPBIN(J+10*K, II), J=1, 10)
957 FORMAT(2X, I3, 5X, 10(I5, 2X))
958 CONTINUE
959 CONTINUE
1000 CONTINUE
      END
*****
**
**          PRIMARY COLLISION SUBROUTINE
**
**
*****
* AANDREW LABUN, SEPTEMBER 14, 1988
*
* THIS SUBROUTINE HANDLES THE PRIMARY ELECTRON'S TRAJECTORY UNTIL THE
* END OF THE CATHODE FALL REGION OR THE ELECTRON IS REABSORBED BY THE
* CATHODE OR ATTACHED.
*
      SUBROUTINE PRICOL (X, Y, Z, VX, VY, VZ, IBAR, ACCLN, ENPREV, POPBIN, TENBAR

```

```

1          , INBAR, L, TEMP, TIME, EN, NCOLCO, NCOLHE,
2          NCOLN2, NCOLL, PRESS, PRESHE, PRESN2, PRESKO)
C
C   PARAMETER (NCOLMN=126, NBIN=200)
C
C   INTEGER IBAR, POPBIN(0:NCOLMN-1, 1:NBIN), INBAR(NCOLMN-1), NCOLCO,
1          NCOLHE, NCOLN2, ICHECK
C
C   REAL X, Y, Z, VX, VY, VZ, ACCLN, ENPREV, TENBAR(NCOLMN-1), L(200), L2,
1          TEMP, TIME, EN, PRESS, R1, R2, T, S,
2          PRESHE, PRESKO, PRESN2, QN2(200, 8), QCO2(200, 10),
3          QHE(200, 4), P1, P2, SPHE(201, 81), SPN2(201, 81), SPCO2(201, 81)
COMMON /XSEC/ SPHE, QHE, SPN2, QN2, SPCO2, QCO2
C
C   10 ICHECK=Z*1000.*PRESS
IF (IBAR.LT.1) IBAR=1
CALL NRGDIS(IBAR, ICHECK, ACCLN, ENPREV, POPBIN, TENBAR, INBAR, EN)
CALL COLLID(X, Y, Z, VX, VY, VZ, S, T, TIME, L, TEMP, EN, ACCLN,
1          PRESHE, PRESN2, PRESKO, QHE, QN2, QCO2, NCOLL, NCOLCO,
2          NCOLHE, NCOLN2, &10, &20)
C
C IF THE PARTICLE HAS BEEN TERMINATED BY PASSING OUT OF THE
C SIMULATED REGION OR HAS BEEN ATTACHED, WE PROCEED TO LABEL 20,
C OTHERWISE WE RETURN TO LABEL 10 AND REITERATE THE COLLISION
C PROCESS.
C
C   20 ICHECK=Z*1000.*PRESS
IF (IBAR.LT.1) IBAR=1
IF (ICHECK.LT.IBAR) GO TO 60
CALL NRGDIS(IBAR, ICHECK, ACCLN, ENPREV, POPBIN, TENBAR, INBAR, EN)
60 RETURN
END
C
C
C *****
C **                                     **
C **           THE FAMOUS SUBROUTINE WHICH INCREMENTS THE ARRAYS           **
C **           WHICH CONTAIN THE ENERGY DISTRIBUTION IN SPACE.           **
C **                                     **
C *****
C
C   SUBROUTINE NRGDIS(IBAR, ICHECK, ACCLN, ENPREV, POPBIN, TENBAR, INBAR,
1          EN)
C
C   PARAMETER (NCOLMN=126, NBIN=200)
C
C   INTEGER IBAR, IENIC, ENBIN, ICHECK, POPBIN(0:NCOLMN-1, 1:NBIN),
1          INBAR(NCOLMN-1)
C
C   REAL ENCHAN, ENIC, ACCLN, ENPREV, TENBAR(NCOLMN-1), ZZ, EN
C
C   IF (ICHECK .GE. IBAR) THEN
C
C IF WE ONLY WANT TO TABULATE THE ENERGY OF REVERSE ELECTRON FLUX
C WE DON'T INCREMENT THE ELECTRONS THAT SATISFY THIS PART OF THE
C IF STATEMENT, BUT MERELY ADVANCE THE CURRENT ELECTRON POSITION
C COUNTER.
C
C   GOTO 15
C
C   DO 10 IC = IBAR, ICHECK - 1
ENCHAN = ACCLN - ENPREV
ENIC = ENPREV
1          + ENCHAN *(FLOAT(IC - IBAR+1)/FLOAT(ICHECK - IBAR+1))**2

```

```

      IENIC = INT(ENIC)
      ZZ = (ENIC - IENIC) * 10.
      IF (ZZ.GT.5) THEN
        ENBIN = IENIC + 1
      ELSE
        ENBIN = IENIC
      END IF
      IF (ENBIN.LT.1) ENBIN = 1
      IF (ENBIN.GT.200) ENBIN = 200
      POPBIN(IC,ENBIN) = POPBIN(IC,ENBIN) + 1
10  CONTINUE
      ENBIN = INT(ACCLEN)
      IF (ENBIN.GT.200) ENBIN = 200
      IF (ENBIN.LT.1) ENBIN = 1
      POPBIN(ICHECK,ENBIN) = POPBIN(ICHECK,ENBIN) + 1
      ENPREV = EN
C
C 15 CONTINUE
C
      TENBAR(ICHECK) = TENBAR(ICHECK) + EN
      INBAR(ICHECK) = INBAR(ICHECK) + 1
      IBAR = ICHECK + 1
C
C IF WE ONLY WANT TO COUNT ELECTRONS PAST THE 'HIGH-WATER MARK'
C THEN IGNORE THE REST OF THE SUBROUTINE
C
C   GOTO 30
C
      ELSE IF (ICHECK .LT. IBAR - 1) THEN
C
C IF WE WANT TO TABULATE ONLY THE FORWARD ELECTRON FLUX, THEN
C WE SKIP THE REMAINDER OF THE IF BLOCK, WITH THE EXCEPTION
C OF THE INCREMENTATION OF THE CURRENT ELECTRON COUNTER
C
      GOTO 25
C
      DO 20 IC=IBAR - 1, ICHECK + 1, -1
        ENCHAN = ACCLEN - ENPREV
        ENIC = ENPREV
1      + ENCHAN *(FLOAT(IBAR - IC)/FLOAT(IBAR - ICHECK-1))**2
        IENIC = INT(ENIC)
        ZZ = (ENIC - IENIC) * 10.
        IF (ZZ .GT. 5) THEN
          ENBIN = IENIC + 1
        ELSE
          ENBIN=IENIC
        END IF
        IF (ENBIN .LT. 1) ENBIN = 1
        IF (ENBIN .GT. 200) ENBIN = 200
C
C IF WE WANT THE TOTAL NO. OF ELECTRONS ON THE PLANE, WE INCREMENT
C POPBIN REGARDLESS OF THE DIRECTION OF THE ELECTRON'S MOTION.
C
      POPBIN(IC,ENBIN) = POPBIN(IC,ENBIN) + 1
C
C IF WE WANT THE NET FLUX OF ELECTRONS THROUGH THE PLANE, WE
C DECREMENT THE BACKWARDS TRAVELLING ELECTRONS FROM POPBIN.
C
      POPBIN(IC,ENBIN) = POPBIN(IC,ENBIN) - 1
C
20  CONTINUE
      TENBAR(ICHECK + 1) = TENBAR(ICHECK + 1) + EN
      INBAR (ICHECK + 1) = INBAR(ICHECK + 1) + 1
      ENPREV = EN

```

```

C
25 CONTINUE
C
      IBAR = ICHECK + 1
      END IF
30 CONTINUE
      RETURN
      END
.....
**
**          A SUBROUTINE TO DETERMINE THE COLLISION TYPE AND
**          THE TRAJECTORY OF THE ELECTRON
**
**
.....
C
      SUBROUTINE COLLID(X,Y,Z,VX,VY,VZ,S,T,TIME, L,TEMP,EN,ACCLN,
1          PRESHE,PRESN2,PRESKO,QHE,QN2,QCO2,NCOLL,
2          NCOLCO,NCOLHE,NCOLN2,*,*)
C
      PARAMETER (NCOLMN=126,NBIN=200,NSTEP=6)
C
      INTEGER NCOLCO,NCOLHE,NCOLN2,NCOLL,IEN
C
      REAL X,Y,Z,VX,VY,VZ,ACCLN,TEMP, L(200),L2,
1          TIME,EN,PRES,R1,R2,T,S,
2          PRESHE,PRESKO,PRESN2,QN2(200,8),QCO2(200,10),
3          QHE(200,4),P1,P2,SPHE(201,81),SPN2(201,81),SPCO2(201,81),
4          ZZ,PQHE,PQN2,PQCO2,SUMQ
C
C GENERATE RANDOM NO. R1 TO DECIDE THE PATH LENGTH OF THE ELECTRON
C BEFORE COLLISION OCCURS.
C
      R1=0.0
      CALL RANDOM(R1)
      CALL ENERGY(VX,VY,VZ,VV,EN)
      IEN=EN
      DO 10 I=1,NSTEP
        IF (IEN.LE.1) IEN=1
        IF (IEN.GE.200) IEN=200.
        L2 = L(IEN) * TEMP / 288.0
        S = -L2 * ALOG(R1) / NSTEP
        CALL ACCEL(X, Y, Z, VX, VY, VZ, S, T, TIME, EN, &50)
        IEN = EN
      10 CONTINUE
      ACCLN = EN
C
C IT IS NECESSARY TO DETERMINE WHICH ATOM THE ELECTRON COLLIDED
C WITH. THIS REQUIRES A KNOWLEDGE OF THE OVERALL CROSS-SECTIONS
C OF THE VARIOUS COMPONENT GASES.
C
      IEN = EN
      ZZ = (EN - IEN) * 10.
      IF (ZZ .GE. 5.) IEN = IEN + 1
      IF (EN .GE. 200.0) IEN = 200
      IF (IEN .LE. 1) IEN = 1
      PQHE = PRESHE * QHE(IEN,1)
      PQN2 = PRESN2 * QN2(IEN,1)
      PQCO2 = PRESKO * QCO2(IEN,1)
      SUMQ = PQHE + PQN2 + PQCO2
C
C DETERMINE TYPE OF COLLISION AND COMPUTE THE NEW STATE OF THE ELECTRON.
C
      NCOLL = NCOLL + 1
      P1 = PQHE / SUMQ

```



```

P2 = (PQHE + PQN2) / SUMQ
CALL RANDOM(R2)
IF (R2 .LT. P1) GO TO 20
IF (R2 .GE. P1 .AND. R2 .LT. P2) GO TO 30
NCOLCO = NCOLCO + 1
CALL COLCO2(X, Y, Z, VX, VY, VZ, EN, TIME, 640, 650)
20 NCOLHE = NCOLHE + 1
CALL COLHE(X, Y, Z, VX, VY, VZ, EN, TIME, 640)
30 NCOLN2 = NCOLN2 + 1
CALL COLN2(X, Y, Z, VX, VY, VZ, EN, TIME, 640)
C
40 RETURN 1
50 RETURN 2
END
*****
**
** SECONDARY COLLISION SUBROUTINE
**
*****
* ANDREW LABUN, SEPTEMBER 14, 1988
*
* THIS SUBROUTINE DOES THE SECONDARY ELECTRONS' TRAJECTORIES UNTIL THE
* END OF THE CATHODE FALL REGION OR THE ELECTRONS ARE REABSORBED BY THE
* CATHODE OR ATTACHED.
*
SUBROUTINE SECCOL (X, Y, Z, VX, VY, VZ, IBAR, ACCLEN, ENPREV, POPBIN, TENBAR
1 , INBAR, L, TEMP, TIME, EN, NCOLCO, NCOLHE,
2 NCOLN2, NCOLL, PRESS, PRESHE, PRESN2, PRESKO)
C
PARAMETER (NCOLMN=126, NBIN=200, NSEC=200)
C
INTEGER IBAR, POPBIN (0:NCOLMN-1, 1:NBIN), NCOLCO,
1 NCOLHE, NCOLN2, ICHECK
C
REAL X, Y, Z, VX, VY, VZ, ACCLEN, ENPREV, L(200), L2, TEMP,
1 TIME, EN, PRESS, R1, R2, T, S,
2 PRESHE, PRESKO, PRESN2,
3 P1, P2
C
INTEGER KIHE, KIN2, KICO2, K6N2, K7CO2
C
DIMENSION SPHE(201, 81), SPN2(201, 81), SPCO2(201, 81), QHE(200, 4),
1 QN2(200, 8), QCO2(200, 10), XIHE(200), YIHE(200),
2 ZIHE(200), VXIHE(200), VYIHE(200), VZIHE(200),
3 ENIHE(200), XIN2(200), YIN2(200), ZIN2(200), VXIN2(200),
4 VYIN2(200), VZIN2(200), ENIN2(200), XICO2(200),
5 YICO2(200), ZICO2(200), VXICO2(200), VYICO2(200),
6 VZICO2(200), ENICO2(200), TIHE(200), TIN2(200),
7 X6N2(200), Y6N2(200), Z6N2(200), VX6N2(200), VY6N2(200),
8 VZ6N2(200), EN6N2(200), X7CO2(200), Y7CO2(200),
9 Z7CO2(200), VX7CO2(200), VY7CO2(200), VZ7CO2(200),
* EN7CO2(200), TICO2(200), XNWHE(200), YNWHE(200),
1 ZNWHE(200), VXNWHE(200), VYNWHE(200), VZNWHE(200)
DIMENSION XNWN2(200), YNWN2(200), ZNWN2(200), VXNWN2(200),
1 VYNWN2(200), VZNWN2(200), XNWCO2(200), YNWCO2(200),
2 ZNWCO2(200), VXNWCO2(200), VYNWCO2(200), VZNWCO2(200),
3 TENBAR(125), INBAR(125), AENBAR(125)
C
COMMON /XSEC/ SPHE, QHE, SPN2, QN2, SPCO2, QCO2
COMMON /CHE/ XIHE, YIHE, ZIHE, VXIHE, VYIHE, VZIHE, ENIHE, TIHE,
1 KIHE, K2HE, KIHE
COMMON /CN2/ XIN2, YIN2, ZIN2, VXIN2, VYIN2, VZIN2, ENIN2, TIN2,
1 X6N2, Y6N2, Z6N2, VX6N2, VY6N2, VZ6N2, EN6N2,
2 K1N2, K2N2, K3N2, K4N2, K5N2, K6N2, KIN2

```

```

COMMON /CCO2/ XICO2, YICO2, ZICO2, VXICO2, VYICO2, VZICO2, ENICO2,
1      X7CO2, Y7CO2, Z7CO2, VX7CO2, VY7CO2, VZ7CO2, EN7CO2,
2      TICO2, K1CO2, K2CO2, K3CO2, K4CO2, K5CO2, K6CO2, K7CO2,
3      KICO2, KACO2
COMMON /SECELS/
1      XNWHE, YNWHE, ZNWHE, VXNWHE, VYNWHE, VZNWHE, XNWN2, YNWN2, ZNWN2,
2      VXNWN2, VYNWN2, VZNWN2, XNWCO2, YNWCO2, ZNWCO2, VXNWCO, VYNWCO,
3      VZNWCO
C
10 ICHECK=Z*1000.*PRESS
   KSIHE=KIHE
   KSIN2=KIN2
   KSICO2=KICO2
   KS6N2=K6N2
   KS7CO2=K7CO2
   IF (IBAR.LT.1) IBAR=1
   CALL NRGDIS (IBAR, ICHECK, ACCLN, ENPREV, POPBIN, TENBAR, INBAR, EN)
   CALL COLLID (X, Y, Z, VX, VY, VZ, S, T, TIME, L, TEMP, EN, ACCLN,
1         PRESHE, PRESN2, PRESKO, QHE, QN2, QCO2, NCOLL, NCOLCO,
2         NCOLHE, NCOLN2, &20, &30)
C
20 IF (KIHE - KSIHE .GT. 0) THEN
   XNWHE(KIHE) = X
   YNWHE(KIHE) = Y
   ZNWHE(KIHE) = Z
   VXNWHE(KIHE) = VX
   VYNWHE(KIHE) = VY
   VZNWHE(KIHE) = VZ
C
   ELSE IF (KIN2 - KSIN2 .GT. 0 .OR. K6N2 - KS6N2 .GT. 0) THEN
   XNWN2(KIN2 + K6N2) = X
   YNWN2(KIN2 + K6N2) = Y
   ZNWN2(KIN2 + K6N2) = Z
   VXNWN2(KIN2 + K6N2) = VX
   VYNWN2(KIN2 + K6N2) = VY
   VZNWN2(KIN2 + K6N2) = VZ
C
   ELSE IF (KICO2 - KSICO2 .GT. 0 .OR. K7CO2 - KS7CO2 .GT. 0) THEN
   XNWCO2(KICO2 + K7CO2) = X
   YNWCO2(KICO2 + K7CO2) = Y
   ZNWCO2(KICO2 + K7CO2) = Z
   VXNWCO(KICO2 + K7CO2) = VX
   VYNWCO(KICO2 + K7CO2) = VY
   VZNWCO(KICO2 + K7CO2) = VZ
C
   END IF
   GO TO 10
C
C IF THE PARTICLE HAS BEEN TERMINATED BY PASSING OUT OF THE
C SIMULATED REGION OR HAS BEEN ATTACHED, WE PROCEED TO LABEL 30,
C OTHERWISE WE RETURN TO LABEL 20 AND REITERATE THE COLLISION
C PROCESS.
C
30 ICHECK=Z*1000.*PRESS
   IF (IBAR.LT.1) IBAR=1
   IF (ICHECK.LT.IBAR) GO TO 60
   CALL NRGDIS (IBAR, ICHECK, ACCLN, ENPREV, POPBIN, TENBAR, INBAR, EN)
60 RETURN
   END
   SUBROUTINE RANDOM(RAND)
C*****
C
C THIS SUBROUTINE GENERATES UNIFORMLY DISTRIBUTED RANDJM NUMBERS
C BETWEEN 0 AND 1.

```

```

C
C   IMPLICIT REAL(A - H,O - Z)
C   REAL DSEED, R(1)
C   COMMON /ARRAND/ DSEED
C   S1 = (7.**5) * DSEED
C   R1 = 2. ** 31 - 1.
C   DSEED = AMOD(S1,R1)
C   RAND = DSEED / (2.**31)
C   RANDOM NUMBER GENERATOR FROM "NUMERICAL RECIPES", PRESS,FLANNERY,
C   TEUKOLSKY, AND VETTERLING, 1986, CAMBRIDGE, P. 196.
C
C   INTEGER IX1,IX2,IX3,J,IFF
C   DIMENSION R(97)
C   PARAMETER (M1=259200,IA1=7141,IC1=54773,RM1=1./M1)
C   PARAMETER (M2=134456,IA2=8121,IC2=28411,RM2=1./M2)
C   PARAMETER (M3=243000,IA3=4561,IC3=51349)
C   DATA IFF /0/
C   IF (DSEED.LT.0.OR.IFF.EQ.0) THEN
C     IFF=1
C     IX1=MOD(IC1-INT(DSEED),M1)
C     IX1=MOD(IA1*IX1+IC1,M1)
C     IX2=MOD(IX1,M2)
C     IX1=MOD(IA1*IX1+IC1,M1)
C     IX3=MOD(IX1,M3)
C     DO 10 J=1,97
C       IX1=MOD(IA1*IX1+IC1,M1)
C       IX2=MOD(IA2*IX2+IC2,M2)
C       R(J) = (FLOAT(IX1)+FLOAT(IX2)*RM2)*RM1
10    CONTINUE
C     DSEED=1.99
C   ENDIF
C   IX1=MOD(IA1*IX1+IC1,M1)
C   IX2=MOD(IA2*IX2+IC2,M2)
C   IX3=MOD(IA3*IX3+IC3,M3)
C   J=1+(97*IX3)/M3
C   IF (J.GT.97.OR.J.LT.1) J=97
C   RAND=R(J)
C   R(J) = (FLOAT(IX1)+FLOAT(IX2)*RM2)*RM1
C   RETURN
C   END
C*****C
C   SUBROUTINE INIT(X,Y, Z, VX, VY, VZ, PRESHE, PRESN2, PRESKO, L)
C*****C
C
C   C THIS SUBROUTINE INITIALISES THE POSITION AND VELOCITY OF AN ELECTRON C
C   C AS IT LEAVES THE CATHODE.
C
C   IMPLICIT REAL(A - H,O - Z)
C   REAL LHEI, LN2I, LCO2I, L(200), MU(19), DC, VC, BO, PRESS, BEAM
C
C   C INITIALISE THE POSITION OF ELECTRON TO 0. ASSUME THAT THE
C   C ELECTRON STARTS OUT WITH A Z-COMPONENT OF VELOCITY WITH AN
C   C ENERGY DISTRIBUTED BETWEEN 0 AND 10 EV PLUS A BEAM ENERGY.
C
C   COMMON /EDATA/ DC, VC, BO, MU, PRESS, BEAM
C   DATA EM /9.1D-31/
C   CALL RANDOM(R1)
C   X = 0.0
C   Y = 0.0
C   Z = 0.0
C   VX = 0.0
C   VY = 0.0
C   VZ = DSQRT(20.*1.6D-19*(R1+BEAM*0.1)/EM)
C   RETURN

```

```

      END
      *****C
      SUBROUTINE ENERGY(VX, VY, VZ, VEL2, EN)
      *****C
      C
      C THIS SUBROUTINE CALCULATES THE ELECTRON ENERGY IN ELECTRON VOLTS(EV).
      C
      IMPLICIT REAL(A - H,O - Z)
      DATA EM /9.1D-31/
      VEL2 = VX * VX + VY * VY + VZ * VZ
      EN = 0.5 * EM * VEL2
      EN = EN / 1.6D-19
      RETURN
      END
      *****C
      SUBROUTINE ACCEL(X, Y, Z, VX, VY, VZ, S, T, TIME, EN,*)
      *****C
      C
      C THIS SUBROUTINE CALCULATES THE ACCELERATION OF AN ELECTRON DUE TO THE
      C ELECTRIC AND MAGNETIC FIELD AND ALSO DETERMINES THE NEW VALUES OF
      C X,Y,Z POSITIONS AND VX,VY,VZ VELOCITIES.
      C
      IMPLICIT REAL(A - H,O - Z)
      REAL M, M2, MU(19)
      COMMON /EDATA/ DC, VC, B0, MU, PRESS, BEAM
      DATA EM /9.1D-31/, QE /-1.6D-19/
      W = QE * B0 / EM
      M = SQRT((W*W) - ((2*QE*VC)/(EM*DC*DC)))
      ZPOSN = 1 - (Z/DC)
      IF (ZPOSN.LE.0.01) ZPOSN = 0.01
      B = -((2*QE*VC)/(M*EM*DC)) * ZPOSN + (W*VY) / M
      WB = W * B
      M2 = M * M
      CALL TIMER(X, Y, Z, VX, VY, VZ, S, T)
      SINE = SIN(M*T)
      COSINE = COS(M*T)
      VXOLD = VX
      VYOLD = VY
      VZOLD = VZ
      X = VX * T + X
      Y = (W*VZOLD/M2) * (COSINE - 1.) + (WB/M2) * SINE + (VYOLD - (WB/
      1M)) * T + Y
      Z = (VZ/M) * SINE - (B/M) * (COSINE - 1) + Z
      VX = VXOLD
      VY = -(W*VZOLD/M) * SINE + (WB/M) * (COSINE - 1.) + VYOLD
      VZ = VZOLD * COSINE + B * SINE
      C
      TIME = TIME + T
      CALL ENERGY(VX, VY, VZ, VEL2, EN)
      C
      IF (Z .LE. 0.0 .OR. (Z .GT. (DC+0.00015) .AND. EN .LT. 15.0))
      IF (Z .LE. 0.0 .OR. Z .GT. DC,
      1 GO TO 20
      10 RETURN
      20 RETURN 1
      END
      *****C
      SUBROUTINE COLHE(X, Y, Z, VX, VY, VZ, EN, TIME,*)
      *****C
      C
      C THE AIM OF THIS SUBROUTINE IS TO DETERMINE WHICH OF THE FOLLOWING
      C TYPES OF COLLISION IS UNDERGONE BY THE ELECTRON.
      C
      C (I) ELASTIC
      C
      C (II) METASTABLE TRIPLET EXCITATION (2 S) WITH
      C

```

```

C          EXCITATION ONSET AT 19.8 EV.                                C
C          (III) EXCITATION TO 2 P LEVEL WITH ONSET AT                C
C          21.5 EV.                                                  C
C          (IV) IONISATION WITH ONSET AT 24.5 EV.                    C
C          IMPLICIT REAL(A - H,Q - Z)
C          DIMENSION XIHE(200), YIHE(200), ZIHE(200), VXIHE(200), VYIHE(200),
1          VZIHE(200), ENIHE(200), QHE(200,4), SPHE(201,81),
2          EHE(3), TIHE(200), SPN2(201,81), QN2(200,8),
3          SPCO2(201,81), QCO2(200,10)
C          COMMON /XSEC/ SPHE, QHE, SPN2, QN2, SPCO2, QCO2
C          COMMON /ARRAND/ ESEED
C          COMMON /CHE/ XIHE, YIHE, ZIHE, VXIHE, VYIHE, VZIHE, ENIHE, TIHE,
1          K1HE, K2HE, KIHE
C          DATA EM /9.1D-31/

C
C DEFINE THE VARIOUS EXCITATION ONSET IN E.S.
EHE(1) = 19.8
EHE(2) = 21.5
EHE(3) = 24.5

C
CALL ENERGY(VX, VY, VZ, VEL2)
VEL = SQRT(VEL2)
IEN = EN
ZZ = (EN - IEN) * 10.
IF (ZZ .GE. 5) IEN = IEN + 1
IF (EN .GE. 200) IEN = 200
IF (IEN .LE. 1) IEN = 1
SUMQ = EHE(IEN,2) + QHE(IEN,3) + QHE(IEN,4)
CALL RANDOM(R2)
DIVQ = SUMQ / QHE(IEN,1)

C
C AN ELASTIC COLLISION IS ASSUMED TO OCCUR IF THE RANDOM NO. R2 IS
C GREATER THAN OR EQUAL TO DIVQ.
C
IF (R2 .GE. DIVQ) GO TO 50

C
C IN CASE OF AN INELASTIC COLLISION DETERMINE WHICH TYPE IT IS.
C
CHECK = 0.0
J = 2
10 CHECK = CHECK + (QHE(IEN,J)/QHE(IEN,1))
IF (R2 .LT. CHECK) GO TO 20

C
C IF R2 IS LESS THAN CHECK THIS MEANS THAT THE LEVEL 'J' IS EXCITED.
C OTHERWISE CHECK FOR LEVEL 'J+1'. IONISATION OCCURS IF J = 4.
C
J = J + 1
IF (J .EQ. 4) GO TO 40
GO TO 10

C
C EXCITATION TO A HIGHER LEVEL OCCURS.
C
20 JK = J - 1
EN = EN - EHE(JK)

C
IF (JK .NE. 1) GO TO 30
K1HE = K1HE + 1
GO TO 50

C
30 K2HE = K2HE + 1
GO TO 50

C
C IONISATION OCCURS.
40 EN = (EN - EHE(3)) / 10

```

```

C
C STORE THE POSITION AND VELOCITY OF IONISED ELECTRONS. KI DENOTES THE
C NUMBER OF IONISED ELECTRONS.
  CALL NEWVEL(KIHE, VXIHE, VYIHE, VZIHE, XIHE, YIHE, ZIHE, ENIHE, X,
  1   Y, Z, EN)
  TIME(KIHE) = TIME
50 IFLAG = 1
  CALL NEWSTA(EN, X, Y, Z, VX, VY, VZ, IFLAG, 160)
C
60 RETURN 1
  END
C*****
  SUBROUTINE COLN2(X, Y, Z, VX, VY, VZ, EN, TIME,*)
C*****
C
C THE AIM OF THIS SUBROUTINE IS TO DETERMINE WHICH OF THE FOLLOWING
C TYPES OF COLLISION IS UNDERGONE BY THE ELECTRON WITH N2.
C (I) ELASTIC
C (II) VIBRATIONAL EXCITATION
C (III) EXCITATION TO 6.22EV LEVEL
C (IV) EXCITATION TO 7.39EV LEVEL
C (V) EXCITATION TO 8.59EV LEVEL
C (VI) EXCITATION TO 11.1EV LEVEL
C (VII) IONISATION WITH ONSET AT 15.7 EV.
C (VIII) DISS. IONIS. WITH ONSET AT 25.0 EV.
C
  IMPLICIT REAL(A - H, O - Z)
  DIMENSION XIN2(200), YIN2(200), ZIN2(200), VXIN2(200), VYIN2(200),
  1   VZIN2(200), ENIN2(200), X6N2(200), Y6N2(200), Z6N2(200),
  2   VX6N2(200), VY6N2(200), VZ6N2(200), EN6N2(200), EN2(7),
  3   TIN2(200), SPHE(201,81), QHE(200,4), SPN2(201,81),
  4   QN2(200,8), SPCO2(201,81), QCO2(200,10)
C
  COMMON /XSEC/ SPHE, QHE, SPN2, QN2, SPCO2, QCO2
  COMMON /ARRAND/ DSEED
  COMMON /CN2/ XIN2, YIN2, ZIN2, VXIN2, VYIN2, VZIN2, ENIN2, TIN2,
  1   X6N2, Y6N2, Z6N2, VX6N2, VY6N2, VZ6N2, EN6N2,
  2   K1N2, K2N2, K3N2, K4N2, K5N2, K6N2, KIN2
  DATA EM /9.1D-31/
C
C DEFINE THE VARIOUS EXCITATION ONSET LEVELS.
  EN2(1) = 1.5
  EN2(2) = 6.22
  EN2(3) = 7.39
  EN2(4) = 8.59
  EN2(5) = 11.1
  EN2(6) = 15.7
  EN2(7) = 25.0
C
  CALL ENERGY(VX, VY, VZ, VEL2, EN)
  VEL = SQRT(VEL2)
  IEN = EN
  IQ = (EN - IEN) * 10.
  IF (ZZ .GE. 5) IEN = IEN + 1
  IF (EN .GE. 200) IEN = 200
  IF (IEN .LE. 1) IEN = 1
  SUMQ = QN2(IEN,2) + QN2(IEN,3) + QN2(IEN,4) + QN2(IEN,5) + QN2(
  1IEN,6) + QN2(IEN,7) + QN2(IEN,8)
  CALL RANDOM(R2)
  DIVQ = SUMQ / QN2(IEN,1)
C
C AN ELASTIC COLLISION IS ASSUMED TO OCCUR IF THE RANDOM NO. R2 IS
C GREATER THAN OR EQUAL TO DIVQ.
C

```

```

      IF (R2 .GE. DIVQ) GO TO 110
C
C IN CASE OF AN INELASTIC COLLISION DETERMINE WHICH TYPE IT IS.
C
      CHECK = 0.0
      J = 2
      10 CHECK = CHECK + (QN2(IEN, J)/QN2(IEN,1))
      IF (R2 .LT. CHECK) GO TO 20
C
C IF R2 IS LESS THAN CHECK THIS MEANS THAT THE LEVEL 'J' IS EXCITED.
C OTHERWISE CHECK FOR LEVEL 'J+1'. IONISATION OCCURS IF J = 7. DISS.
C IONISATION OCCURS IF J=8.
C
      J = J + 1
      IF (J .EQ. 8) GO TO 20
      GO TO 10
C
C EXCITATION TO A HIGHER LEVEL OCCURS.
C
      20 JK = J - 1
      IF (JK .EQ. 6 .OR. JK .EQ. 7) GO TO 30
      EN = EN - EN2(JK)
      GO TO 40
      30 EN = (EN - EN2(JK)) / 2.
      GO TO 90
C
      40 IF (JK .NE. 1) GO TO 50
      K1N2 = K1N2 + 1
      GO TO 110
      50 IF (JK .NE. 2) GO TO 60
      K2N2 = K2N2 + 1
      GO TO 110
      60 IF (JK .NE. 3) GO TO 70
      K3N2 = K3N2 + 1
      GO TO 110
      70 IF (JK .NE. 4) GO TO 80
      K4N2 = K4N2 + 1
      GO TO 110
      80 IF (JK .NE. 5) GO TO 90
      K5N2 = K5N2 + 1
      GO TO 110
      90 IF (JK .NE. 6) GO TO 100
      CALL NEWVEL(K6N2, VXIN2, VYIN2, VZIN2, XIN2, YIN2, ZIN2, ENIN2, X,
      1      Y, Z, EN)
      TIN2(KIN2) = TIME
      GO TO 110
C
C DISSOCIATIVE IONISATION OCCURS. K6 DENOTES THE NUMBER OF
C DISSOCIATIVE-IONISED ATOMS OF N2. STORE THE POSITION AND
C VELOCITY OF IONISED ELECTRONS.
C
      100 CALL NEWVEL(K6N2, VX6N2, VY6N2, VZ6N2, X6N2, Y6N2, Z6N2, EN6N2, X,
      1      Y, Z, EN)
      110 IFLAG = 2
      CALL NEWSTA(EN, X, Y, Z, VX, VY, VZ, IFLAG, &120)
C
      120 RETURN 1
      END
C*****C
      SUBROUTINE CO2CO2(X, Y, Z, VX, VY, VZ, EN, TIME,*,*)
C*****C
C
C THE AIM OF THIS SUBROUTINE IS TO DETERMINE WHICH OF THE FOLLOWING
C TYPES OF COLLISION IS UNDERGONE BY THE ELECTRON.

```

```

C      (I) ELASTIC
C      (II) VIBRATIONAL EXCITATION
C      (III) EXCITATION TO 3.1EV LEVEL
C      (IV) EXCITATION TO 6.1EV LEVEL
C      (V) EXCITATION TO 7.0EV LEVEL
C      (VI) EXCITATION TO 10.5EV LEVEL
C      (VII) EXCITATION TO 11.5EV LEVEL
C      (VIII) IONISATION WITH ONSET AT 13.3 EV.
C      (IX) DISS. IONIS. WITH ONSET AT 25.0 EV.
C      (X) DISS. ATTACH. WITH ONSET AT 3.0 EV.
C
C      IMPLICIT REAL(A - H,O - Z)
C      DIMENSION XICO2(200), YICO2(200), ZICO2(200), VXICO2(200),
1          VYICO2(200), VZICO2(200), ENICO2(200), X7ICO2(200),
2          Y7ICO2(200), Z7ICO2(200), VX7ICO2(200), VY7ICO2(200),
3          VZ7ICO2(200), EN7ICO2(200), ECO2(9), TICO2(200),
4          SPHE(201,81), QHE(200,4), SPN2(201,81), QN2(200,8),
5          SPCO2(201,81), QCO2(200,10)
C      COMMON /XSEC/ SPHE, QHE, SPN2, QN2, SPCO2, QCO2
C      COMMON /ARRAND/ DSFED
C      COMMON /CCO2/ XICO2, YICO2, ZICO2, VXICO2, VYICO2, VZICO2, ENICO2,
1          X7ICO2, Y7ICO2, Z7ICO2, VX7ICO2, VY7ICO2, VZ7ICO2, EN7ICO2,
2          TICO2, K1CO2, K2CO2, K3CO2, K4CO2, K5CO2, K6CO2, K7CO2,
3          K1CO2, K4CO2
C      DATA EM /9.1D-31/
C
C      DEFINE THE VARIOUS EXCITATION ONSET LEVELS.
C      ECO2(1) = 0.0
C      ECO2(2) = 3.1
C      ECO2(3) = 6.1
C      ECO2(4) = 7.0
C      ECO2(5) = 10.5
C      ECO2(6) = 11.5
C      ECO2(7) = 13.3
C      ECO2(8) = 25.0
C      ECO2(9) = 3.0
C
C      CALL ENERGY(VX, VY, VZ, VEL2, EN)
C      EL = SQRT(VEL2)
C      IEN = EN
C      ZZ = (EN - IEN) * 10.
C      IF (ZZ .GE. 5) IEN = IEN + 1
C      IF (EN .GE. 200) IEN = 200
C      IF (IEN .LE. 1) IEN = 1
C      SUMQ = QCO2(IEN,2) + QCO2(IEN,3) + QCO2(IEN,4) + QCO2(IEN,5) +
1      QCO2(IEN,6) + QCO2(IEN,7) + QCO2(IEN,8) + QCO2(IEN,9) + QCO2(IEN,
2      10)
C      CALL RANDOM(R2)
C      DIVQ = SUMQ / QCO2(IEN,1)
C
C      AN ELASTIC COLLISION IS ASSUMED TO OCCUR IF THE RANDOM NO. R2 IS
C      GREATER THAN OR EQUAL TO DIVQ.
C
C      IF (R2 .GE. DIVQ) GO TO 130
C
C      IN CASE OF AN INELASTIC COLLISION DETERMINE WHICH TYPE IT IS.
C
C      CHECK = 0.0
C      J = 2
C      10 CHECK = CHECK + (QCO2(IEN,J)/QCO2(IEN,1))
C      IF (R2 .LT. CHECK) GO TO 20
C
C      IF R2 IS LESS THAN CHECK THIS MEANS THAT THE LEVEL 'J' IS EXCITED.
C      OTHERWISE CHECK FOR LEVEL 'J+1'. IONISATION OCCURS IF J = 6. DISS.

```



```

C IONISATION OCCURS IF J=9, DISS. ATT. OCCURS IF J=10.
C
  J = J - 1
  IF (J .EQ. 11) GO TO 20
  GO TO
C
C EXCITATION TO A HIGHER LEVEL OCCURS.
C
  20 JK = J - 1
  IF (JK .EQ. 7 .OR. JK .EQ. 8) GO TO 30
  EN = EN - ECO2(JK)
  GO TO 40
  30 EN = (EN - ECO2(JK)) / 2.
  GO TO 110
C
  40 IF (JK .NE. 1) GO TO 50
  K1CO2 = K1CO2 + 1
  GO TO 130
  50 IF (JK .NE. 2) GO TO 60
  K2CO2 = K2CO2 + 1
  GO TO 130
  60 IF (JK .NE. 3) GO TO 70
  K3CO2 = K3CO2 + 1
  GO TO 130
  70 IF (JK .NE. 4) GO TO 80
  K4CO2 = K4CO2 + 1
  GO TO 130
  80 IF (JK .NE. 5) GO TO 90
  K5CO2 = K5CO2 + 1
  GO TO 130
  90 IF (JK .NE. 6) GO TO 100
  K6CO2 = K6CO2 + 1
  GO TO 130
  100 KACO2 = KACO2 + 1
  GO TO 150
  110 IF (JK .NE. 7) GO TO 120
  CALL NEWVEL(KICO2, VXICO2, VYICO2, VZICO2, XICO2, YICO2, ZICO2,
  1 ENICO2, X, Y, Z, EN)
  TICO2(KICO2) = TIME
  GO TO 130
C
C DISSOCIATIVE IONISATION OCCURS. K7 DENOTES THE NUMBER OF
C DISSOCIATIVE-IONISED ATOMS OF CO2. STORE THE POSITION AND
C VELOCITY OF IONISED ELECTRONS.
C
  120 CALL NEWVEL(K7CO2, VX7CO2, VY7CO2, VZ7CO2, X7CO2, Y7CO2, Z7CO2,
  1 EN7CO2, X, Y, Z, EN)
  130 IFLAG = 3
  CALL NEWSTA(EN, X, Y, Z, VX, VY, VZ, IFLAG, &140)
C
  140 RETURN 1
  150 RETURN 2
  END
C*****C
  SUBROUTINE NEWVEL(KI, VXI, VYI, VZI, XI, YI, ZI, ENI, X, Y, Z, EN)
C*****C
C
C THIS SUBROUTINE CALCULATES THE VELOCITY COMPONENTS OF THE
C SECONDARY ELECTRON CREATED BY AN EXCITATION COLLISION.
C
  IMPLICIT REAL(A - H, O - Z)
  DIMENSION VYI(200), VYI(200), VZI(200), ENI(200), XI(200),
  1 YI(200), ZI(200)
  COMMON /ARRAND/ DSEED

```

```

DATA EM /9.1D-31/
KI = KI + 1
IF (EN .LE. 0.0) EN = 0
CONST = 2.0 * EN * 1.6E-19 / EM
CALL RANDOM(R1)
CALL RANDOM(R2)
CALL RANDOM(R3)
RTOT = R1 + R2 + R3
VXI(KI) = SQRT(CONST*R1/RTOT)
VYI(KI) = SQRT(CONST*R2/RTOT)
VZI(KI) = SQRT(CONST*R3/RTOT)
CALL RANDOM(R11)
CALL RANDOM(R21)
CALL RANDOM(R31)
IF (R11 .GE. 0.5) VXI(KI) = -VXI(KI)
VXI(KI) = -VXI(KI)
IF (R21 .GE. 0.5) VYI(KI) = -VYI(KI)
VYI(KI) = -VYI(KI)
IF (R31 .GE. 0.5) VZ(KI) = -VZ(KI)
VZ(KI) = -VZ(KI)
XI(KI) = X
YI(KI) = Y
ZI(KI) = Z
ENI(KI) = EN
RETURN
END
C*****C
SUBROUTINE NEWSTA(EN, X, Y, Z, VX, VY, VZ, IFLAG,*)
C*****C
C
C THE AIM OF THIS SUBROUTINE IS TO DETERMINE THE STATE OF THE ELECTRON
C AFTER A COLLISION HAS OCCURED. TWO RANDOM NUMBERS R3 AND R4 ARE USED
C TO DETERMINE THE ANGLES THETA AND PHI RESPECTIVELY. C
C
IMPLICIT REAL(A - H,O - Z)
DIMENSION SPHE(201,81), QHE(200,4), SPN2(201,81), QN2(200,8),
1 SPCO2(201,81), QCO2(200,10)
COMMON /ARRAND/ DSLED
COMMON /XSEC/ SPHE, QHE, SPN2, QN2, SPCO2, QCO2
DATA EM /9.1D-31/
CALL RANDOM(R3)
X1 = R3 / 0.0125
IIX = X1
Y1 = (X1 - IIX) * 10.
IF (Y1 .GE. 5) IIX = IIX + 1
IIX = IIX + 1
IEN = EN
Z1 = (EN - IEN) * 10.
IF (Z1 .GE. 5) IEN = IEN + 1
IEN = IEN + 1
IF (EN .GE. 101.) IEN = 101
IF (IEN .LE. 1) IEN = 1
IF (IEN .GE. 101) IEN = 101
IF (EN .LE. 0) EN = 0.00001
C
IF (IFLAG .GE. 2) GO TO 10
THETAC = SPHE(IEN,IIX) * 3.1415927 / 180.0
GO TO 30
10 IF (IFLAG .EQ. 3) GO TO 20
THETAC = SPN2(IEN,IIX) * 3.1415927 / 180.0
GO TO 30
20 THETAC = SPCO2(IEN,IIX) * 3.1415927 / 180.0
C
30 CALL RANDOM(R4)

```

```

PHIC = 2. * 3.1415927 * P4
V1 = SQRT(VX*VX + VY*VY + VZ*VZ)
V = DSQRT(2.*EN*1.6D-19/EM)
IF (V1 .EQ. 0.0) GO TO 40
VZ11 = VZ / V1
IF (VZ11 .GE. 1.0) VZ11 = 1.0
THETA1 = ACOS(VZ11)
GO TO 50
40 THETA1 = 0.0
50 PHII = FCNPHI(VX,VY)
C
C IMPLEMENT FORWARD SCATTERING BY MAKING ALL ANGLES ZERO
C
C THETAC=0.0
C THETA1=0.0
C PHII=0.0
C PHIC=0.0
C
SINPI = SIN(PHII)
COSPI = COS(PHII)
SINPC = SIN(PHIC)
COSPC = COS(PHIC)
SINTI = SIN(THETA1)
COSTI = COS(THETA1)
SINTC = SIN(THETAC)
COSTC = COS(THETAC)
VX = V * (COSPI*COSTI*SINTC*COSPC
1      -SINPI*SINTC*SINPC
2      +COSPI*SINTI*COSTC)
VY = V * (SINPI*COSTI*SINTC*COSPC
1      +COSPI*SINTC*SINPC
2      +SINPI*SINTI*COSTC)
VZ = V * (-SINTI*SINTC*COSPC
1      +COSTI*COSTC)
RETURN 1
END
C*****#C
      FUNCTION FCNPHI(VX, VY)
C*****C
C
C FCNPHI CALCULATES ANGLE PHII (INITIAL ANGLE PHI) WHICH THE
C VELOCITY VECTOR JUST BEFORE COLLISION MAKES ON THE X-Y PLANE
C WITH THE X-AXIS.
C
      IMPLICIT REAL(A-H,O-Z)
      IF (VX .EQ. 0.0) THEN
        IF (VY .GT. 0.0) THEN
          FCNPHI = 3.1415927/2.0
        ELSE
          FCNPHI = 3*3.1415927/2.0
        ENDIF
      ELSE
        IF (VX .GT. 0.0) THEN
          FCNPHI = ATAN(VY/VX)
        ELSE
          FCNPHI = 3.1415927 + ATAN(VY/VX)
        ENDIF
      ENDIF
      RETURN
      END
*****
* A SUBROUTINE TO PROVOKE A NOMINAL EXIT IN THE CASE OF A RUN LIKELY
* TO EXCEED ITS TIME LIMIT.
*

```

```

* ILEFT IS HOW MANY STU'S REMAIN AVAILABLE TO THE PROGRAM OF THE
* ORIGINAL LIMIT AFTER THE OVERHEAD HAS BEEN DEDUCTED. IT IS
* SET TO ZERO AT THE START OF THE MAIN PROGRAM AND THIS VALUE IS
* CHECKED FOR AT THE START OF THE SUBROUTINE.
* EXPTL. VERSION 1 05-16-88 ANDREW LABUN
*
      SUBROUTINE CHKCPU(STAY, ILEFT)
C
      LOGICAL STAY
      REAL ALEFT, ATIME1, CPUBUF, SBU, STIME1, STU, TLEFT, TUSED, ATIME1
      1      , ZTLEFT
C      INTEGER ILEFT
      REAL ILEFT
C
C EVALUATE THE NUMBER OF CPU SECONDS REMAINING AND SET STAY=.TRUE.
C UNTIL THE TIME REMAINING IS BELOW SOME CRITICAL VALUE CPUBUF.
C
      CALL Q5GETACT('SYSTIME=', STIME1, 'CPUTIME=', ATIME1, 'SYSCHRG=',
      1      STU, 'USRCHRG=', SBU)
      STIME1 = STIME1 * 1.E-6
      ATIME1 = ATIME1 * 1.E-6
      STU = STU * 1.E-6
      SBU = SBU * 1.E-6
      ZTIME1=AMAX1(ATIME1, SBU, 0)
      CALL Q5GETTL('OLDTIME=', ZTLEFT)
      ZTLEFT=ZTLEFT*1.0E-6
      IF (ILEFT.LE.0.0) ILEFT=ZTLEFT-STU
      ALEFT=ILEFT-ZTIME1
      TLEFT=AMIN1(ALEFT, ZTLEFT)
      TUSED=ATIME1
C
C NOW WE CHECK OUR TIME LEFT AND DECIDE WHETHER TO STAY OR NOT.
C
      STAY=.TRUE.
      CPUBUF=120.
      IF (TLEFT.LT.CPUBUF) STAY=.FALSE.
C
C      WRITE(6,10) ALEFT, ATIME1, SBU, STU, ZTLEFT
C 10  FORMAT(1X, E9.2, ' SEC LEFT ', E7.2, '=ATIME1 ', E7.2, '=SBU ',
C      1      E7.2, '=STU ', E7.2, '=ZTLEFT')
C      ILEFT=1.0
      RETURN
      END
C
C*****
      SUBROUTINE TIMER(X, Y, Z, VX, VY, VZ, S, T)
C*****
      IMPLICIT REAL(A - H, O - Z)
      REAL M, MU(19)
      EXTERNAL F
      COMMON /EDATA/ DC, VC, B0, MU, PRESS, LAMB
      COMMON /PARS/ A0, A1, A2, A3, A4, A5
      DATA EM /9.1D-31/, QE /-1.6D-19/
      W = QE * B0 / EM
      M = SQRT((W*W) - ((2*QE*VC)/(EM*DC*DC)))
      ZPOSN = 1 - Z/DC
      B1 = -((2*QE*VC)/(M*EM*DC)) * ZPOSN + (W*VY) / W
      WB = W * B1
      DELTA = S
      V = SQRT(VX*VX + VY*VY + VZ*VZ)
      T = S / 1.33E6
      IF (V .NE. 0.0) T = S / V
      A0 = VX
      A1 = -W * VZ / M

```

```

A2 = WB / M
A3 = VY
A4 = VZ
A5 = B1
A = C.0
ACC = 1.0E-5
DXMAX = 3.0
USUM = S * M
B = M * T
CALL UNSIMP(F, A, B, ACC, USUM, ERROR, AREA, DXMAX, IFLAG)
C
C DISABLE UNSIMP ERROR MESSAGE TO SHORTEN OUTPUT FILE
IFLAG=1
C
B = B + ERROR
T = B / M
C
IFLAG = 1 FOR NORMAL RETURN.
C
= 2 IF IT IS NECESSARY TO GO TO 30 LEVELS OR USE A SUB-
C
INTERVAL TOO SMALL FOR MACHINE WORD LENGTH. ERROR
C
MAY BE UNRELIABLE IN THIS CASE.
C
= 3 IF MORE THAN 2000 FUNCTION EVALUATIONS ARE
C
USED. ROUGH APPROXIMATIONS ARE USED TO COMPLETE
C
THE COMPUTATIONS AND ERROR IS USUALLY UNRELIABLE.
C
= 4 IF THE ALGORITHM FAILS DUE TO F(X) BEING
C
PREDOMINANTLY NEGATIVE ON SOME SUB-INTERVAL.
C
IF (IFLAG .EQ. 1) GO TO 30
WRITE (6,10)
10 FORMAT (1X, 'IFLAG = 1 ----> NORMAL RETURN', /, 1X,
1 'IFLAG = 2 ----> NECESSARY TO GO TO 40 LEVELS OR USE A ', /
2 ', 17X, 'SUB-INTERVAL TOO SMALL FOR MACHINE WORD', /, 17X,
3 'LENGTH. THE ANSWER RETURNED IS NOT CORRECT.', /, 1X,
4 'IFLAG = 3 ----> MORE THAN 5000 FUNCTION EVALUATIONS', /,
5 1X, 'IFLAG = 4 ----> F(X) IS PREDOMINANTLY -VE ON', 1X,
6 'SOME SUB-INTERVAL')
WRITE (6,20) IFLAG
20 FORMAT (1X, 'IFLAG = ', I4)
C
STOP
30 RETURN
END
C*****C
FUNCTION F(X)
C*****C
IMPLICIT REAL(A - H,O - Z)
COMMON /PARS/ A0, A1, A2, A3, A4, A5
COSX = COS(X)
SINX = SIN(X)
Z1 = A0 * A0
Z2 = (A1*SINX + A2*(COSX - 1.) + A3) ** 2
Z3 = (A4*COSX + A5*SINX) ** 2
F = SQRT(Z1 + Z2 + Z3)
RETURN
END
C*****C
SUBROUTINE UNSIMP(F, A, B, ACC, USUM, ERROR, AREA, DXMAX, IFLAG)
C*****C
C
C UNSIMP IS AN ADAPTIVE, ITERATIVE CODE BASED ON SIMPSON'S RULE.
C IT IS DESIGNED TO EVALUATE THE UPPER LIMIT OF INTEGRATION REQUIRED
C TO MAKE THE DEFINITE INTEGRAL OF A CONTINUOUS NON-NEGATIVE FUNCTION
C CLOSE TO A USER SPECIFIED SUM.
C
C
C
C F ----- NAME OF FUNCTION TO BE INTEGRATED. THE
FUNCTION NAME F MUST APPEAR IN AN EXTERNAL STATE-

```

```

C          MENT IN THE CALLING PROGRAM.
C
C      A --- LOWER LIMIT OF INTEGRATION.
C      B --- UPPER LIMIT OF INTEGRATION. ON ENTRY THIS IS SET
C          TO INITIALIZE THE SEARCH. UNSIMP WILL SEARCH
C          FOR THE UPPER LIMIT WHICH MAKES THE DEFINITE
C          INTEGRAL CLOSE TO USUM, THE VALUE
C          SPECIFIED BY THE USER. COMPUTATION WILL BE QUICKER
C          IF THE INITIAL VALUE OF B GIVEN TO THE ROUTINE IS AN
C          UNDERESTIMATION.
C      ACC --- THE DESIRED ACCURACY OF THE FINAL UPPER LIMIT (B).
C          THE CODE TRIES TO MAKE THE ERROR IN B LESS THAN
C          ACC*B.
C      USUM -- THE USER-SPECIFIED VALUE OF THE INTEGRAL OF F(X).
C      ERROR - ESTIMATED ERROR OF B. USER MAY WISH TO EXTRAPOLATE
C          BY FORMING B+ERROR TO GET WHAT IS OFTEN A MORE
C          ACCURATE RESULT. BUT NOT ALWAYS.
C      AREA -- THE CALCULATED INTEGRAL OF F(X) FROM X=A TO X=B,
C          WHERE B REPRESENTS THE FINAL VALUE OF B.
C
C      DXMAX - THE MAXIMUM LIMIT ON THE WIDTH OF A
C          SUB-INTERVAL TO BE USED TO YIELD
C          AN ACCEPTABLE VALUE OF THE INTEGRAL. FOR
C          PERIODIC FUNCTIONS, DXMAX SHOULD BE SET
C          TO THE PERIOD (OR SMALLER) TO PREVENT
C          UNDESIRABLE TERMINATION OF THE ALGORITHM
C          IN CASE OF PREMATURE CONVERGENCE OF
C          SIMPSON'S RULE.
C
C      IFLAG = 1 FOR NORMAL RETURN.
C          = 2 IF IT IS NECESSARY TO GO TO 40 LEVELS OR USE A SUB-
C          INTERVAL TOO SMALL FOR MACHINE WORD LENGTH.
C          THE ANSWER RETURNED IS NOT CORRECT.
C          = 3 IF MORE THAN 5000 FUNCTION EVALUATIONS ARE
C          USED.
C          THE ANSWER RETURNED IS NOT CORRECT.
C          = 4 IF THE ALGORITHM FAILS DUE TO F(X) BEING
C          PREDOMINANTLY NEGATIVE ON SOME SUB-INTERVAL.
C          THE ANSWER RETURNED IS NOT CORRECT.
C
C      DIMENSION LORR(40), F1T(40), F2T(40), F3T(40), DAT(40), ESTT(40),
C          1 PSUM(40)
C      REAL F, F1T, F2T, F3T, DAT, ESTT, PSUM, ACC, ALPHA, DA, DX, A, B,
C          1 EST, ESTL, ESTR, WT, DELSUM, USUM, SUM, AREA, PAREA, ERROR,
C          2 DXMAX, PDIFF, DIFF, FV1, FV2, FV3, FV4, FV5, B2
C
C      SET U TO APPROXIMATE THE UNIT ROUND-OFF OF SPECIFIC MACHINE.
C      HERE IBM 360/370 : L.
C
C      U = 2.220E-16
C      FOURU = 4.0 * U
C      IFLAG = 1
C      KOUNT = 3
C      LVL = 1
C      PSUM(LVL) = 0.0
C      ALPHA = A
C      PAREA = 0.0
C      PDIFF = 0.
C
C      10 LORR(LVL) = 1
C          DA = B - ALPHA
C          FV1 = F(ALPHA)
C          FV3 = F(ALPHA + 0.5*DA)

```

```

      FV5 = F(ALPHA + DA)
      WT = DA / 6.0
      EST = WT * (FV1 + 4.0*FV3 + FV5)
C
C 'BASIC STEP'. HAVE ESTIMATE EST OF INTEGRAL ON (ALPHA, ALPHA+DA)
C BISECT AND COMPUTE ESTIMATES ON LEFT AND RIGHT HALF INTERVALS.
C
20 DX = 0.5 * DA
   FV2 = F(ALPHA + 0.5*DX)
   FV4 = F(ALPHA + 1.5*DX)
   KOUNT = KOUNT + 2
   WT = DX / 6.0
   ESTL = WT * (FV1 + 4.0*FV2 + FV3)
   ESTR = WT * (FV3 + 4.0*FV4 + FV5)
   SUM = ESTL + ESTR
   DIFF = EST - SUM
C
C IF ERROR IS ACCEPTABLE, GO TO 80. IF INTERVAL IS TOO SMALL OR
C TOO MANY LEVELS OR TOO MANY FUNCTION EVALUATIONS, SET A FLAG
C AND GO TO 80 ANYWAY.
C
   IF (SUM .LT. 0.) GO TO 110
   AREA = PAREA + SUM
   B2 = ALPHA + DA
   IF (ABS(ABS(USUM - AREA) - ABS(PDIFF)) + ABS(DIFF) .GT. FV5*ACC*(
1   B2 - A)) GO TO 30
   ERROR = (USUM - AREA - (PDIFF + DIFF)/15) / FV5
   B = B2
   RETURN
30 IF (ABS(USUM - AREA) .LE. ABS(PDIFF + DIFF)) GO TO 50
   IF (USUM .GT. AREA) GO TO 40
   PSUM(1) = PAREA
   LVL = 1
   LORR(LVL) = 1
   GO TO 50
40 IF (ABS(DIFF) .LE. FV5*ACC*DA .AND. DA .LE. DXMAX) GO TO 60
50 IF (LVL .GE. 40) GO TO 90
   IF (ABS(DX) .LE. FOURU*ABS(ALPHA)) GO TO 90
   IF (KOUNT .GE. 5000) GO TO 100
C
C HERE TO RAISE LEVEL. STORE INFORMATION TO PROCESS RIGHT HALF
C INTERVAL LATER. INITIALISE FOR 'BASIC STEP' SO AS TO TREAT
C LEFT HALF INTFRVAL.
C
   LVL = LVL + 1
   PSUM(LVL) = 0.
   LORR(LVL) = 0
   F1T(LVL) = FV3
   F2T(LVL) = FV4
   F3T(LVL) = FV5
   DA = DX
   DAT(LVL) = DX
   EST = ESTL
   ESTT(LVL) = ESTR
   FV5 = FV3
   FV3 = FV2
   GO TO 20
C
C ACCEPT APPROXIMATE INTEGRAL SUM. IF IT WAS ON A LEFT INTER-
C VAL. GO TO 'MOVE RIGHT'. IF A RIGHT INTERVAL, ADD RESULTS
C TO FINISH AT THIS LEVEL. ARRAY LORR (MNEMONIC FOR LEFT OR
C RIGHT) TELLS WHETHER LEFT OR RIGHT INTERVAL AT EACH LEVEL.
C
60 PDIFF = PDIFF + DIFF

```

```

70 IF (LORR(LVL) .EQ. 0) GO TO 80
   SUM = PSUM(LVL) + SUM
   PAREA = PAREA - PSUM(LVL)
   LVL = LVL - 1
   IF (LVL .GE. 1) GO TO 70
   LVL = 1
   PSUM(LVL) = SUM
   PAREA = SUM
   ALPHA = ALPHA + DA
   B = 2 * B - A
   GO TO 10
C
C 'MOVE RIGHT'. RESTORE SAVED INFORMATION TO PROCESS RIGHT
C HALF INTERVAL.
C
80 PSUM(LVL) = SUM
   PAREA = PAREA + SUM
   LORR(LVL) = 1
   ALPHA = ALPHA + DA
   DA = DAT(LVL)
   FV1 = F1T(LVL)
   FV3 = F2T(LVL)
   FV5 = F3T(LVL)
   EST = ESTT(LVL)
   GO TO 20
C
C ACCEPT 'POOR' VALUE. SET APPROPRIATE FLAGS.
C
90 IFLAG = 2
   RETURN
100 IFLAG = 3
   RETURN
110 IFLAG = 4
   RETURN
   END
C
C*****C
C      SUBROUTINE VELHE(I1, I2, INEGHE, YIHE, ZIHE, TIHE, TOTVHE)
C*****C
C
C THIS PROGRAM CALCULATES THE DISCHARGE VELOCITY
C (DUE TO THE HALL FORCE) OF THE HELIUM GAS
C COMPONENT IN A LASER GAS MIXTURE.
C
C REAL MUHE, MU(19), YIHE(200), ZIHE(200), TIHE(200)
C COMMON /EDATA/ DC, VC, BO, MU, PRESS, BEAM
C
C DO 60 I = I1, I2
   EHE = (2*VC/DC) * (1 - (ZIHE(I)/DC))
   IF (EHE .EQ. 0) GO TO 50
   EDIVP = EHE / PRESS
   IE = EDIVP / 1000
C
   IF (IE .GE. 1) GO TO 10
   MUHE = 0.85
   GO TO 40
10  IF (IE .GT. 10) GO TO 20
   MUHE = MU(IE)
   GO TO 40
20  IF (IE .GE. 100) GO TO 30
   IE = (IE/10.) + 9
   MUHE = MU(IE)
   GO TO 40
30  MUHE = 0.16

```



```

C
C 40 TIONHE = ZIHE(I) / (MUHE*EHE)
C
C USE CORRECTLY INTEGRATED TRAVEL TIME FOR IONS IN DECAYING E
C
C 40 TIONHE=-1*DC*DC*LN(1-ZIHE(I)/DC)/(2*MUHE*VC)
TOTTHE = TIONHE + TIHE(I)
HEVEL = YIHE(I) / TOTTHE
TOTVHE = TOTVHE + HEVEL
GO TO 60
50 INEGHE = INEGHE + 1
60 CONTINUE
C
C RETURN
C END
C
C *****C
C SUBROUTINE VELN2(I1, I2, INEGN2, YIN2, ZIN2, TIN2, TOTVN2)
C *****C
C
C THIS PROGRAM CALCULATES THE DISCHARGE VELOCITY
C (DUE TO THE HALL FORCE) OF THE NITROGEN GAS
C COMPONENT IN A LASER GAS MIXTURE.
C
C REAL MUN2, MU(19), YIN2(200), ZIN2(200),
COMMON /EDATA/ DC, VC, BO, MU, PRESS, BE
C
C DO 20 I = I1, I2
C EN2 = (2*VC/DC) * (1 - (ZIN2(I)/DC))
IF (EN2 .EQ. 0) GO TO 10
C
C MUN2 = 0.2
C TIONN2 = ZIN2(I) / (MUN2*EN2)
C
C USE CORRECTLY INTEGRATED TRAVEL TIME FOR ION IN DECAYING E FIELD
C
C TIONN2 = -1*DC*DC*LN(1-ZIN2(I)/DC)/(2*MUN2*VC)
TOTTN2 = TIONN2 + TIN2(I)
N2VEL = YIN2(I) / TOTTN2
TOTVN2 = TOTVN2 + N2VEL
GO TO 20
10 INEGN2 = INEGN2 + 1
20 CONTINUE
C
C
C *****C
C SUBROUTINE VELCO2(I1, I2, INEGCO, YICO2, ZICO2, TICO2, TOTVCO)
C *****C
C
C THIS PROGRAM CALCULATES THE DISCHARGE VELOCITY
C (DUE TO THE HALL FORCE) OF THE CARBON-DIOXIDE GAS
C COMPONENT IN A LASER GAS MIXTURE.
C
C REAL MUCO2, MU(19), YICO2(200), ZICO2(200), TICO2(200)
COMMON /EDATA/ DC, VC, BO, MU, PRESS, BEAM
C
C DO 20 I = I1, I2
C ECO2 = (2.*VC/DC) * (1 - (ZICO2(I)/DC))
IF (ECO2 .EQ. 0) GO TO 10
C
C MUCO2 = 0.073
C TIONCO = ZICO2(I) / (MUCO2*ECO2)

```

```
C
C USE CORRECTLY INTEGRATED TRAVEL TIME FOR ION IN DECAYING E FIELD
C
      TIONCO = -1*DC*DC*LN(1-ZICO2(I)/DC)/(2*MUCO2*VC)
      TOTTCO = TIONCO + TICO2(I)
      CO2VEL = YICO2(I) / TOTTCO
      TOTVCO = TOTVCO + CO2VEL
      GO TO 20
10  INEGCO = INEGCO + 1
20  CONTINUE
C
      RETURN
      END
```